

VIBRATION ANALYSIS OF A STEEL TWIN I-GIRDER PEDESTRIAN  
BRIDGE: STRUCTURAL IDENTIFICATION AND EVALUATION OF  
PEDESTRIAN EXCITATION MODELS

by

Jonathan Michael Moss

A thesis submitted to the faculty of  
The University of North Carolina at Charlotte  
in partial fulfillment of the requirements  
for the degree of Master of Science in  
Civil Engineering

Charlotte

2015

Approved by:

---

Dr. Matthew J. Whelan

---

Dr. David C. Weggel

---

Dr. Hongbing Fang

©2015  
Jonathan Michael Moss  
ALL RIGHTS RESERVED

## ABSTRACT

JONATHAN MICHAEL MOSS. Vibration analysis of a steel twin I-girder pedestrian bridge: structural identification and evaluation of pedestrian excitation Models. (Under the direction of DR. MATTHEW J. WHELAN)

Excessive vibration of footbridges caused by pedestrian excitation is an important design consideration that has received increased attention in recent years following serviceability-related failures of several notable pedestrian bridges. Numerous models have been proposed and modified for simulating both individual pedestrian footfall excitations as well as groups of persons. However, experimental validation of pedestrian load modeling has yet to be extensively performed for this challenging human-structure interaction problem. This thesis evaluates the performance of published pedestrian load models by comparing time history simulations from a calibrated finite element model of a pedestrian bridge to experimental data obtained from full-scale testing of the structure.

Operational modal analysis of a steel twin I-girder span is conducted through ambient vibration monitoring using a distributed wireless sensor network with triaxial accelerometers. The experimentally obtained estimates of the modal parameters are then used to calibrate a finite element model of the structure through structural identification, or finite element model updating, using a genetic algorithm optimization routine. Following this field calibration of the dynamic properties of the model, modal superposition time history analyses of the response of the span obtained using the finite element model with published pedestrian load models are compared to experimental measurements acquired during controlled pedestrian loading. The com-

comparisons reveal that published pedestrian load models significantly underpredict the measured peak accelerations for this case study. Parameter identification of variables within each model through optimization of the model correlation with the measured response was performed to calibrate coefficients within each model to the case study data. The results indicate that, for this structure, a single harmonic periodic load with a force amplitude larger than recommended in standardized models produced strong correlation with the measurement data.

## ACKNOWLEDGMENTS

I would like to express my gratitude to those who have made the completion of this thesis possible through their ongoing support.

This thesis would not have been possible without the continued guidance of my advisor Dr. Matthew J. Whelan, whose technical knowledge, understanding, and patience have been crucial throughout the course of this research. His guidance as my advisor, committee chair, and professor has contributed immeasurably to every aspect of this thesis. I am further grateful to Dr. David C. Weggel for his thorough critique of my work, suggestions for improvements to my thesis, and ideas on how to further implement the research. Recognition is given to Dr. Howie Fang for his meaningful insight and review of this work.

I would also like to thank Mr. Caleb Martin for his assistance during experimentation, and further recognition for technical assistance is given to Mr. Houston Skipper. I am furthermore thankful for the continued support and assistance that I have received from my fellow graduate research assistants and classmates.

I cannot express enough gratitude to my family for their significant support and patience throughout this pursuit. I am specifically grateful to my parents for their unwavering support and understanding, without which I could not have completed this work. Above all I thank God for this opportunity and the ability to see it through to completion.

## TABLE OF CONTENTS

LIST OF TABLES	ix
LIST OF FIGURES	xi
CHAPTER 1: INTRODUCTION	1
1.1. Introduction	1
1.2. Anticipated Contribution of the Research Effort	3
1.3. Organization of Thesis	5
CHAPTER 2: LITERATURE REVIEW	6
2.1. Overview of Pedestrian-Induced Vibrations	6
2.1.1. Serviceability Recommendations for Comfort Levels	7
2.1.2. Influence of Dynamic Structural Properties on Pedestrian Excited Response	11
2.2. Review of Experimental Studies on Pedestrian-Induced Vibration of Footbridges	13
2.3. Pedestrian Footfall Models for Single Pedestrian Loading	17
2.4. Pedestrian Footfall Models for Groups of Pedestrians	22
2.5. Finite Element Model Updating	26
CHAPTER 3: EXPERIMENTAL VIBRATION TESTING OF A STEEL TWIN I-GIRDER PEDESTRIAN BRIDGE	31
3.1. Description of Test Structure	31
3.2. Instrumentation and Ambient Vibration Monitoring	35
3.3. Characteristics of Recorded Vibration Response	41
3.4. Operational Modal Analysis	42

3.5. Measured Response to Pedestrian Excitation	48
CHAPTER 4: FINITE ELEMENT MODELING OF THE SPAN AND STRUCTURAL IDENTIFICATION	54
4.1. Description of the Finite Element Model	54
4.2. Structural Identification for Model Calibration	70
4.2.1. Parameterization of the Model	70
4.2.2. Global Optimization Using Genetic Algorithm	77
4.2.3. Comparison of Field Calibrated Model to Experimental Data	83
CHAPTER 5: COMPARISON OF PEDESTRIAN FOOTFALL MODELS TO EXPERIMENTAL DATA	87
5.1. Modal Superposition Time History Simulation of Pedestrian Excitation	87
5.2. Performance Evaluation of Standardized Pedestrian Excitation Models	90
5.3. Evaluation of Single Pedestrian Loading Models Using Recommended Coefficients	91
5.3.1. American Institute of Steel Construction (AISC) Model	93
5.3.2. International Standards Organization (ISO) Model	93
5.3.3. British Standards Institute (BSI) Model	96
5.4. Evaluation of Calibrated Single Pedestrian Excitation Loading Models	96
5.4.1. Optimization of Single Pedestrian Excitation Models	96
5.4.2. Evaluation of Field Calibrated AISC Loading Model	100
5.4.3. Evaluation of Calibrated ISO Loading Model	102

	viii
5.4.4. Evaluation of Field Calibrated BSI Loading Model	103
5.5. Summary of Comparisons Before and After Calibration	105
5.6. Evaluation of Multiple Pedestrian Loading Models	109
CHAPTER 6: CONCLUSIONS	112
6.1. Summary of Research and Key Findings	112
6.2. Recommendations for Future Work	114
REFERENCES	116
APPENDIX A: SAP2000 MATRIX EXTRACTION CODE	119
APPENDIX B: SCRIPTS USED TO OPTIMIZE COEFFICIENTS IN PEDESTRIAN FOOTFALL MODELS	123

## LIST OF TABLES

TABLE 1: Eurocode recommended peak acceleration (Eurocode, 2001)	10
TABLE 2: AISC recommended dynamic coefficients for walking pedestrians (Murray et al., 2003)	21
TABLE 3: Summary of ambient accelerations	41
TABLE 4: Summary of pedestrian-induced peak accelerations across local measurement axes	50
TABLE 5: Number of nodes and elements in the idealized finite element model	65
TABLE 6: Comparison of modal estimates obtained through experimentation and predicted by the idealized finite element model	69
TABLE 7: Global coordinate degree of freedom assignments for the link elements used in model updating	74
TABLE 8: Sensitivity analysis of the uncertain parameter for the column link stiffness	76
TABLE 9: Summary of uncertain parameters included in the structural identification routine	77
TABLE 10: Comparison of idealized and updated finite element model parameters	84
TABLE 11: Comparison of modal parameters obtained through experimentation and predicted by the field calibrated finite element model	85
TABLE 12: AISC recommended dynamic coefficients for one pedestrian walking (Murray et al., 2003)	94
TABLE 13: ISO recommended coefficients for one pedestrian walking (ISO, 2007)	95
TABLE 14: BSI recommended coefficients for one pedestrian walking (BSI, 2008)	96

TABLE 15: Optimization of AISC forcing function: lower bounds, upper bounds, and field calibrated parameters	101
TABLE 16: Optimization of ISO forcing function: lower bounds, upper bounds, and field calibrated parameters	103
TABLE 17: Optimization of BSI forcing function: lower bounds, upper bounds, and field calibrated parameters	105
TABLE 18: Peak analytical accelerations before and after calibration compared to the experimentally measured peak acceleration	107

## LIST OF FIGURES

FIGURE 2.1: Recommended peak accelerations for various structures (Reproduced from Murray et al (2003))	9
FIGURE 2.2: Recommended peak lateral accelerations based on human perception (Reproduced from ISO 2631-2 (1989))	10
FIGURE 2.3: Typical footfall forcing function following Bachmann and Ammann (1987)	19
FIGURE 2.4: Typical footfall forcing function following AISC design guidance	21
FIGURE 2.5: Amplification of applied force for multiple pedestrian load- ing following Matsumoto et al (1978)	23
FIGURE 2.6: Typical footfall forcing function following the British Annex to Eurocode	25
FIGURE 3.1: Pedestrian bridge experimentally tested within research program	32
FIGURE 3.2: Elevation view of bridge	33
FIGURE 3.3: Typical cross-section	33
FIGURE 3.4: Framing plan of the instrumented span	34
FIGURE 3.5: Bridge deck (top left). Bridge framing (top right). Pin and hanger assembly (bottom left). Girder stiffener (bottom right).	34
FIGURE 3.6: Sensor placement on bridge span	37
FIGURE 3.7: Sensors on bridge deck (top left). Individual accelerometer (top right). Wireless accelerometer (bottom left). Receiving antenna (bottom right)	39
FIGURE 3.8: Mechanical shaker oriented to provide excitation in the vertical direction (left) and in the longitudinal direction (right)	39
FIGURE 3.9: Pedestrian load cases examined	40

FIGURE 3.10: Time history acceleration plots at midspan under ambient conditions	42
FIGURE 3.11: Average normalized power spectral density computed across ambient vibration time histories	43
FIGURE 3.12: Selection of modes in SPICE	45
FIGURE 3.13: Average power spectral density plot including locations of modal estimates	48
FIGURE 3.14: Experimental modal parameter estimates	49
FIGURE 3.15: Time history of accelerations measured at midspan for one person walking	51
FIGURE 3.16: Time history of accelerations measured at midspan for two persons walking	51
FIGURE 3.17: Time history of accelerations measured at midspan for three persons walking	52
FIGURE 3.18: Time history of accelerations measured at midspan for three persons walking single file	52
FIGURE 3.19: Comparison of peak acceleration to number of persons walking	53
FIGURE 4.1: Bridge deck and corresponding elements of model	58
FIGURE 4.2: Bridge bearings and corresponding boundary conditions in model	60
FIGURE 4.3: Pin and hanger assemblies and corresponding modeling approach	61
FIGURE 4.4: Bridge columns and corresponding modeling approach	62
FIGURE 4.5: Different methods used to model connections between bridge deck and I-girders	64
FIGURE 4.6: Finite element model of instrumented pedestrian bridge in SAP2000	66

FIGURE 4.7: First twelve modal parameter estimates produced from the idealized finite element model	68
FIGURE 4.8: Comparison of modal parameters from the idealized finite element model to experimental estimates	70
FIGURE 4.9: Minimum objective scores obtained when varying deck unit weight and thickness	83
FIGURE 4.10: Comparison of modal parameters from field calibrated finite element model to experimental estimates	86
FIGURE 5.1: SAP2000 model displaying frame elements used to prescribe pedestrian loading	89
FIGURE 5.2: Peak amplitude acceleration time histories of the experimental load cases used for comparison to the predicted response	92
FIGURE 5.3: Experimental bridge deck response compared to AISC loading model predicted response	94
FIGURE 5.4: Experimental bridge deck response compared to ISO loading model predicted response	95
FIGURE 5.5: Experimental bridge deck response compared to BSI loading model predicted response	97
FIGURE 5.6: Experimental acceleration compared to field calibrated AISC loading model predicted acceleration	102
FIGURE 5.7: Experimental acceleration compared to field calibrated ISO loading model predicted acceleration	104
FIGURE 5.8: Experimental acceleration compared to field calibrated BSI loading model predicted acceleration	105
FIGURE 5.9: Experimental acceleration response compared to the AISC predicted response calculated using the AISC recommended forcing function in conjunction with the calibrated value for the first harmonic coefficient	108
FIGURE 5.10: Single pedestrian footfall loading models using (a) recommended coefficients and (b) calibrated coefficients	109

FIGURE 5.11: Experimentally measured response from two pedestrians (top) compared to the analytically predicted response for the same load case

## CHAPTER 1: INTRODUCTION

### 1.1 Introduction

Pedestrian induced vibrations in footbridges present a challenge in that they can create serviceability issues, even in circumstances when the pedestrian bridge has been adequately designed to resist static and dynamic strength limit states. Due to the dynamic nature of pedestrian footfall loading, bridges intended for use by pedestrian traffic require special considerations to mitigate pedestrian induced serviceability concerns, such as resonance of the structure due to synchronization of the pacing frequency of pedestrians (Bachmann and Ammann, 1987). Pedestrian-induced excessive vibrations can be problematic for both the structural integrity of the pedestrian bridge and for the comfort of the pedestrians present at the time of the vibrations (Murray et al., 2003). Therefore, minimizing excessive vibrations is an important but challenging aspect to the design and maintenance of pedestrian bridges.

The importance of adequately anticipating the dynamic response under pedestrian loading is exemplified by the case of the London Millennium Bridge, which despite being adequately designed for structural limit states, was closed to traffic on its second day of operation due to excessive vibrations that resulted from resonance of the bridge superstructure by pedestrian crowd loading during normal service (Dallard et al., 2001). The vibrations in the Millennium Bridge resulted in displacements of up

to 70 mm (2.75 in), providing a stark example of the potential effects of pedestrian induced vibrations. In order to reduce the vibrations to an acceptable level, this bridge required an extensive seven million dollar retrofit with associated closure of the bridge until the work had been completed (Roberts, 2005). Although extensive research had been previously performed in the area of pedestrian induced vibrations, this highly publicized incident in June of 2000 has brought wider attention to pedestrian loading and led to more research on footfall loading, crowd loading, and the causes of excessive vibrations within human-structure interaction problems (Zivanovic et al., 2010).

Adequately designing for pedestrian loading requires the use of an accurate representation of footfall loads. This too is exemplified by the case of the Millennium Bridge, where footfall loading was initially accounted for in the design process through the use of a then-current but now outdated design guidance for modeling footfall loading (Dallard et al., 2001). Such methods for modeling pedestrian loading vary by governing or voluntary design standard, although most design guides are similar in their prescribed methodology to account for pedestrian loading. For design purposes, design guides typically recommend use of a time varying forcing function to represent the pedestrian footfall loads progressing along the walking surface. While this method accounts for the moving load associated with footfall loading, the modeling of the time varying forces applied to the structure during a footstep presents a challenge due to the unknown interaction of the structural response with the mechanics of the footfall producing the loading. The current forcing functions prescribed to model footfall loading rely on limited experimentally measured footfall forces to approximate the expected dynamic loads using Fourier series representations (Bachmann

and Ammann, 1987). Amplitude and phase coefficients for harmonic contributions to the footfall force have been recommended by various organizations to anticipate the changes in the nature of the applied loading due to expected human-structure interaction in commonly encountered design scenarios. However, these models do not explicitly consider the human-structure interaction and therefore it is expected that significant discrepancies between predicted and measured response may occur when they are applied to specific structures.

In summary, the predicted response of structures, particularly lively footbridges, to pedestrian loads remains a challenging and practically relevant problem. Prediction of these dynamic forces requires the use of an accurate loading model to replicate the actual forces created by pedestrian footfalls, but there is a lack of well documented case studies evaluating the predictive accuracy of the various published footfall models relative to field measurements obtained from full-scale structures. Methodology for performing such assessments of pedestrian footfall models incorporating dynamic calibration of the underlying analytical model of the structure has also not been sufficiently addressed.

## 1.2 Anticipated Contribution of the Research Effort

This research will evaluate the performance of standardized pedestrian footfall functions using experimental measurements and a field calibrated finite element model. As described, there are currently multiple design guides that recommend methods for modeling pedestrian footfall loading. However, these design guides vary by location, with various countries and organizations using different standards and loading models.

The objective of this research is to examine several different load models sourced from the literature to identify potential shortcomings in the current recommended functions. To facilitate this research, full-scale vibration testing of a pedestrian bridge was conducted to perform operational modal analysis of the structure and obtain vibration response measurements under controlled pedestrian excitation. Modal parameter estimates derived through operational modal analysis are used to calibrate the dynamic properties of a finite element model developed of the structure to ensure consistency with the actual in-service behavior. The calibrated finite element model is then leveraged to perform linear dynamic analysis of the response of the bridge to pedestrian loads. Through comparison of the analytical acceleration time histories obtained to experimental measurements, the forcing functions are evaluated and methodology to field calibrate the coefficients in each model to the experimental measurements is developed.

This study seeks multiple contributions to research in this area of structural dynamics. The methods used to develop the idealized and updated finite element models will be described in detail, contributing to applied research on structural identification by providing a case study for finite element model updating using genetic algorithms. Furthermore, a process for evaluating the predictive accuracy of various pedestrian footfall loading models is explained, and the applied results obtained through comparisons with experimental test data are presented. Lastly, a methodology for calibrating coefficients within these functions to achieve improved model correlation with the experimentally measured response is developed to offer insight into the characteristics of the actual applied pedestrian excitation in the presence of

human-structure interaction for this case study.

### 1.3 Organization of Thesis

The outline of this thesis is as follows:

- Chapter 2 presents a literature review on the mechanics of pedestrian footfall loading and the different models used for modeling footfall loads. Furthermore, a review of finite element model updating using genetic algorithms for parameter identification is presented.
- Chapter 3 presents a description of the instrumentation, vibration testing, and operational modal analysis of a pedestrian bridge used as the case study structure for this research.
- Chapter 4 presents details of a finite element model developed for the case study pedestrian bridge and the use of genetic algorithm for structural identification to improve the correlation between the dynamic properties of the model and the experimentally estimated modal parameters.
- Chapter 5 presents an evaluation of various footfall forcing functions using recommended amplitude and phase coefficients for single pedestrian excitation during walking. A methodology is also presented to calibrate the coefficients in these models to the field measurements to identify the characteristics of the pedestrian excitation observed in this case study.
- Chapter 6 summarizes conclusions of the research effort and provides recommendations for future work in this area of research.

## CHAPTER 2: LITERATURE REVIEW

In this chapter, a literature review on pedestrian-induced vibrations and finite element model updating is presented. This literature review examines the background behind pedestrian-induced vibrations, acceptable vibration comfort levels, and the methods used to model pedestrian loading, followed by a review of finite element model updating techniques.

### 2.1 Overview of Pedestrian-Induced Vibrations

Pedestrian loads are the loads generated by the footfalls of walking pedestrians. These loads and the resulting vibrations are subjects that have been studied extensively, particularly in Bachmann and Ammann (1987). Pedestrian loads can be categorized as a type of dynamic loading and, more specifically, these loads are a type of periodic dynamic loading, meaning that the load is repeated at a regular interval. This is due to the repetitive motion of one foot being placed in front of the other, resulting in a rhythmic application of the load. Because the load is applied at the pacing rate of the pedestrian, the vibrational excitation will also be generated at this rate. The periodic loading translates into vibrations induced through dynamic response of the structure, although this response of the structure is influenced by human-structure interaction (Dallard et al., 2001). Furthermore, it has been found that the loads applied by the pedestrians act in both the vertical and horizontal

planes, with the vertical forces being significantly greater than those acting in the horizontal plane (Ricciardelli and Pizzimenti, 2007). Therefore, pedestrians induce both vertical and lateral vibrational responses in structures as they walk. The magnitude of these vibrations is affected by various factors, such as the type of structure, weight of the pedestrian, and the pacing rate of the pedestrian relative to the natural frequencies of the structure. As reviewed subsequently in this chapter, multiple methods have been proposed for approximating footfall forces through mathematical models.

### 2.1.1 Serviceability Recommendations for Comfort Levels

Human perception and comfort levels play a critical role in vibration analysis of civil structures. Often, the vibrations experienced in structures are not significant enough to cause structural damage but are enough to cause discomfort. For this reason, standards and design guidance have been developed to not only address structural integrity concerns related to dynamic loads, but to also account for human comfort. Examples of such standards and design guides are AISC Design Guide 11 (Murray et al., 2003), ISO 2631-2 (ISO, 1989), ISO 10137 (ISO, 2007), and the British Annex to Eurocode 1 (BSI, 2008). In all of these publications, guidelines are set forth based on human perception and acceptance of structural vibrations. The criteria established in each of these standards will be reviewed to develop an understanding of serviceability concerns and acceptance thresholds associated with pedestrian induced vibrations.

In Murray et al (2003) and ISO 10137 (2007), significant portions of the design guidance is focused on human comfort and vibration acceptance. According to Murray

et al (2003), human perception and tolerance of structural vibrations varies according to multiple factors. The factors that play the most significant roles in vibration comfort levels are the type of structure and the activity of the occupants. For example, the guide specifies that vibrations are more accepted on an outdoor footbridge than in a residential structure due to both user expectations and impact on use of and activity within the structures. Because of this, the guide recommends a comparison of the actual vibrations within a structure, measured by accelerometers monitoring vibrations during service, to predetermined human comfort limits. The acceleration limits, first developed in ISO 2631-2 (1989) and then expounded upon in both AISC Design Guide 11 and ISO 10137 (2007), are presented in the form of a chart that prescribes the maximum acceptable magnitude of vertical accelerations for various structures. In this chart, the magnitude of the peak acceptable acceleration varies by structure type and the frequency of the vibrations. The lowest amplitude curve was developed as a baseline acceleration acceptance limit, while the various limits for other structures were developed through the use of multiplication factors applied to the baseline curve. The acceptable level of vibration varies with the frequency of the vibration due to the nature of human perception, which causes vibrations to be more noticeable at certain frequencies than at others. This chart, which is replicated in Figure 2.1 based on Murray et al (2003), indicates that vibrations are most accepted in outdoor footbridges and structures subjected to rhythmic activities, where vibrations would be both generally expected and less noticeable due to the nature of the activity. Similarly, the same baseline curve is used in ISO 10137 (2007) but with more detailed multiplication factors. In that case, factors reflecting time of

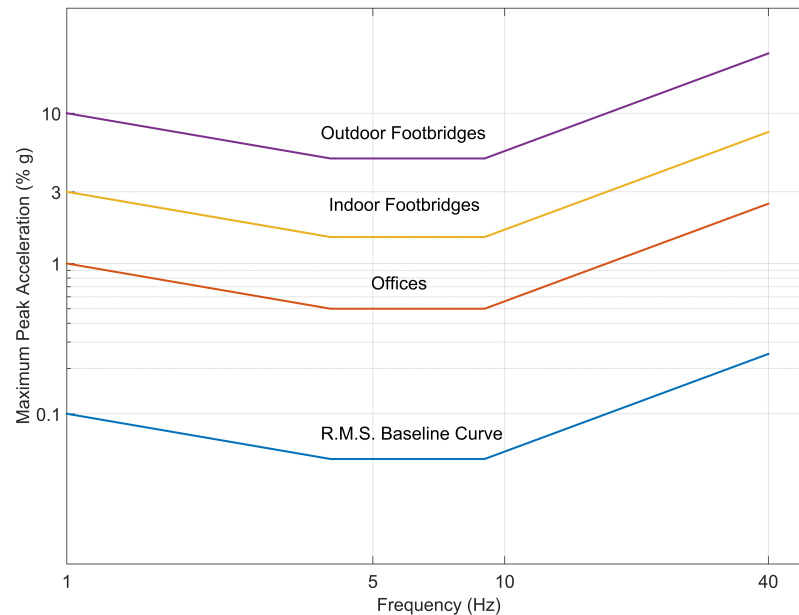


FIGURE 2.1: Recommended peak accelerations for various structures (Reproduced from Murray et al (2003))

day and number of people using the structure are presented.

Similar to the case of vertical accelerations, peak lateral acceleration limits were developed in ISO 10137 (2007). Consistent with the prior design charts, a baseline curve to which multiplication factors are applied to extend the baseline curve to structure-specific cases is presented. This plot is replicated in Figure 2.2 with the baseline lateral acceleration curve and the peak acceleration curve for the case of outdoor footbridges. The peak acceleration curves provide a useful method of evaluating measurements from in-service vibration monitoring in relation to human comfort levels. If the accelerations obtained through testing or analysis of a structure are higher than the recommended peak accelerations, the structure presents serviceability concerns.

Similar to the recommended limits set forth in AISC Design Guide 11 and in ISO

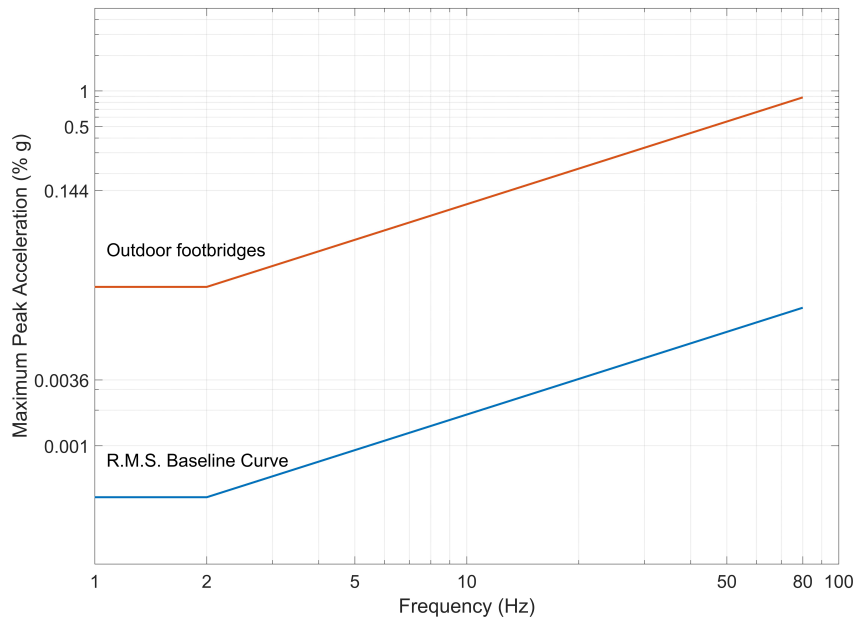


FIGURE 2.2: Recommended peak lateral accelerations based on human perception (Reproduced from ISO 2631-2 (1989))

TABLE 1: Eurocode recommended peak acceleration (Eurocode, 2001)

Case	Peak Accelerations (g's)
Vertical accelerations	0.0714
Horizontal accelerations under typical loading	0.0204
Horizontal accelerations under crowd loading	0.0408

10137, peak acceleration recommendations have also been established in Eurocode standards formed by the European Committee for Standardization. In the Eurocode (2001), peak acceleration limits for the vertical and lateral response have been established for pedestrian bridges. While it is noted in the Eurocode (2001) that the peak acceptable acceleration may vary by project, the given limits that are applicable in most cases are presented in Table 1.

In the British Annex to the Eurocode, recommended serviceability limits are further defined (BSI, 2008). This standard recommends a peak design acceleration magnitude

of less than the peak design acceleration limit calculated as

$$a_{limit} = 1.0k_1k_2k_3k_4 \text{ [m/s}^2\text{]} \quad (1)$$

where  $k_1$  is a site usage factor ranging from 0.6 to 1.6,  $k_2$  is a route redundancy factor ranging from 0.7 to 1.3,  $k_3$  is a structure height factor ranging from 0.7 to 1.1, and  $k_4$  is an exposure factor that is typically assumed to be equal to 1.0, unless otherwise determined on an individual basis. Furthermore, the peak design acceleration limit is restricted between 0.5 m/s<sup>2</sup> and 2.0 m/s<sup>2</sup>.

### 2.1.2 Influence of Dynamic Structural Properties on Pedestrian Excited Response

As was seen in the case of the peak acceptable acceleration chart presented in Figure 2.1, vibrations are more tolerated in certain structures than in others. While this can be attributed in part to the intended use of the structure, it is also due to the dynamic properties possessed by the structure. Two of these properties that will be focused on in this section are the natural frequencies and relative damping factors.

The natural frequencies of a structure affect the amplitude and perception of vibrations within that structure. The natural frequencies of a structure are defined as the characteristic frequencies at which the structure will vibrate if initially displaced and then allowed to freely respond absent of any external driving forces (Tedesco et al., 1999). If the frequency of external applied loads on a structure coincide with a natural frequency, the amplitude of acceleration, velocity, and displacement of the structure will increase relative to excitation at other frequencies. This phenomenon is known as resonance and should be avoided when significant dynamic service loads

are present.

According to Murray et al (2003), the fundamental natural frequency, which is the lowest, is typically of the most concern when considering excitations due to human activities. When feasible, low fundamental natural frequencies within the bandwidth excited by human activities should be intentionally avoided in structures where such loads are prevalent. Specifically, in the case of structures subject to pedestrian loading, natural frequencies between 1.6 Hz and 2.4 Hz should be avoided, since the pacing frequency of pedestrian loads typically falls within this range (Bachmann and Ammann, 1987). Furthermore, the American Association of State Highway and Transportation Officials LRFD Guide Specifications for the Design of Pedestrian Bridges recommends that the fundamental natural frequency of vertical modes exceed 3.0 Hz and the fundamental natural frequency of lateral modes exceed 1.3 Hz (AASHTO, 2009).

The relative damping factor is another important dynamic property that influences the response of structures to pedestrian loads. Structural damping is a mechanism of energy dissipation within a structure introduced by internal and external friction, drag, and other means of mechanical energy loss (Tedesco et al., 1999). Since the relative damping applies to mechanical energy during vibration, structures with increased damping are more effective at dissipating vibrations than structures with otherwise similar properties and therefore experience lower amplitudes of peak acceleration.

According to Bachmann and Ammann (1987), damping can be increased by the presence of non-structural items, such as railings or joints, which serve to dissipate energy by means of friction. Furthermore, the same authors concluded that pedes-

trian bridges typically have less damping than other structures due to an absence of non-structural fixtures. While the relative damping factor associated with individual modes of a particular structure can be determined through instrumentation and experimental analysis of the dynamic response, several studies have been performed in an effort to establish reliable estimates of the relative damping typically exhibited by pedestrian bridges. In Bachmann and Ammann (1987), a study of numerous pedestrian bridges found the relative damping factor to typically range from two to six percent. For design calculations, a relative damping factor of 0.005 was recommended in Bachmann and Ammann (1987) for concrete on steel girder structures, while 0.01 was recommended in Murray et al (2003). As identified within the case studies reviewed in this chapter, the addition of damping through active and passive control devices is also a viable means of reducing excessive vibrations.

## 2.2 Review of Experimental Studies on Pedestrian-Induced Vibration of Footbridges

There have been multiple studies regarding pedestrian-induced vibrations in footbridges, and many of these case studies focus on particular incidents of excessive vibrations encountered in noteworthy structures. In this section, relevant case studies, including details of the specific structures, causes of the reported vibrations, and solutions to the problems, will be reviewed and their findings summarized.

One of the most notable case studies related to pedestrian induced vibrations of footbridges is the London Millennium Bridge. This bridge was opened on June 10th of 2000 and experienced excessive vibrations on the same day (Dallard et al., 2001).

Excessive motion of the bridge span occurred in the lateral direction as a crowd of between 80,000 and 100,000 people crossed the bridge. These vibrations caused up to 70 mm of lateral deflection at the center span. Due to concerns over the excessive motion, the bridge was closed for investigation and retrofitting on June 12th, 2000 (Dallard et al., 2001). Investigations revealed that the probable cause of the vibrations was the synchronization of footfall loads from the crowd crossing the bridge (Roberts, 2005). Synchronization can occur when the individuals within a crowd walk in step with each other and instinctively step in unison with the harmonic motion of the bridge. This causes the forces to be applied at the resonant frequency of the structure leading to large accelerations and, furthermore, the synchronization becomes more pronounced as the motion of the structure increases. Consequently, this leads to additional amplification as the crowd becomes increasingly synchronized as the movements of the bridge increase (Dallard et al., 2001). The solution to prevent future excessive vibrations in the Millennium Bridge was determined to be the introduction of dampers to the structure to increase the relative damping factor of the resonant mode (Dallard et al., 2001).

Another case of excessive vibration occurring in a pedestrian bridge was analyzed in Fujino et al (1993). In this study, which took place seven years prior to the highly publicized Millennium Bridge incident, excessive motion was observed in a cable-stayed pedestrian bridge during crowd loading. This structure was a two-span, continuous steel girder bridge, with the longest span being 134 m. It was found that when crowds of up to 2000 pedestrians were simultaneously crossing the bridge, excessive vibrations in both the vertical and lateral directions became apparent. As

with the Millennium Bridge, it was concluded that pedestrian loading was amplifying the resonance of the structure through synchronization. Applied research revealed that small initial vibrations led the pedestrians to instinctively change their stride to match the bridge movement and walk approximately at the natural frequency of the first lateral mode of the bridge, which occurred at 0.9 Hz. Measurement of the pacing frequency of the pedestrians revealed that, on average, the crowd of pedestrians adjusted their footfall frequency to 0.883 Hz. As the motions increased, over 20 percent of the pedestrians synchronized their movements to the bridge, causing the amplitude of vibrations to increase. However, the study found that, although the vibrations were apparent, many of the pedestrians had grown accustomed to the movements and did not seem concerned. The researchers also noted that only vertical vibrations were considered during the initial design, as the potential problems associated with lateral vibrations were not yet well known. As with the Millennium Bridge, the solution developed to remediate the problem was installation of dampers on the structure (Fujino et al., 1993).

A pedestrian bridge of much shorter span length than the previous two case studies was analyzed in Pan (1992). The bridge in this study had a single span of 43.3 m and consisted of a steel framed superstructure with a concrete deck. In contrast to the previous other two case studies, this bridge was found to experience excessive accelerations in only the vertical direction. Accelerometers were deployed to monitor the response of the bridge and it was found that the fundamental natural frequency associated with the first vertical mode was 2.65 Hz. This moderately low frequency, coupled with heavy pedestrian traffic was identified as the reason for the excessive

vertical vibration. Suggested retrofit of the structure included both the introduction of dampers and an additional support column to the structure.

Operational modal analysis and subsequent finite element model updating of a pedestrian bridge located in Montenegro was presented in Zivanovic et al (2006), which is of particular relevance to the current study. This pedestrian bridge superstructure consisted of a main, central span of 78 m and two shorter spans of 13 m. The cross section of the bridge spans utilized a stiffened steel box girder with a concrete deck. This pedestrian bridge was described as lively, and was thus used as a case study structure in Zivanovic et al (2006). The excessive vibrations in this case had been observed since the bridge opened in the 1970s and were attributed to the low natural frequency of the bridge that was likely an issue due to a lack of serviceability design standards at the time of construction. Prior to the operational modal testing described in Zivanovic et al (2006), a retrofit of the bridge had been carried out to increase the stiffness of the structure, but was neutralized by a corresponding increase in the mass of the bridge. Therefore, the fundamental natural frequency of the bridge was still within the range of typical pedestrian pacing frequencies during the modal testing. In this study, the objective of the research was to develop a finite element model capable of replicating the response of the experimentally tested structure. The authors found that while an idealized finite element model of the structure could yield estimates of its dynamic properties, tuning of the finite element model yielded far superior model correlation between the analytical and experimental dynamic responses. The recommendation of this study was that finite element models used to model existing structures for dynamic analysis should be calibrated to field

measurements from the actual structure using structural identification to ensure the accuracy of the predictions.

### 2.3 Pedestrian Footfall Models for Single Pedestrian Loading

Several footfall loading functions have been developed in an effort to accurately model pedestrian loading of structures (Bachmann and Ammann, 1987, BSI, 2008, Murray et al., 2003). These models typically involve the use of a time dependent forcing function to represent the footfall force exerted by the pedestrian.

In Bachmann and Ammann (1987), it was found that there are certain aspects of pedestrian loading that must be considered. While it was known that walking loads were periodic, it was also known that footsteps could not simply be applied as a heaviside step load at a set time interval. This is due to the stepping motion of a pedestrian, in which the exerted force moves from the heel to the ball of the pedestrian's foot. The amplitude of the applied force varies throughout the duration of the step with peak forces occurring at the beginning and end of each footstep. The result of these two amplitude peaks is a saddle shape in the forcing function as the force increases, decreases, and then increases again. Furthermore, the forcing function should account for the fact that a walking pedestrian will always have a foot in contact with the ground. This constant ground contact results in a slight overlap of footsteps when the heel of the leading foot touches the ground as the ball of the trailing foot leaves the ground. This overlap results in an increase in amplitude of the first peak within the saddle shaped graph, as this peak is the sum of the forces of both the leading and trailing feet. These different factors were taken into considera-

tion in Bachmann and Ammann (1987), in which a Fourier series representation was developed to model single pedestrian loading. This function is given by

$$F_P(t) = G + \Delta G_1 \sin(2\pi f_s t) + \Delta G_2 \sin(4\pi f_s t - \psi_2) + \Delta G_3 \sin(6\pi f_s t - \psi_3) \quad (2)$$

where  $F_P(t)$  is the time dependent footfall force,  $G$  is the weight of the pedestrian,  $f_s$  is the pacing frequency of the pedestrian in Hz, and  $\Delta G_n$  and  $\psi_n$  are the load amplitude and phase angle of the  $n^{\text{th}}$  harmonic, respectively. Two of the most significant variables in this function are the weight of the pedestrian, which is directly proportional to the amplitude of the applied force, and the pacing frequency of the pedestrian. The pacing frequency varies by the speed and stride length of the pedestrian, with increasing frequencies corresponding to an increase in walking speed or decrease in the stride length. For the case of a pedestrian moving at a normal walking speed, the pacing rate has been found to typically fall between 1.7 Hz and 2.3 Hz. The expected amplitude of the fundamental driving frequency appearing in the forcing function has been determined to be between  $0.4G$  for a pacing frequency of 2.0 Hz and  $0.5G$  for a pacing frequency of 2.4 Hz (Bachmann and Ammann, 1987). Interpolation has been proposed as a valid method for determining the amplitude in the case of different pacing frequencies. For the amplitude of the second and third harmonics,  $0.1G$  was proposed as a reasonable value. For all harmonics, the phase angle was specified as  $\pi/2$ . The typical forcing function represented in this model with the recommended variable assignments for a pedestrian weighing 0.8 kN (180 lb) and walking at a pacing frequency of 2.0 Hz is presented in Figure 2.3.

It was also noted in Bachmann and Ammann (1987) that the periodic footfall forces

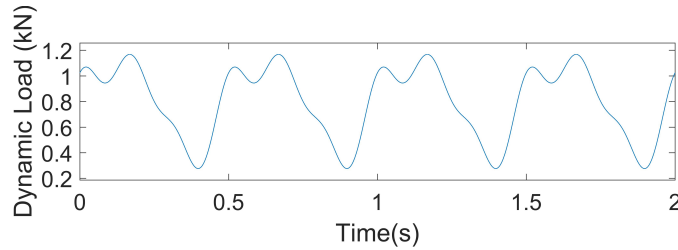


FIGURE 2.3: Typical footfall forcing function following Bachmann and Ammann (1987)

occurred in both the vertical and horizontal directions. Naturally, the vertical load exerted by pedestrians is far greater than the horizontal force due to the direction of gravity. However, the amplitude of the horizontal forces, while only approximately 10 percent of the vertical forces, also occurred with each footstep. This is due to the sway of a person as he or she walks, as the swaying creates a horizontal force component on the walking surface. The horizontal force develops similarly to the vertical force, as both result from the same step. However, it should be noted that while the vertical force exerted by each footstep consistently applies a downward force, the horizontal load will alternate in the direction of load application with each step. Therefore, the horizontal force should be applied in each horizontal direction at half the rate of the vertical force.

The pedestrian loading function developed in Bachmann and Ammann (1987) is a commonly used model for representing the loading from a single pedestrian. A similar Fourier series representation is recommended for vibration analysis by the International Standards Organization in ISO 2631-2 (1989) and ISO 10137 (2007). According to these standards, the function can be used to model both vertical and horizontal loads, with the only difference being a slight variation in the recommended

amplitude coefficients associated with the harmonics. It is also recommended in ISO 10137 (2007) that the number of harmonics included in the forcing function may vary depending on the structure being analyzed. However, tables listing recommended numerical values for the dynamic coefficients in both the vertical and horizontal directions are provided in ISO 10137 (2007) for the first five harmonics. The values of the harmonics vary by both direction of the force and by the pacing frequency.

A similar time history function is described for modeling pedestrian loading in Murray et al (2003). This function is referenced by the American Institute of Steel Construction in AISC Design Guide 11: Floor Vibrations Due to Human Activity. While similar to the loading function recommended in ISO 10137 (2007), the time history function found in Murray et al (2003) recommends a different number of harmonics and slightly different amplitude and phase assignments for each harmonic. The recommended forcing function is given by

$$F_n(t) = P[1 + \sum \alpha_n \cos(2\pi n f_s t + \psi_n)] \quad (3)$$

where  $P$  is the weight of the pedestrian, and  $\alpha_n$  is the force amplitude of the  $n^{th}$  harmonic. The other variables in the equation are consistent with the notation in the prior model. It is recommended in the design guide that the weight of the pedestrian be taken as 0.7 kN (157 lb), while the harmonic force component coefficients are specific to the pacing frequency and are provided in Table 2. Furthermore, although it is stated that the above function is a reliable pedestrian loading model, it is also permitted for simplicity to consider only the first harmonic for design purposes. This is permitted because the harmonics occurring after the first are of lower amplitude

TABLE 2: AISC recommended dynamic coefficients for walking pedestrians (Murray et al., 2003)

Harmonic	$f$ (Hz)	$\alpha$	$\psi$
1	1.6-2.2	0.5	0
2	3.2-4.4	0.2	$\pi/2$
3	4.8-6.6	0.1	$\pi/2$
4	6.4-8.8	0.05	$\pi/2$

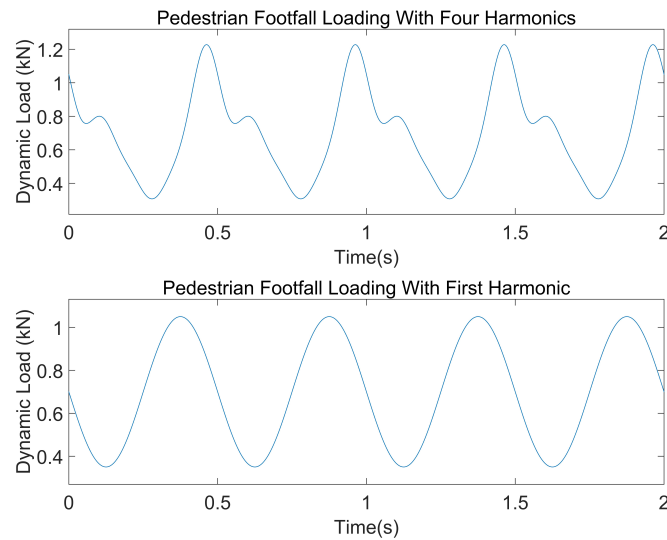


FIGURE 2.4: Typical footfall forcing function following AISC design guidance

and are less likely to induce significant perceptible vibrations through the higher frequency modes of the structural response. Plots of the typical excitation time histories associated with the full model featuring four harmonics and the simplified single harmonic function are presented in Figure 2.4.

An additional pedestrian loading model is described in the British National Annex to the Eurocode 1 Structural standard (BSI, 2008). In this standard, a generalized function is presented to represent the dynamic loading introduced by pedestrian traffic for both single and multiple pedestrians. The applicability of the function to single pedestrian and crowd loading is accomplished through the use of various adjustment

factors within the function. These factors vary with different load scenarios, and recommended values for the factors are provided in the BSI (2008). Since this function can be used to model either single or multiple pedestrian loading, the functional form of the model will be presented and discussed in more detail in the following section concerning multiple pedestrian loading.

## 2.4 Pedestrian Footfall Models for Groups of Pedestrians

The pedestrian footfall models presented in the previous section dealt with single pedestrian loading. In this section, current methods for modeling multiple pedestrian loading will be discussed. Modeling the loads induced by groups of pedestrians presents challenges that are not present during loading by a single pedestrian. Aside from the increase in force created by multiple pedestrians, the effects of synchronization are amplified, as pointed out in the case studies.

Several of the previously discussed single pedestrian load models have been adapted to approximate loads from groups of pedestrians. An early attempt to model crowd loading using a multiplier to represent the number of pedestrians was proposed in Matsumoto et al (1978). This method was referenced in Bachmann and Ammann (1987) as being untested in the field but verified through computer simulations. The method is relatively simple and uses the mean flow rate of pedestrians across the bridge deck and the time taken to cross the length of the bridge to calculate the number of pedestrians occupying the deck at a given time. The square root of the number of pedestrians is then used as a multiplier to amplify the forcing function

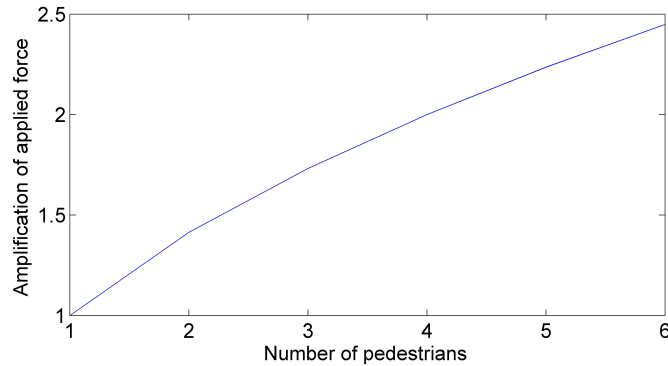


FIGURE 2.5: Amplification of applied force for multiple pedestrian loading following Matsumoto et al (1978)

associated with a single pedestrian. This is shown mathematically by

$$F_m(t) = mF_p(t) \quad (4)$$

$$m = \sqrt{\lambda T_0}$$

where  $F_m(t)$  is the forcing function for multiple pedestrian loading,  $m$  is an amplification factor to account for the loading from multiple pedestrians,  $\lambda$  is the mean flow rate of pedestrians over the bridge, and  $T_0$  is the time required for a pedestrian to cross the span length of the bridge. Use of this method results in a nonlinear increase in the applied force as the number of pedestrians increases, as illustrated in Figure 2.5.

A similar method to that developed by Matsumoto et al (1978) is recommended in ISO 10137 (2007). The recommended method is also based on the concept of using a multiplier to amplify the forcing function developed for a single pedestrian. The function takes the form

$$F_N(t) = C(N)F_p(t) \quad (5)$$

where  $C(N)$  is a coordination factor, which is a function of the number of pedestrians,  $N$ .

In this approach, the forcing function appears the same as in the case of a single pedestrian, except the pedestrian weight is taken as the estimated weight of the group of pedestrians, while the multiplier is a reduction factor, referred to as the coordination factor. The premise of reducing the force is based on the assumption that a lack of coordination will reduce the force on the surface. Therefore, perfect coordination would have the same effect as a single pedestrian of equal weight to the entire group of pedestrians, because the coordination factor would be equal to one. Values for the coordination factor are prescribed in ISO 10137 (2007) for different levels of coordination. For the case of a complete lack of coordination, the presented coordination factor is recommended.

$$C(N) = \frac{\sqrt{N}}{N} \quad (6)$$

As previously mentioned, the BSI (2008) presents a generalized pedestrian loading function applied for simulating either single or groups of pedestrians. This standard recommends the forcing function

$$F = F_0 k(f_v) \sqrt{1 + \lambda(N - 1)} \sin(2\pi f_v t) \quad (7)$$

where  $F_0$  represents the reference amplitude of the applied force,  $N$  is the number of pedestrians considered, and  $f_v$  defines the natural frequency of the vertical mode being evaluated. A combined factor, denoted as  $k(f_v)$ , is used to account for effects of the pedestrian traffic, harmonic responses, and pedestrian sensitivity to structural

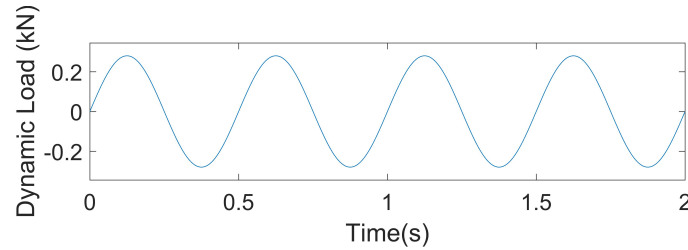


FIGURE 2.6: Typical footfall forcing function following the British Annex to Eurocode

accelerations. A reduction factor, denoted by  $\lambda$ , is used to account for unsynchronized pedestrian movement. A typical footfall model for a single pedestrian developed using this function is presented in Figure 2.6 for a reference amplitude of 0.28 kN (63 lb) and a pacing frequency of 2 Hz.

Through adjustment of the variables in the equation, the forcing function can be applied for any number of pedestrians. Several tables and figures are provided in the BSI (2008) to determine recommended values of the coefficients. The combined factor varies by the natural frequency of the structure, while the synchronization reduction factor varies by the number of pedestrians and the relative damping ratio of the structure. For design and analysis purposes, the forcing function is modeled as a moving dynamic load along the deck of the bridge with a reference amplitude of 0.28 kN. The response of the bridge is then calculated at the most unfavorable location on the bridge deck. It is further specified that the load model should be applied considering not only the fundamental mode shape but also the other modes of the structure.

All of the methods reviewed are relatively simplistic in that the amplitude of the force is assumed to steadily increase with the number of pedestrians. Furthermore,

the multiplier does not account for differences among pedestrians, such as weights and pacing rates, that introduce stochastic characteristics to the loading model. This is because the methods use a scalar factor to simply amplify the loading model for a single pedestrian. The forcing function is therefore based on one specific pedestrian and cannot account for the differences in others.

## 2.5 Finite Element Model Updating

Analysis of the dynamic response of structures to loads varying in time and space is readily facilitated using either direct time history analysis or modal superposition time history analysis with finite element models (Weaver and Johnston, 1987). However, due to differences between the predicted dynamic properties of the analytical model and those of the actual structure, significant errors can arise from the use of finite element models to predict dynamic responses without first verifying and, if warranted, field calibrating the dynamic properties of the model (Friswell and Motterhead, 1995). These discrepancies can arise from uncertainties regarding geometric and material properties of the structure, modeling idealizations, and discretization errors in the finite element model. In order to minimize the effects of these differences and to improve the accuracy of the predictions developed by finite element models, various methods of finite element model updating, or structural identification, have been proposed and evaluated through application to laboratory and full-scale field structures (Çatbaş et al., 2013).

Finite element model updating is accomplished by selectively changing certain parameters within the finite element model while other parameters remain fixed (Friswell

and Mottershead, 1995). These parameter changes are associated with changes in the stiffness and mass matrices of the finite element model, and consequently lead to changes in the predicted response and dynamic structural properties of the model. The effectiveness of the changes can be evaluated through the use of an objective function, which is developed to quantitatively compare the analytically predicted response to the experimentally measured structural response. Therefore, an improvement in the objective score reflects improved model correlation with the change in the uncertain parameters updated, with the objective being to determine the globally optimal solution of parameters for the model. Additional information on parameterization of finite element models and model correlation using an objective function is presented in Chapter 4. The following review of structural identification is specific to the use of genetic algorithms to field calibrate finite element models, which is investigated in this study using field measurements from a case study structure.

Multiple local and global optimization techniques for locating the optimum solution have been favored over recent years as computational techniques and computing power have improved (Mottershead et al., 2011, Zárata and Caicedo, 2008). One of the emerging techniques gaining popularity for structural identification is the global optimization method of genetic algorithms (Levin and Lieven, 1998). This method of optimization uses the principles of natural selection and genetics to search for globally optimal solutions for a given set of parameters (Goldberg, 1989). As with most conventional optimization techniques, a set of uncertain parameters in the finite element model are selected for optimization within a prescribed range of plausible values defined by specified lower and upper bounds for each parameter. Therefore, while the

optimization is completed by the genetic algorithm, the method still requires human discretion to properly update the model. In order to determine the optimal solution, the genetic algorithm evaluates individual sets of candidate parameter assignments, referred to as individuals, across a population of combinations covering the range of possible parameter assignments, or the search space. The quality of each individual is evaluated through the objective function, and the genetic algorithm uses the objective scores across the population to identify the best individual solutions from the population. In this way, the method of genetic algorithm updating uses a survival of the fittest approach to retain and pass on the characteristics of these best individual solutions when recursively generating and evaluating a new population in the search for a globally optimum solution (Goldberg, 1989).

The method parallels natural selection by forming subsequent generations using the surviving individuals, or elites, from each previous population. The subsequent generations developed consist of either crossover, mutation, or elite individuals. Following this methodology, crossover individuals consist of combinations of two previous parameter sets, mutation individuals involve random changes applied to parameters in an individual, and elite individuals represent the unchanged set of best parameter sets according to the objective function (Levin and Lieven, 1998). By the presence of the elite individuals, the best objective score in each subsequent population must either increase or remain unchanged, leading to an eventual convergence on an optimal solution.

Genetic algorithm optimization has been proven effective for use with finite element model updating across multiple studies. In Levin and Lieven (1998), genetic algorithm

optimization was successfully applied to a finite element model updating problem, in which a genetic algorithm routine was used to update a finite element model of a wing shaped plate structure. In this relatively simple evaluation, the genetic algorithm updating routine was found to improve the correlation between the modal results obtained through experimental testing and through finite element analysis.

Genetic algorithm optimization was further used in Nguyen et al (2015) to update a finite element model of a vehicle bridge located in Croatia in order to improve the correlation between the experimental and analytical modal property estimates of the structure. The test structure in the study was an arch bridge constructed using fiber reinforced concrete and having an overall length of 157 m divided across nine spans. In this case, the MATLAB computing environment was used to complete the genetic algorithm updating routine of the finite element model, which was developed using the Abaqus software. Comparison of the properties of the finite element model to experimentally estimated modal parameters was used to conclude that a significant improvement in the correlation of the modal results could be obtained following implementation of the genetic algorithm updating routine.

The extension of genetic algorithm optimization for finite element model updating of civil structures to vibration-based damage detection was explored in Friswell et al (1998), in which a genetic algorithm was used in conjunction with vibration data to predict the location of damage in a finite element model of a cantilever beam. The effectiveness of the genetic algorithm led to the conclusion that the genetic algorithm is a robust method of finite element model updating and is well suited to solving difficult optimization problems. Genetic algorithms were further used for finite ele-

ment model updating and damage detection in Kernicky et al (2015). In this study, a genetic algorithm was used to field calibrate a finite element model of a masonry infill wall in a full-scale structure to experimentally obtained modal parameter estimates acquired both prior to and after the introduction of damage. The optimization routine was successfully used to calibrate an idealized finite element model to improve the correlation between the experimental and predicted modal parameters of the case study wall. Subsequent structural identification of the finite element model using modal parameters measured after subjecting the wall to blast loading was used in this study to predict localized changes in the stiffness of the masonry wall. The predicted locations of damage were found to be plausible with respect to field observations of damage and dynamic nonlinear simulations of the blast response of the wall.

These examples serve to verify the successful use of genetic algorithm optimization for finite element model updating. In all of the cases, the genetic algorithm was found to improve the correlation between experimental and analytical dynamic responses through updating of finite element model parameters.

## CHAPTER 3: EXPERIMENTAL VIBRATION TESTING OF A STEEL TWIN I-GIRDER PEDESTRIAN BRIDGE

In this chapter, operational modal analysis of a pedestrian bridge that serves as a case study structure in this thesis is presented. The test structure, a steel twin I-girder bridge, was vibration tested under both ambient excitation and under a series of prescribed pedestrian load cases. Vibration test results were analyzed to determine the modal characteristics of the structure and to determine the peak accelerations of the bridge throughout the tests. The details of the test structure, experimental modal analysis, and experimental pedestrian-induced vibration results are presented.

### 3.1 Description of Test Structure

Full-scale instrumentation and ambient vibration monitoring was conducted on the longest span of a steel twin I-girder pedestrian bridge for the purposes of operational modal analysis and pedestrian-induced vibration analysis. The bridge, shown in Figure 3.1, is a concrete deck on steel girder superstructure consisting of four spans of unequal length. The bridge serves as a crossing for pedestrian and bicycle traffic over a multi-lane highway. The total length of the bridge, detailed in the as-built construction plans, is 102.49 meters, with the longest span being 35.69 meters. An elevation view drawing of the bridge, which indicates the location of the instrumented span, is shown in Figure 3.2. The framing of the bridge consists of two steel built-up I-shape girders in the cross-section that are independent for each span. The plate



FIGURE 3.1: Pedestrian bridge experimentally tested within research program

girders for each span feature pin and hanger assemblies to connect the adjacent spans. Due to the placement of the columns supporting the bridge, each span is supported on one end by either a column or ramp, while the other end is connected to the next span by the pin and hanger assembly. As seen in the elevation view, the bridge is supported by three columns, located approximately at the end of each span, and by ramps at each end of the bridge. At the abutments at each of these ramps, the bridge is supported by a pair of rocker bearings placed under the end diaphragms of the respective spans. The columns consist of hollow tubular steel sections of two foot six inch diameter filled with concrete.

The girders feature transverse stiffeners formed by T-shape cross sections welded between the upper and lower flanges of the girders. Steel C12x25 channels serve as diaphragms between the girders and support the reinforced concrete deck, which is located approximately at the mid-height of the main girder depth. The bridge features a composite deck with steel decking beneath the reinforced concrete deck

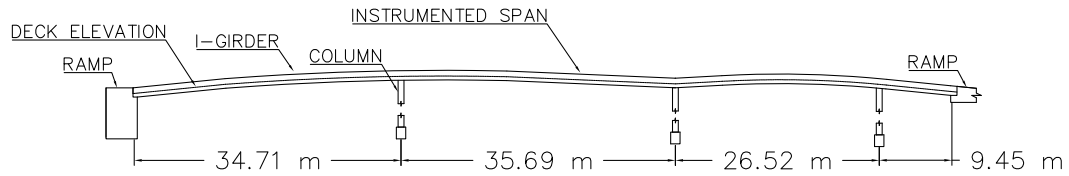


FIGURE 3.2: Elevation view of bridge

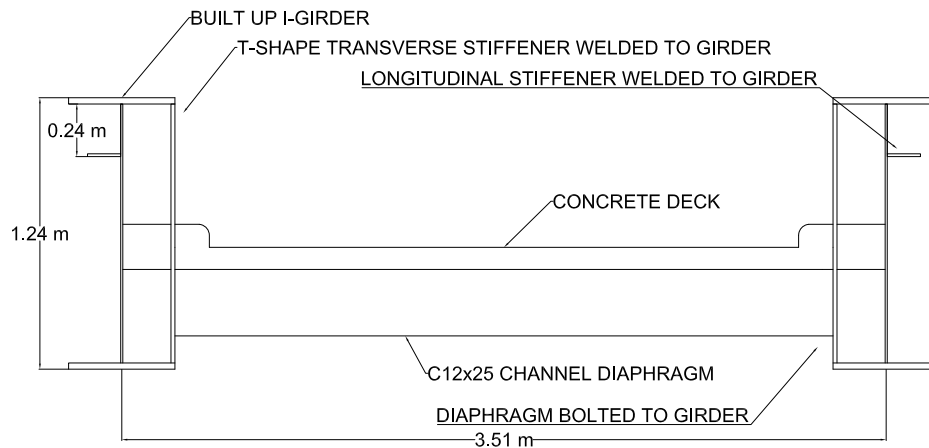


FIGURE 3.3: Typical cross-section

slab. It should be noted that the details of the composite design of the deck were not known. The steel channel framing is connected through the use of simple bolted shear connections. A typical cross section is illustrated in Figure 3.3. It is notable that construction of this design type, with the deck located at the mid-height between twin girders, is considered to be especially susceptible to excessive vibrations (Murray et al., 2003).

The framing plan of the instrumented span of the bridge is presented in Figure 3.4. The bridge is braced laterally by steel ST6x17.5 beams running diagonally between the girders, as shown in the framing plan. Each diagonal spans two diaphragm sections, but is connected to the intermediate diaphragm with a simple shear connection. It is

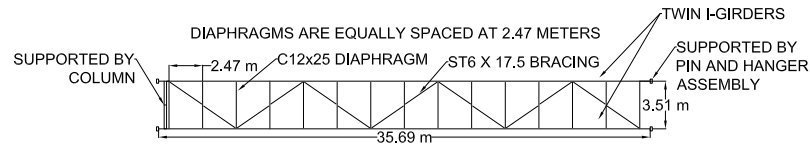


FIGURE 3.4: Framing plan of the instrumented span



FIGURE 3.5: Bridge deck (top left). Bridge framing (top right). Pin and hanger assembly (bottom left). Girder stiffener (bottom right).

also noteworthy that the deck of the bridge is cast directly to both the diaphragms and the twin I-girders in a manner suggesting composite action. In addition to being cast directly to the top of the steel diaphragms, the concrete deck was poured in a way that it surrounds the transverse stiffeners of the main girders, thereby facilitating some degree of composite action with the steel superstructure. Photographs of the bridge deck, steel framing, pin and hanger connections, and the concrete deck surrounding the transverse stiffeners can be seen in Figure 3.5.

### 3.2 Instrumentation and Ambient Vibration Monitoring

In order to obtain acceleration time histories for vibration analysis and for the experimental estimation of the modal parameters of the instrumented span of the bridge for finite element model calibration, field testing of the structure was performed with a distributed array of accelerometers. This field testing was completed on a clear day with mild temperatures and minimal winds. Consequently, ambient vibrations recorded throughout the experimental test program can be attributed to pedestrian loading and vibrations induced by vehicles passing beneath the bridge. To facilitate testing, a network of 16 wireless sensors, each acquiring data from a Kionix KXR 94-2283 triaxial accelerometer, was attached to the deck of the longest span of the bridge. The accelerometers were sampled at a rate of 125 Hz, thereby offering an effective measurement bandwidth from 0 to 56.3 Hz. Digital anti-alias filters and oversampling techniques designed into the wireless sensor network hardware maximize this measurement bandwidth and ensure rejection of any high frequency response or noise in the recorded measurements. The nominal sensitivity of the accelerometers used in the testing was 1000 mV per g, the noise density was  $45 \mu\text{g}/\sqrt{\text{Hz}}$ , and the full-scale range was  $\pm 2$  g. The accelerometers were oriented to record accelerations primarily in the longitudinal, vertical, and lateral directions of the bridge. However, since the accelerometer cases were mounted directly to the deck surface and since the deck profile had a mild slope, the local vertical direction was established as the direction locally normal to the bridge deck, while the local longitudinal direction was established locally tangent to the deck in the lengthwise direction. The deck profile from

the original plans was used to estimate the local orientation of each sensor relative to the gravitational direction and then correct the measurements to the global directions used in the subsequent finite element model described in the following chapter. The local lateral direction of each sensor was naturally lateral to the actual deck and required no correction due to the deck profile. The sensors were attached to the bridge deck through the use of a small amount of wax adhesive, which kept the sensors fixed in place without the need for permanent attachments. The sensors were installed symmetrically along the bridge deck, with sensor locations selected as the locations where the lateral bracing connects to the girders. This layout is shown in Figure 3.6. The selected placement provided uniform spacing along the length of the bridge span and was sufficient to monitor critical peak accelerations in all three directions across the full span. This layout also provided enough spatial density to reconstruct mode shape estimates of the bridge span from the acceleration data. Since each triaxial accelerometer provided three local measurements of acceleration, the network of 16 sensors resulted in a total of 48 measurement channels that were streamed in real-time to a host receiver using a wireless transmission protocol developed in Whelan and Janoyan (2009). The receiving antenna for the sensors was located at the end of the span that corresponded to sensors 15 and 16. Images of the wireless sensors and testing apparatus are shown in Figure 3.7.

The objective of the ambient vibration monitoring program was to collect data both with and without deliberate pedestrian excitation. The data sets without pedestrian excitation are subsequently used to develop modal parameter estimates of the bridge through output-only system identification, or operational modal analysis. The data

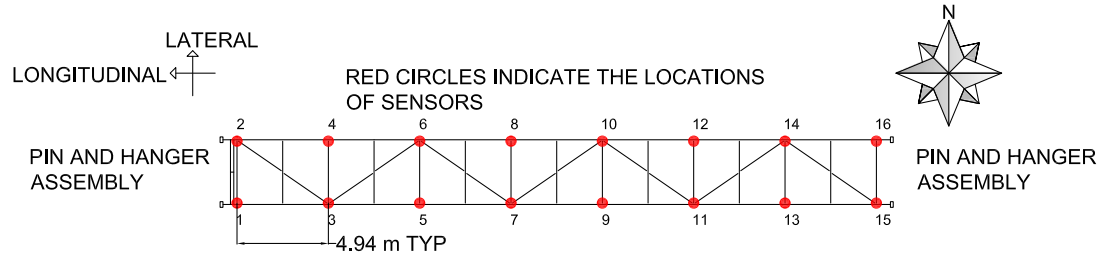


FIGURE 3.6: Sensor placement on bridge span

sets with pedestrian excitation are used in this study to determine the peak accelerations induced in the bridge under specific pedestrian loading scenarios to assess the performance of pedestrian excitation models. Data sets with pedestrian excitation could not be used for operational modal analysis since the excitation from pedestrian loading introduces strong harmonic excitations that violate the assumption of broadband excitation required for operational modal analysis.

Ambient vibration monitoring without pedestrian excitation was performed first, since these results were used to immediately determine the fundamental resonant frequency of the span for subsequent controlled pedestrian testing. The testing without pedestrian excitation consisted of two types of tests. One set of tests was carried out using a mechanical shaker to excite the bridge, while the other set was carried out under ambient conditions without applying additional external excitation with the shaker. Initially, the mechanical shaker, shown in Figure 3.8, was positioned on the bridge deck to induce accelerations in the bridge through prescribed motion of the reaction masses. Using this approach, the shaker provided excitation additional to the ambient vibration sources using a slow swept sine motion of the reaction masses over the full measurement bandwidth while the accelerometers acquired the vibra-

tion response data. Accelerations higher than ambient levels would have ideally been developed with the aid of the shaker to facilitate improved modal parameter estimation through increased signal-to-noise ratio of the measurements. However, while attempting to complete the testing with the shaker, it was found that the vibrations induced by the shaker were not significant enough to produce accelerations notably in excess of those developed under ambient conditions. Since tests involving the shaker required reallocating one of the sensors from the bridge to measure the input excitation from the motion of the masses, it was ultimately determined that the modal parameter estimates would be produced using the data from ambient vibration monitoring without this additional excitation. For the remainder of the ambient vibration cases, it was necessary to collect data when the bridge was not subject to unusual or strongly periodic external excitations. Therefore, the ambient data was collected during intervals when there was either an absence of pedestrian traffic or the presence of only light traffic. Furthermore, it should be noted that both the ambient vibration data and the shaker data were collected with vehicular traffic flowing underneath the bridge. However, the presence of vehicular traffic passing under the bridge can be considered acceptable for operational modal analysis, as these occurrences are generally random and non-periodic. Over the course of the ambient vibration monitoring, data records of 190 second duration were repeatedly obtained to form a basis for developing and averaging modal parameter estimates. Since there were occasional disruptions in the usual flow of pedestrian traffic, including bicyclists, joggers, and pedestrians stopping to examine the sensors, a large number of sets of ambient data were collected. Ultimately, the test program yielded seven data sets absent of pedes-



FIGURE 3.7: Sensors on bridge deck (top left). Individual accelerometer (top right). Wireless accelerometer (bottom left). Receiving antenna (bottom right)



FIGURE 3.8: Mechanical shaker oriented to provide excitation in the vertical direction (left) and in the longitudinal direction (right)

trian induced resonance, which are used for the operational model analysis described in Section 3.4.

After the ambient testing had been completed, the bridge was tested under prescribed pedestrian loading cases. The objective was to measure the dynamic response of the bridge under several cases of pedestrian excitation in order to quantify the peak accelerations developed by a single person walking and by small groups of people walking in different configurations. The various pedestrian load cases that



FIGURE 3.9: Pedestrian load cases examined

were tested included the cases of one person walking, two persons walking shoulder-to-shoulder, three persons walking shoulder-to-shoulder, and three persons walking in single file. Photographs illustrating these pedestrian load cases are presented in Figure 3.9. For each loading case, the footfalls were timed to a metronome set to approximately match, and thus excite, the resonant frequency of the fundamental vertical bending mode. Examination of the previously obtained ambient data determined that the resonant frequency associated with this mode was approximately 2.1 Hz. Therefore, the metronome was set to 126 beats per minute, as this results in 2.1 beats per second. For each loading scenario, three runs were completed, so that the results for each load case could later be averaged. Furthermore, these data sets were obtained during closure of the bridge to all other pedestrian traffic to ensure that the measured response could be attributed predominantly to the prescribed walking loads associated with each test with minimal vibration interference.

TABLE 3: Summary of ambient accelerations

Case	Peak Longitudinal Acceleration (mg)	Sensor	Peak Vertical Acceleration (mg)	Sensor	Peak Lateral Acceleration (mg)	Sensor
1	2.52	15	8.18	14	4.15	15
2	2.35	8	9.53	3	3.69	15
3	2.48	16	10.96	12	4.17	16
4	4.14	16	23.04	8	5.99	15
5	2.43	7	9.36	3	5.86	16
6	2.74	11	12.97	10	5.11	16
7	2.71	16	11.58	13	9.76	16
Average	2.77		11.29		5.53	

### 3.3 Characteristics of Recorded Vibration Response

Prior to developing estimates of the modal parameters of the instrumented span, the data recorded during the ambient testing was analyzed to determine the peak accelerations recorded on the span in the three measured directions of motion. This statistic was used to identify time histories without significant pedestrian excitation. The results are presented in Table 3 and provide measurements of the peak accelerations obtained across the instrumented bridge span. The sensor number is included to show the location where the respective peak acceleration was recorded. Figure 3.10 presents a typical time history acceleration response graph for the midspan of the bridge during ambient vibration conditions.

In order to characterize the frequency response of the instrumented span, an average normalized power spectral density plot (ANPSD) was developed using the data collected through field testing. The ANPSD represents an estimate of the averaged strength of the acceleration measured across the bridge as a function of frequency.

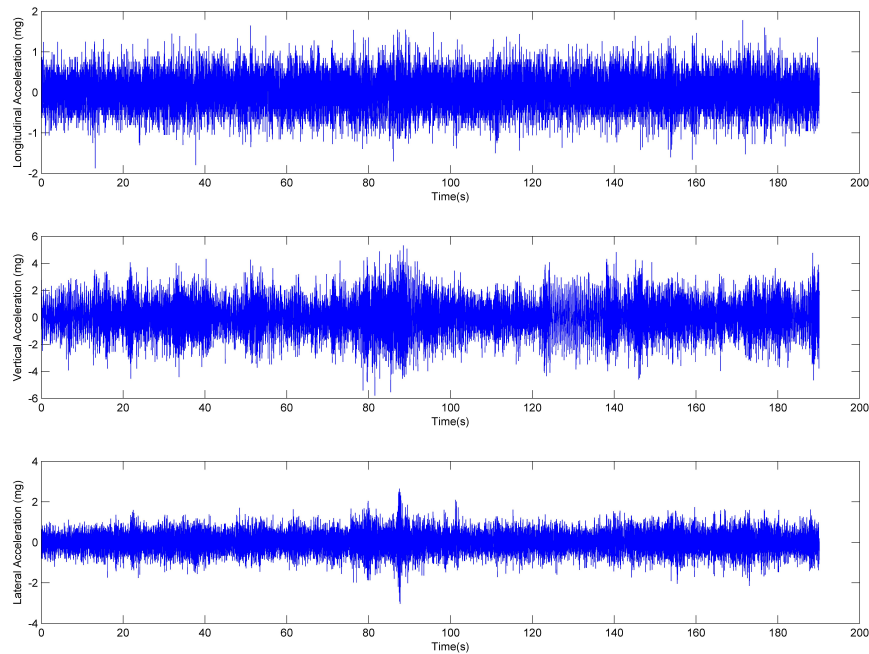


FIGURE 3.10: Time history acceleration plots at midspan under ambient conditions

As such, peaks in signal strength can be identified on the ANSPD at the frequencies at which they occur. For the purpose of this research, the ANSPD was developed within the MATLAB computing environment using Welch's method (Brandt, 2011) to determine the power spectral density. The resulting ANSPD is presented in Figure 3.11. This plot can be a useful reference when locating the resonant frequencies of the structure, which correspond closely with the undamped natural frequencies of the structure for most typical cases of structural damping.

### 3.4 Operational Modal Analysis

For each data set collected during ambient vibration testing, operational modal analysis, or output-only system identification, can be applied on the recorded acceleration time histories to develop estimates of the natural frequencies, relative damping

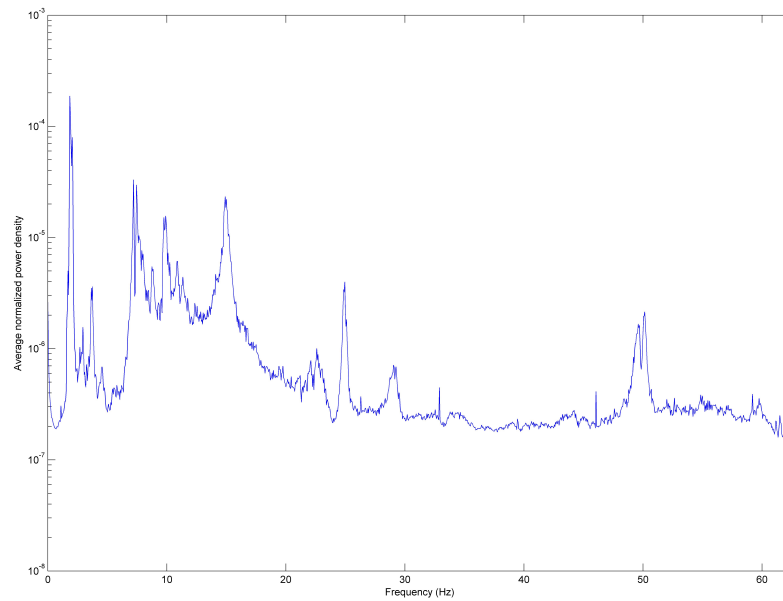


FIGURE 3.11: Average normalized power spectral density computed across ambient vibration time histories

factors, and mode shapes expressed in the measured response for the span under test. The system identification performed on this structure was completed in the MATLAB computing environment using a toolbox developed at the Katholieke Universiteit Leuven. This software is entitled Signal Processing in Civil Engineering (SPICE), or in later versions Modal Analysis on Civil Engineering Constructions (MACEC) (Van den Branden et al., 1999) and implements the stochastic subspace state-space system identification (SSI) algorithm developed in Van Overschee and De Moor (1996). The SSI algorithm is a time domain method of system identification. This method works by regression of a state space model, consisting of state variables, to the measurement data in order to develop a mathematical model for the response of the structure that is consistent with the ordinary differential equation of mechanical vibration. Following regression of the state space model, modal parameter estimation

is performed by eigendecomposition of the estimated state matrix. As the method makes the assumption that the applied force is random, it is especially useful when the input forces, such as winds or traffic underneath the bridge, are not measured due to either logistical or economic reasons (Peeters and Roeck, 2001). This allows for analysis based only on measured response data and provides a means for vibration monitoring of large civil structures under ambient conditions that do not require temporary closure of the structure.

Using the SSI algorithm within the SPICE software, stabilization plots for each data set were generated to extract estimates of stable poles in the system models. An example of such a plot is shown in Figure 3.12. As can be seen in the representative plot, stable poles can be identified by columns of data points, which typically correspond to locations of a resonance peak within the frequency response spectra. Each pole corresponds to a single modal parameter estimate, consisting of a natural frequency, damping ratio, and mode shape for a potential structural mode. Since each row of poles corresponds to an estimate of the system model with a given model order, five modal parameter estimates were obtained for each identified potential structural mode from each data set. These five estimates were taken for each mode and across each data set for the purpose of averaging the data and model order used for the modal parameter estimation when developing the final estimate for each mode. This selection process was completed for each of the seven ambient data sets, until five modal parameter estimates had been compiled for each potential mode identified within each data set. Since several data sets were averaged, it was necessary to pair consistent modal parameter estimates prior to averaging. To achieve this, estimates

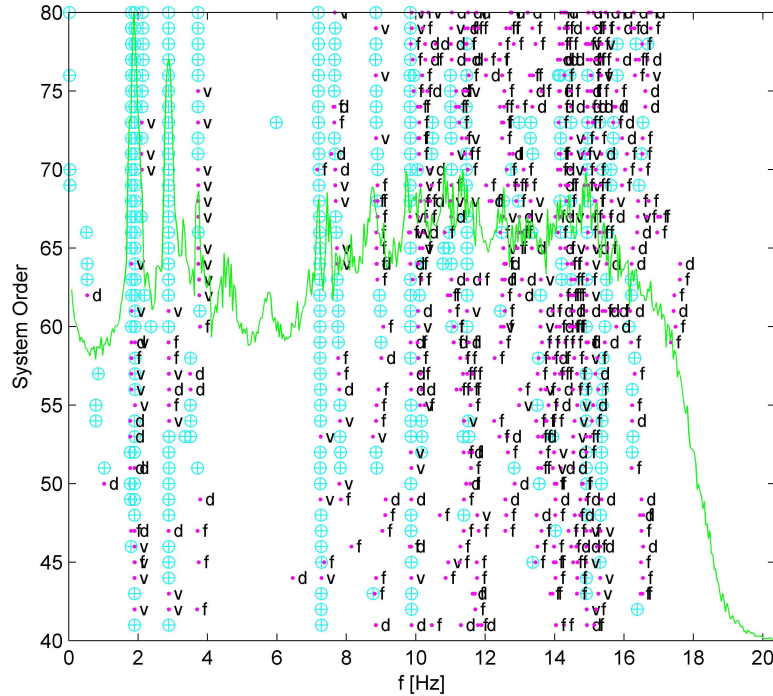


FIGURE 3.12: Selection of modes in SPICE

were initially grouped together based solely on similarities in the undamped natural frequencies. However, it was possible that different mode shapes could occur at similar frequencies and that some modal parameter estimates may be inconsistent due to the pole selection process. Since the averaging of distinctly different modes would produce inaccurate results, the modal assurance criteria (MAC) was calculated across the grouped sets of modal parameter estimates to ensure selection of consistent modes prior to averaging. The MAC is a commonly used statistical measure of modal vector consistency that can be used to verify that a pair of mode shape estimates are actually estimates of the same mode (Ewins, 1984). The equation used to calculate the MAC value is

$$MAC = \frac{|[\phi_j][\phi_i]^T|^2}{([\phi_j][\phi_j]^T)([\phi_i][\phi_i]^T)} \quad (8)$$

where  $\phi_j$  is the measured mode shape to which another mode is compared, and  $\phi_i$  is

the mode shape being compared to the first mode. The MAC value was applied to individual groups of mode shape estimates with similar natural frequencies through the use of a cross-MAC estimator, which returns a matrix of MAC values for all pairs of modes in the group. Higher MAC values indicate greater correlation between the modes. For example, the MAC value computed for two identical mode shapes would be equal to 100 percent. For each set of averaged modes, a minimum threshold value of 85 percent was established for the cross-MAC of each modal parameter estimate used within averages. To expedite this process, the matrix of MAC values computed over each group were represented using a 2D color plot. This provides a means of evaluating the cross-MAC to identify sets of consistent modal parameters for each set of estimates.

After the modes had been reduced to sets of consistent estimates according to the MAC criteria established, averaging could be directly performed across the natural frequencies of the paired modes. The relative damping factors could also be averaged at this point since those are also unbiased estimates. However, due to uncertainties created by outliers in the relative damping factor estimates, the mean and standard deviation of the set of estimates for each mode were first calculated. All values outside the range of the mean plus and minus the standard deviation were discarded. The remaining values were then averaged to obtain a final estimate of the relative damping factor for the mode. In contrast to the natural frequencies and relative damping factors, the mode shape estimates are of relative scale and arbitrary phase. Consequently, it is necessary to apply a normalization to correct the scale and direction of the mode shape estimates prior to averaging. To perform this normalization, the

modal scale factor (Allemang, 2003), presented by

$$MSF = \frac{[\phi_j]^T[\phi_i]}{[\phi_i]^T[\phi_i]} \quad (9)$$

was applied to the common set estimates of the same modes. Each mode shape was scaled to the first mode shape in the corresponding set to ensure that the individual vectors were averaged both in-phase and in an unbiased manner. In Equation 9,  $\phi_j$  is the reference mode to which other modes are normalized, and  $\phi_i$  is the mode subject to normalization. Following normalization, the mode shapes were averaged to produce a single mode shape estimate for each natural frequency.

It was lastly necessary to determine which estimated mode shapes were reliable representations of the structural modes in order to minimize the possibility of including either a false or poorly estimated mode shape within the final set of modal parameter estimates. This was accomplished through the use of the ANSPD of the time history data recorded in the ambient data sets. The estimated natural frequencies were compared to the resonance peaks in this plot to confirm that the estimates occurred where sufficient excitation of the mode during the field test was reflected in the measured strength of vibration. Modal estimates that did not correspond to peaks or occurred at exceptionally low amplitudes on the plot were regarded as potentially spurious modes or unreliable estimates and were discarded. This comparison is illustrated in Figure 3.13, which indicates the locations of the undamped natural frequencies of the averaged modal parameter estimates below 25 Hz superimposed on the ANSPD estimate. The final set of averaged modal parameter estimates for the instrumented span is presented in Figure 3.14. Both isometric and plan views

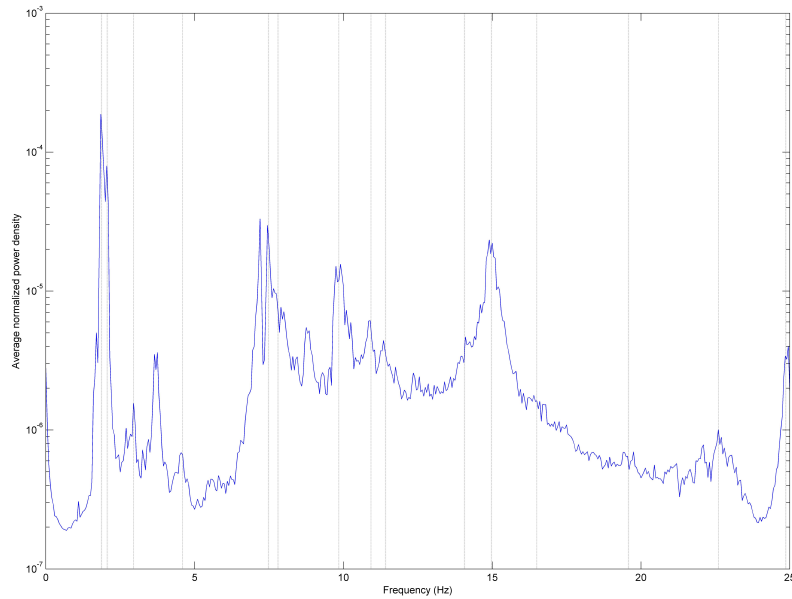


FIGURE 3.13: Average power spectral density plot including locations of modal estimates

of the instrumented span are presented for each mode to permit for identification of both vertical and lateral bending present within each mode. It should be noted that some modes look redundant. However, these similarities arise from the interaction of the connected spans and therefore some of the modes being predominantly driven by resonance within the other spans. This is illustrated later in Chapter 4 through the use of the finite element model developed to simulate the response of the full structure.

### 3.5 Measured Response to Pedestrian Excitation

The accelerations induced by the cases of prescribed pedestrian loading were evaluated to determine the peak accelerations experienced at the instrumented locations of the measured span. For each data set of each prescribed loading scenario, the acceler-

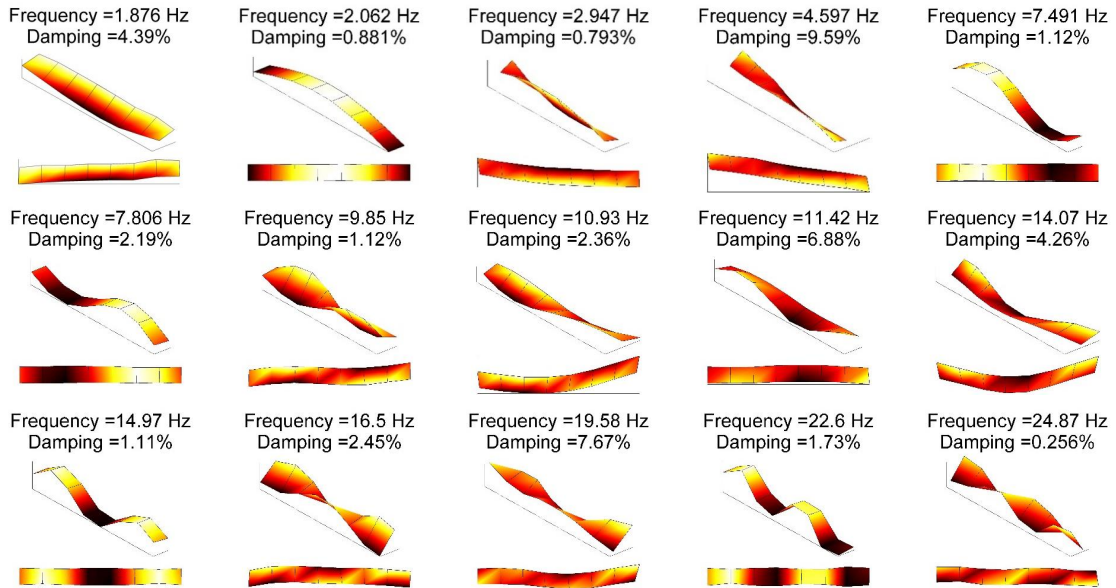


FIGURE 3.14: Experimental modal parameter estimates

ation of each accelerometer along the deck of the structure was evaluated. The peak acceleration measured within each direction was extracted from the recorded data and is compiled in Table 4. It was observed that the peak longitudinal and vertical accelerations occurred at the accelerometers closest to the midspan of the structure (sensors 7 through 10). In contrast, the peak lateral acceleration was typically found to occur toward either end of the span. Time history plots of representative acceleration data recorded during prescribed pedestrian excitation, showing typical accelerations of the deck at midspan, are presented in Figures 3.15, 3.16, 3.17, and 3.18. It can also be observed that the peak accelerations recorded on the bridge increased with an increase in the number of pedestrians providing the loading. This is illustrated by Figure 3.19, showing the peak accelerations plotted against the number of persons walking across the span. Furthermore, a line following the power law was also plotted with the peak vertical accelerations. This was included in order to compare the

TABLE 4: Summary of pedestrian-induced peak accelerations across local measurement axes

Pedestrian Load Case	Peak Longitudinal Accel. (mg)	Sensor	Peak Vertical Accel. (mg)	Sensor	Peak Lateral Accel. (mg)	Sensor
1 Person Walking	4.79	7	43.79	8	8.40	14
1 Person Walking	4.67	7	33.89	8	4.98	16
1 Person Walking	5.62	7	41.97	9	4.50	16
1 Person Average	5.03		39.89		5.96	
2 Persons Walking	8.36	7	70.63	9	5.86	6
2 Persons Walking	7.76	7	58.13	10	6.50	16
2 Persons Walking	9.55	7	73.30	10	10.40	16
2 Person Average	8.56		67.35		7.59	
3 Persons Walking	8.42	7	64.36	8	6.67	2
3 Persons Walking	10.91	7	73.77	9	6.48	16
3 Persons Walking	10.55	7	83.29	7	5.86	2
3 Person Average	9.96		73.81		6.34	
3 Persons Single File	8.69	7	65.00	9	7.06	6
3 Persons Single File	9.00	7	72.76	9	7.02	6
Single File Average	8.84		68.88		7.04	

experimental data to certain pedestrian load models discussed in Chapter 2. These pedestrian load models indicate that a multiplier should be applied to the acceleration induced by a single pedestrian in order to determine the acceleration induced by multiple pedestrians. This multiplier is equal to the square root of the number of pedestrians. Therefore, the line plotted in Figure 3.19 indicates the peak vertical acceleration from the case of a single pedestrian multiplied by the square root of the number of pedestrians. The experimental data indicates that this power law under predicts the peak vertical accelerations induced by the small groups of pedestrians on this structure.

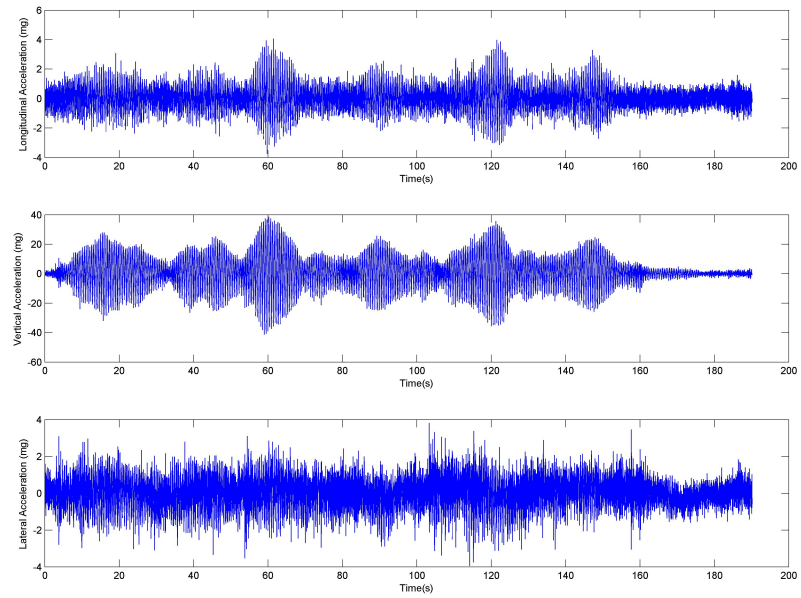


FIGURE 3.15: Time history of accelerations measured at midspan for one person walking

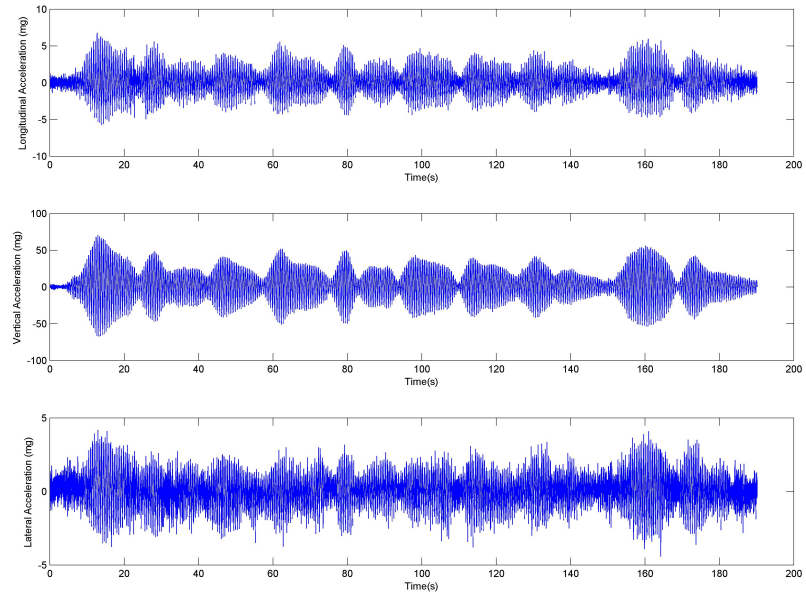


FIGURE 3.16: Time history of accelerations measured at midspan for two persons walking

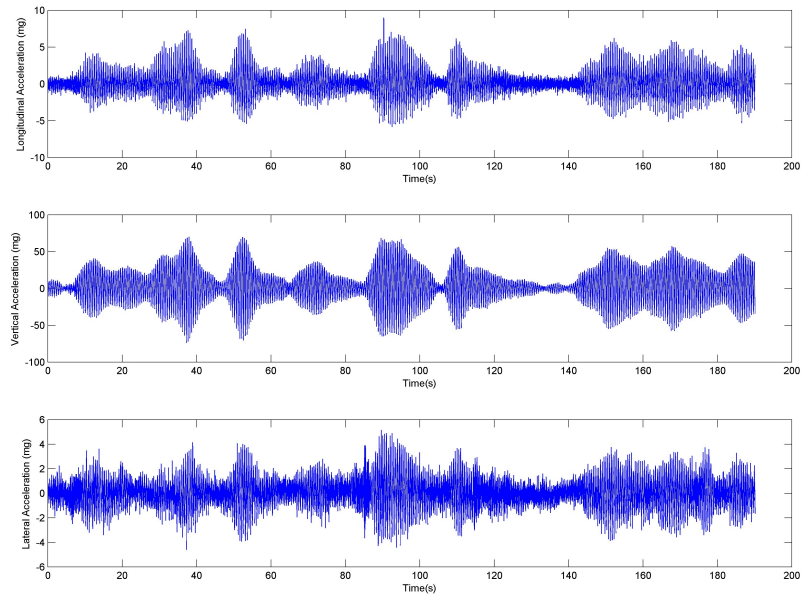


FIGURE 3.17: Time history of accelerations measured at midspan for three persons walking

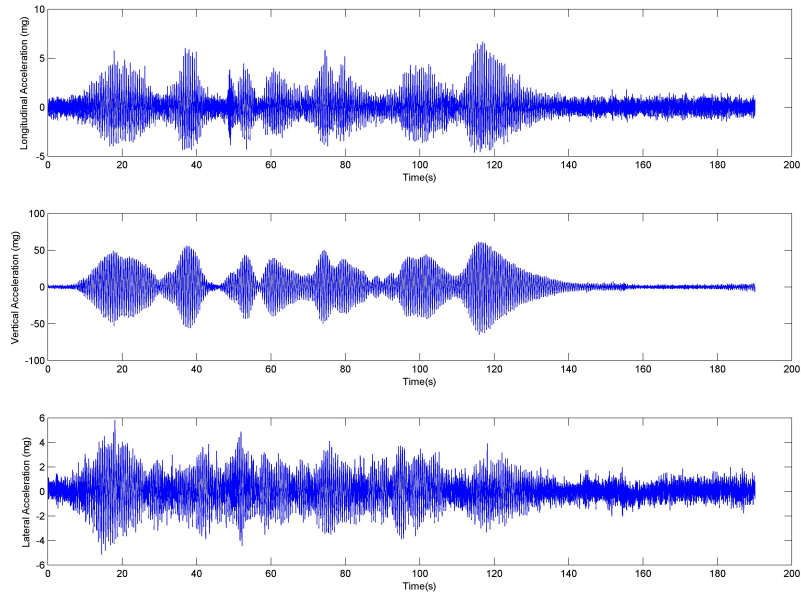


FIGURE 3.18: Time history of accelerations measured at midspan for three persons walking single file

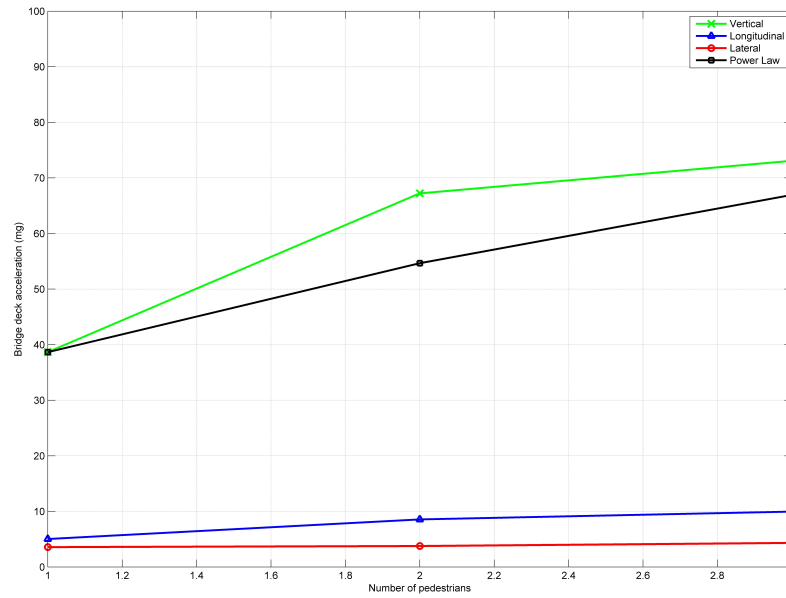


FIGURE 3.19: Comparison of peak acceleration to number of persons walking

## CHAPTER 4: FINITE ELEMENT MODELING OF THE SPAN AND STRUCTURAL IDENTIFICATION

In this chapter, the development of a finite element model of the case study structure used for structural identification and subsequent linear dynamic analysis is presented. The initial section of this chapter describes the methodology, idealizations, and assumptions used when modeling the structure within the commercial finite element analysis software SAP2000. Subsequent sections describe the structural identification routine used to update uncertain parameters within the finite element model for the purpose of improving the correlation between the modal properties of the finite element model and the measured modal parameter estimates obtained through the field testing and system identification described in the previous chapter. The correlation between the experimental modal parameter estimates and those predicted by the updated finite element model are presented at the conclusion of this chapter and serve to validate the use of the model for further linear dynamic analysis under prescribed pedestrian footfall loadings.

### 4.1 Description of the Finite Element Model

The purpose of developing the finite element model was to create a field calibrated representation of the case study pedestrian bridge using software capable of performing linear dynamic analysis. Following validation of the modal parameters of the field calibrated finite element model through comparison to the experimentally obtained

estimates, the this model could be reliably used to simulate pedestrian loading across the bridge span. The first step in producing the field calibrated finite element model was to create an idealized model of the test structure that reflects only engineering judgment in developing the modeling assumptions and assigning material properties. The idealized finite element model, which was modeled using the geometries specified in the original as-built plans of the structure and by observations made during field instrumentation, served as a preliminary model to be later improved by structural identification. Therefore, the idealized finite element model did not attempt to correct uncertainties within the structural model. This idealized model serves as a baseline to document improvements in model correlation afforded by the structural identification.

In developing the idealized finite element model of the structure, it was determined that the entire length of the pedestrian bridge should be represented within the model, despite that the operational modal analysis was carried out on only the longest span of the bridge. The reason for this decision was that it was likely that the dynamic responses and the modal parameters observed in the instrumented span were influenced by coupled interaction with the other spans, since the pin and hanger assemblies do not produce truly independent spans. By modeling the entire span of the structure, the idealized finite element model should more properly simulate the non-ideal boundary conditions at the ends of the instrumented span and account for how the behavior of the span of interest was affected by the adjacent spans. However, since the operational modal analysis was limited to a single span, the experimental modal parameter estimates are incomplete with respect to the response of the full structure

and therefore did not include direct evidence of the behavior of adjacent spans. This presented unique challenges in the model correlation and updating routines that are addressed later in this chapter.

Finite element modeling of the structure was performed using SAP2000 v.15, a commercial finite element analysis software developed by Computers and Structures, Inc. This software can be used to perform both linear and nonlinear dynamic analyses of structures and is especially useful for structural identification research as it allows for assembling and exporting the stiffness and mass matrices of the model for processing within external codes. Additionally, an open-source application programming interface (API) allows for assembly, modification, and analysis of SAP2000 models from the MATLAB computing environment, which was used extensively throughout the model updating process to expedite time consuming and error prone manual manipulation of the finite element model.

The process of developing the idealized finite element model was completed within SAP2000 using the program's graphical user interface, which provides a relatively user-friendly method of modeling structures using frame, area, and solid elements. For this research, the model was developed using only planar area, frame, and link elements. The nodes were initially placed within the x, y, and z planes at points corresponding to each diaphragm of the bridge. These locations had been determined from the as-built plans, which included dimensioned drawings of the structure. The nodes then served as a framework to which other elements could be added. The procedure of specifying nodes and then adding connecting elements approximates the camber of the plate girders and the associated curvature of the deck. In this

approximation, the diaphragms, and thus the nodes, were spaced closely together to approximate the gradual changes in elevation sufficiently to represent the geometry of the structure without the need for curved elements.

The majority of the elements forming the model consisted of those used to model the twin I-girders and the concrete deck. These elements were assigned as thin shell area elements with their respective material properties. The steel girder was assigned an elastic modulus of 199,900 MPa (29,000 ksi) and mass density of 800.38 kg/m<sup>3</sup> (490 lb/ft<sup>3</sup>), while the concrete deck was assumed to be a lightweight concrete with an elastic modulus of 18,561.24 MPa (2692 ksi) and mass density of 196.01 kg/m<sup>3</sup> (120 lb/ft<sup>3</sup>). It should be noted that the actual unit weight and elastic modulus of the concrete was not known, as it was not provided in the as-built construction plans. Furthermore, the actual bridge deck was constructed with formed steel decking that contributes additional stiffness to the concrete deck. The steel decking is not included in the finite element model, which uses the concrete alone as the decking material. This is in part due to the exclusion of the steel decking from the as-built construction plans, since the current deck is not original to the structure. Since design details for the replacement deck were not available, the details for the original deck were used as a guideline. Consequently, the deck was modeled according to the given thickness of 10.16 centimeters (4 inches), although it was unknown whether the same thickness was used for the replacement deck. Observations made during the field experimentation revealed the presence of a concrete curb running the length of the deck surface adjacent to each I-girder. This curb, which was not present in the as-built plans, is approximately 15.24 centimeters (6 inches) tall by 33.02 centimeters

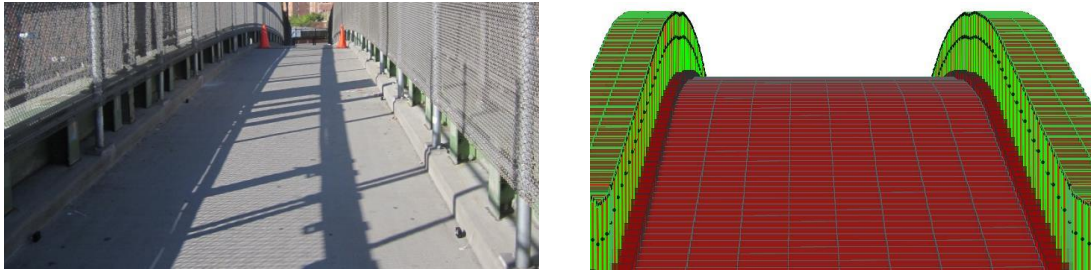


FIGURE 4.1: Bridge deck and corresponding elements of model

(13 inches) wide. As this could potentially affect the results of the modal analysis due to increases in both mass and stiffness, this layer was included in the finite element model. This can be seen in Figure 4.1, which displays both a photograph of the actual deck and an extruded representation of the finite element mesh used for representation of the deck and curb. In contrast to the concrete deck, the dimensions of the twin I-girders and stiffening elements were found to be consistent with the as-built plans and were thus modeled with the original geometries detailed in the plans.

The steel framing of the bridge was modeled using frame elements sized to the specified members in the as-built plans and connected to the girders and other framing elements through the use of ideal simple shear connections. All steel framing was assigned the same material properties as the plate girders. The columns serving as bridge piers were also modeled using frame elements. However, unlike the cross sections of the steel frame elements, the columns could not be selected from the library of standard shapes, as the columns are a composite design consisting of a cylindrical steel tube section filled with concrete. It was therefore necessary to compute the composite cross-sectional properties, which was facilitated through the use of the cross section designer feature of SAP2000. The cross section designer is an interface that

allows users to manually input the cross sectional dimensions and associated materials for a frame element. The dimensions and assumed material properties for the composite columns were specified within this section designer, which then computed the geometric properties of the frame element using an equivalent stiffness referenced to the material properties and mass density of a normal weight concrete. Therefore, although the column cross sections were modeled with both steel and concrete, SAP2000 represents the columns with different dimensions than those specified in the as-built plans. However, the equivalent stiffness and mass match that of the assumed cross section. As the model is used for only a linear elastic analysis, these equivalent properties are sufficient for representing the behavior of the composite columns and are reflected in the global stiffness matrix assembled by the software.

In the initial idealized finite element model, boundary conditions of the model were assigned to nodes of frame elements at the locations where the bridge spans were supported at the abutments. These boundary conditions simulate the simple supports provided in the superstructure as ideal pin restraints that allow freedom of rotation while restraining the local translational degrees of freedom. These boundary conditions were applied to a diaphragm member rather than the plate girder to match the observed bridge design. A comparison of the bearing provided on the actual structure and the idealized boundary enforced on the finite element model is presented in Figure 4.2.

Throughout the finite element model, there were several aspects of the structure where link elements were used to simulate behavior of members or assemblies. Link elements are two-dimensional elements that can be used to connect two nodes with

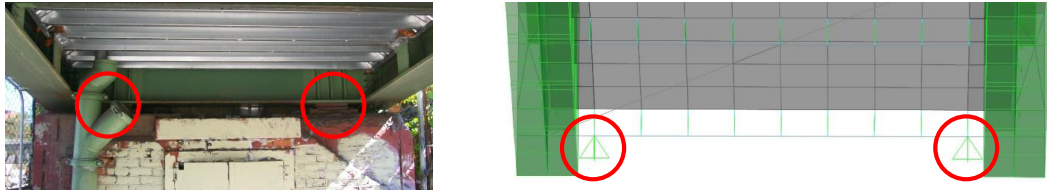


FIGURE 4.2: Bridge bearings and corresponding boundary conditions in model

prescribed translational and rotational stiffness assignments. Therefore, they are especially useful when two elements are connected by a member or mechanism providing either full or partial restraint in a limited number of degrees of freedom. One of the bridge components modeled through the use of link elements was the pin and hanger assemblies used to connect adjacent spans. The pin and hanger assemblies featured on the bridge are assumed in the idealized finite element model to act as translationally rigid elements permitting freedom of rotation associated with major axis bending and minor axis bending of the plate girder, but not torsion. The use of the link element to model the pin and hanger assembly is shown in Figure 4.3, which provides a photograph of the actual connection and a rendering of the mesh of the plate girder webs with the link element used to simulate the behavior of the pin and hanger assembly.

Link elements were also used to model the connection between the column piers and the end diaphragms of the superstructure that they support. Each column of the actual structure is connected to its respective span through the use of a bearing plate on top of the column. Two W18x118 beams spanning between the twin I-girders are anchored to this bearing plate through a bolted connection. In order to model this connection in a simplified manner without introducing solid elements

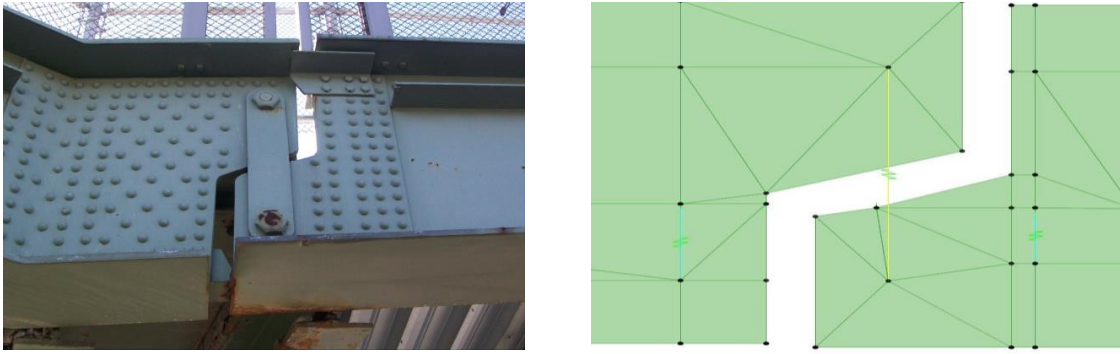


FIGURE 4.3: Pin and hanger assemblies and corresponding modeling approach

to the model, link elements were used to connect the end diaphragms to the top of the pier. Use of these link elements permits the beam elements to be positioned in the correct geometric location with respect to the pier and provides for specification of idealized connection behavior. For the idealized model, all translational degrees of freedom and the rotation about the lateral axis were fixed for this element. This connection is displayed in Figure 4.4, which compares the actual connection to the modeled connection in SAP2000 in both element and extruded representations. The use of link elements for simulation of this connection and the pin and hanger connection also provides a means for model updating, as the stiffness of these elements in each translational and rotational direction can be established as uncertain parameters rather than relying on idealized assignments.

The final aspect of the idealized model that involved the use of link elements was representation of the composite nature of the bridge deck. As previously stated, the deck of the actual bridge was poured in a way suggesting some degree of composite action between the deck and the steel diaphragms and also between the deck and the twin I-girders. To model the connections between the deck and steel diaphragms,

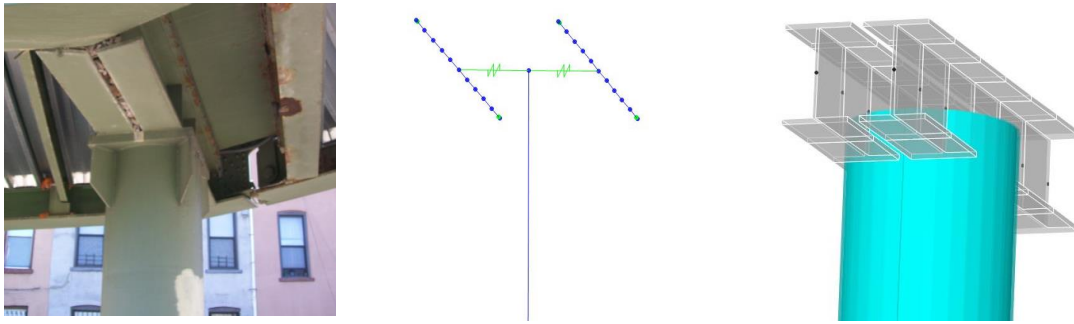


FIGURE 4.4: Bridge columns and corresponding modeling approach

link elements were connected between nodes of the bridge deck and corresponding nodes of the diaphragms below. These link elements were fixed in their translational degrees of freedom but provided no rotational restraint at their nodes. Additionally, since the concrete deck was cast around the tee-shaped transverse stiffeners on the plate girders, as seen in Figure 4.5, it was expected that some degree of composite behavior would occur between the deck and twin I-girders that should be included in the finite element model. However, since the degree of stiffness provided at this interface between the deck and girders could not be easily estimated, several different modeling approaches were taken to develop a representation most agreeable with the measured modal parameter estimates. The first of these modeling approaches featured no connection between the plate girders and the deck, thereby relying only on the diaphragms to transfer loads from the deck to the girders. This approach was discarded after a comparison between the modal parameter estimates of the model to those experimentally measured revealed that the plate girders lacked significant torsional stiffness in many of the modes where such stiffness would likely be contributed to by the casting of the deck to the girder. Therefore, the model was revised so that

the external nodes of the deck were shared with nodes on the web of the girders. While this increased the torsional stiffness of the girder modes, the finite element model had a tendency to return mode shape estimates dominated by flexure in the girders that did not significantly engage the deck. Therefore, the model was revised so that nodes from the transverse stiffeners were also shared with the deck to introduce another connection increasing the composite stiffness of the section. This, however, appeared to increase the torsional stiffness of the model well beyond the experimentally observed response. Lastly, the model was revised so that the deck no longer shared nodes directly with the girders or transverse stiffeners. Instead, link elements were added to the model to connect the nodes on the exterior edges of the deck elements to nodes on the girder web. In order to implement this approach, a small gap was added between the deck and the web of each I-girder to ensure that connectivity between these elements was limited to only the link elements. This approach allowed for the translational degrees of freedom of the connecting link elements to be fixed without inhibiting the rotational degrees of freedom. With respect to the future structural identification routine, these links also provide a stiffness parameter assignment that could be modified during the model updating process to identify the optimal degree of partial fixity to represent the composite action in the structure. Consequently, the link element approach was adopted in the idealized finite element model and was used in the subsequent structural identification routine. Each of the four approaches investigated for modeling this connection is represented in Figure 4.5, which shows the modeling techniques investigated leading up to and including the final idealized model. Although the renderings of these modeling approaches often appear to be

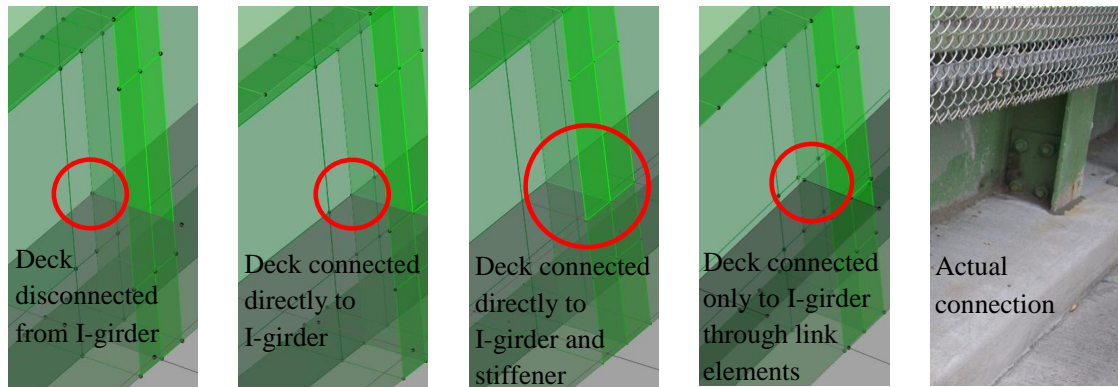


FIGURE 4.5: Different methods used to model connections between bridge deck and I-girders

identical, the difference between the first two models is that the deck and girder do not share connectivity at the nodes along the edge of the deck in the first model, while the second model features connectivity between these elements at these nodes. This connectivity cannot be discerned through visual observation of the model. The third and fourth modeling approaches are more discernible, as the nodes where the deck and I-girders are connected can be identified by the meshes of the components. The gap between the deck and web of the girder is also apparent in the final modeling approach.

Since modal parameters of a structure are sensitive to mass and mass distribution, it is important to consider the added mass of nonstructural elements in addition to the mass and stiffness contributions of structural members. The structure tested supports aluminum fencing along each girder consisting of an aluminum railing original to the bridge and a second, taller chain-link fence that was presumably added at a later time. Both of these fixtures span the entire length of the bridge and, while they were assumed to contribute minimal stiffness to the bridge, they contribute to the mass

TABLE 5: Number of nodes and elements in the idealized finite element model

Nodes	11053
Shell Elements	10169
Frame Elements	727
Link Elements	941

distribution of the structure. The added mass of this fencing was estimated from the dimensions of the fencing and the density of aluminum. The estimated mass was then uniformly distributed along the length of the bridge to the nodes of the girders at the diaphragms where the fencing was supported.

In the same respect, a highway sign is directly supported by one of the plate girders, as observable in the photograph of the structure in the prior chapter (Figure 3.1). Since this added mass was asymmetrically applied to the structure, it may affect the torsional and lateral behavior of the instrumented bridge span. Consequently, the added mass contribution from the sign was accounted for by application of additional masses to the nodes of the model corresponding to the locations of the supporting columns of the sign. For the idealized model, the mass of the sign was estimated to be 250 kg (551 lb) divided evenly across the three nodes.

The final idealized finite element model is presented in an isometric view in Figure 4.6. The number of nodes and each element type used within the model is summarized in Table 5. The number of degrees of freedom present in the final idealized model was 63,410.

While it was anticipated that the idealized finite element model would require model updating to achieve optimal correlation with the experimentally measured modal parameter set, the natural frequencies and mode shapes produced by eigenanalysis

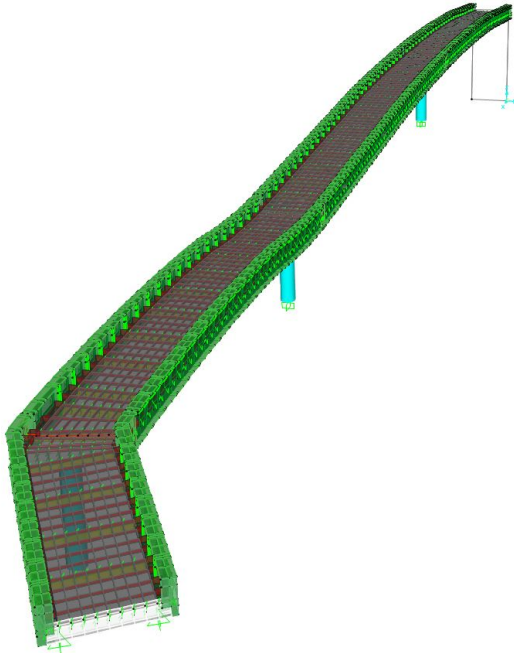


FIGURE 4.6: Finite element model of instrumented pedestrian bridge in SAP2000

of the idealized model serve to characterize the initial correlation in the model prior to application of the structural identification routine. The first twelve mode shape estimates generated by the finite element model are presented in Figure 4.7, where the modes are labeled with their corresponding natural frequency. In these figures, the full model is displayed in the isometric view, while the instrumented span is shown in detail in the plan view. This set of modal parameter estimates serves to illustrate many of the challenges faced when matching experimental modes to the results of the finite element eigenanalysis. Foremost, it can be seen that many of the modes are predominantly associated with resonance occurring in spans other than the instrumented span. In some cases, these modes feature interaction with the instrumented span, while in others the response is essentially isolated. Consequently, the decision to model the full structure rather than idealize the support provided to

the instrumented span is justified. However, by modeling the full span there is a significantly larger set of modes that must be calculated than the set experimentally measured. More significantly, because of the interaction between the spans there are often several modes that appear identical when only the response of the instrumented span is observed. For instance, the modes from the finite element model present at 5.31 Hz, 5.754 Hz, and 6.605 Hz all appear to produce similar behavior in the instrumented span even though they are distinct modes in the full model. This presents challenges in properly matching the modes when the experimental data is limited to a single span when such interaction is present. Strategies for automating the mode pairing in the presence of this challenge are discussed in a subsequent section.

Using the natural frequencies and mode shapes computed from the finite element model, an initial statistical comparison was made to the experimental modal parameter estimates. Mode pairing between the two sets of modal parameter estimates was performed based on the percentage error in natural frequencies, the modal assurance criterion (MAC) correlation, and visual pairing of mode shapes to determine the subset of analytical modes that best corresponded to experimental mode shapes. A strategy used when pairing modal parameter estimates was to assess the relative amplitude of the mode shape within the instrumented span. This relative amplitude measure was taken as the maximum absolute amplitude of the unit normalized eigenvector of each mode shape limited to the measurement locations on the instrumented span. High relative amplitudes indicated that the mode was primarily driven by the dynamics of the instrumented span, while low relative amplitudes indicated that the

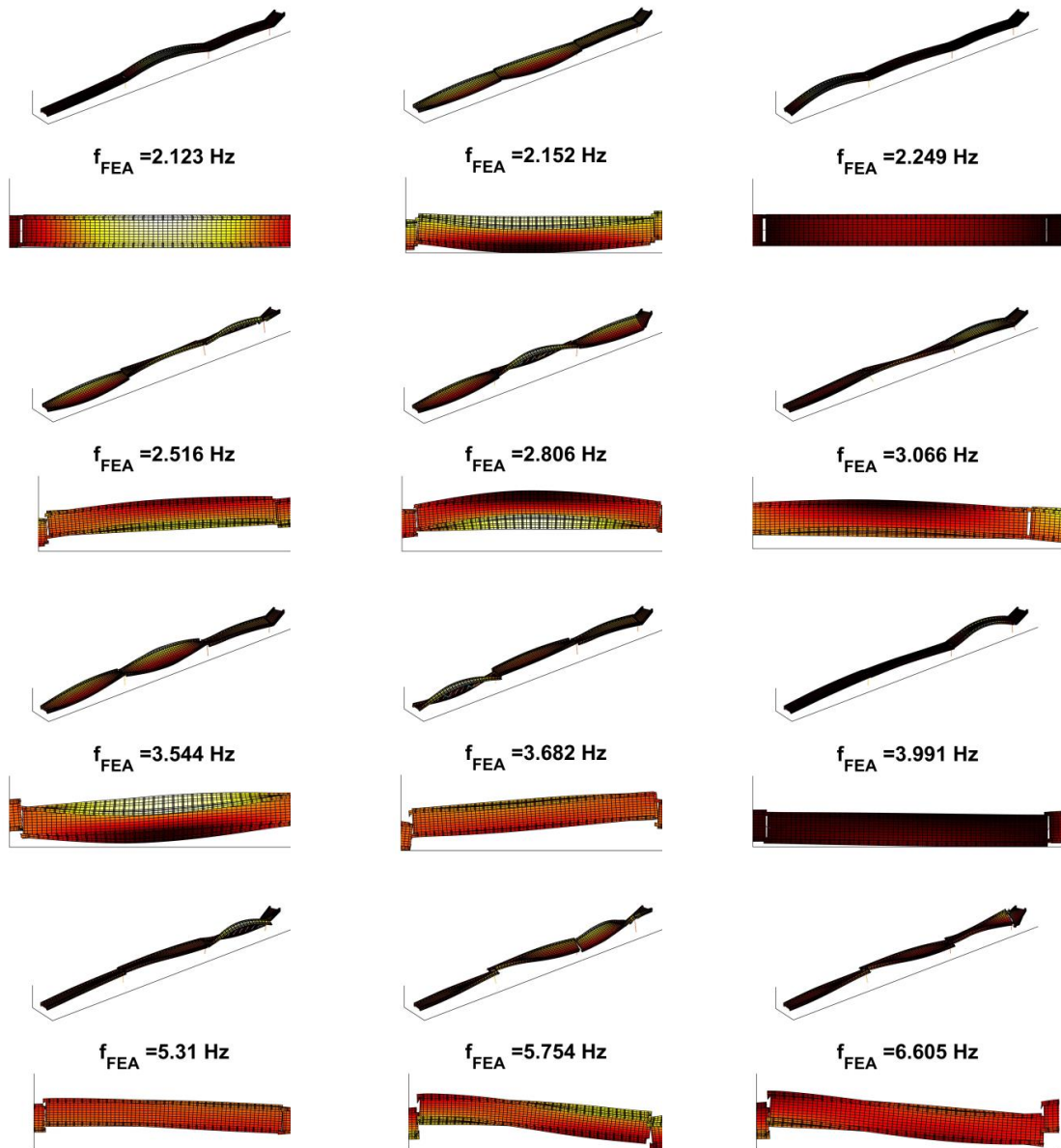


FIGURE 4.7: First twelve modal parameter estimates produced from the idealized finite element model

mode primarily featured resonance in another span. This comparison was crucial to identifying the set of modes that were most likely to be well excited and well measured by the limited instrumentation on the single span of the bridge. The modes from the idealized finite element analysis that were found to best correlate with the

TABLE 6: Comparison of modal estimates obtained through experimentation and predicted by the idealized finite element model

Mode	$f_{exp}$ (Hz)	$f_{FEA}$ (Hz)	% difference	MAC
1	1.876	2.152	14.704	0.938
2	2.062	2.123	2.965	0.988
3	2.947	2.806	-4.806	0.611
4	4.597	5.754	25.162	0.792
5	7.491	7.944	6.056	0.996
6	7.806	8.583	9.963	0.192
7	9.850	10.336	4.931	0.548
8	10.933	10.490	-4.051	0.724
9	11.420	16.435	43.902	0.313
10	14.070	14.250	1.272	0.834
11	14.970	15.712	4.986	0.963
12	16.499	17.435	5.675	0.700
13	19.577	20.429	4.350	0.713
14	22.597	21.718	-3.888	0.735
15	24.872	26.202	5.348	0.364

15 experimental mode shape estimates are presented in Figure 4.8. The experimentally measured modal parameter estimates corresponding to these modes are included in the comparison, and the mode shapes from the finite element model are plotted only at the corresponding sensor locations to facilitate a direct comparison. Table 6 presents a quantitative comparison of the modal parameter estimates from the idealized finite element model and the experimental estimates. As evidenced by the percentage errors in natural frequencies and the MAC values, some of the estimates obtained through finite element eigenanalysis compare well with the modal parameter estimates while others exhibit relatively poor correlation. Due to a desire to improve the model correlation, especially for the lowest frequency modes of the model, structural identification was pursued to field calibrate the model to the measured modal parameter estimates.

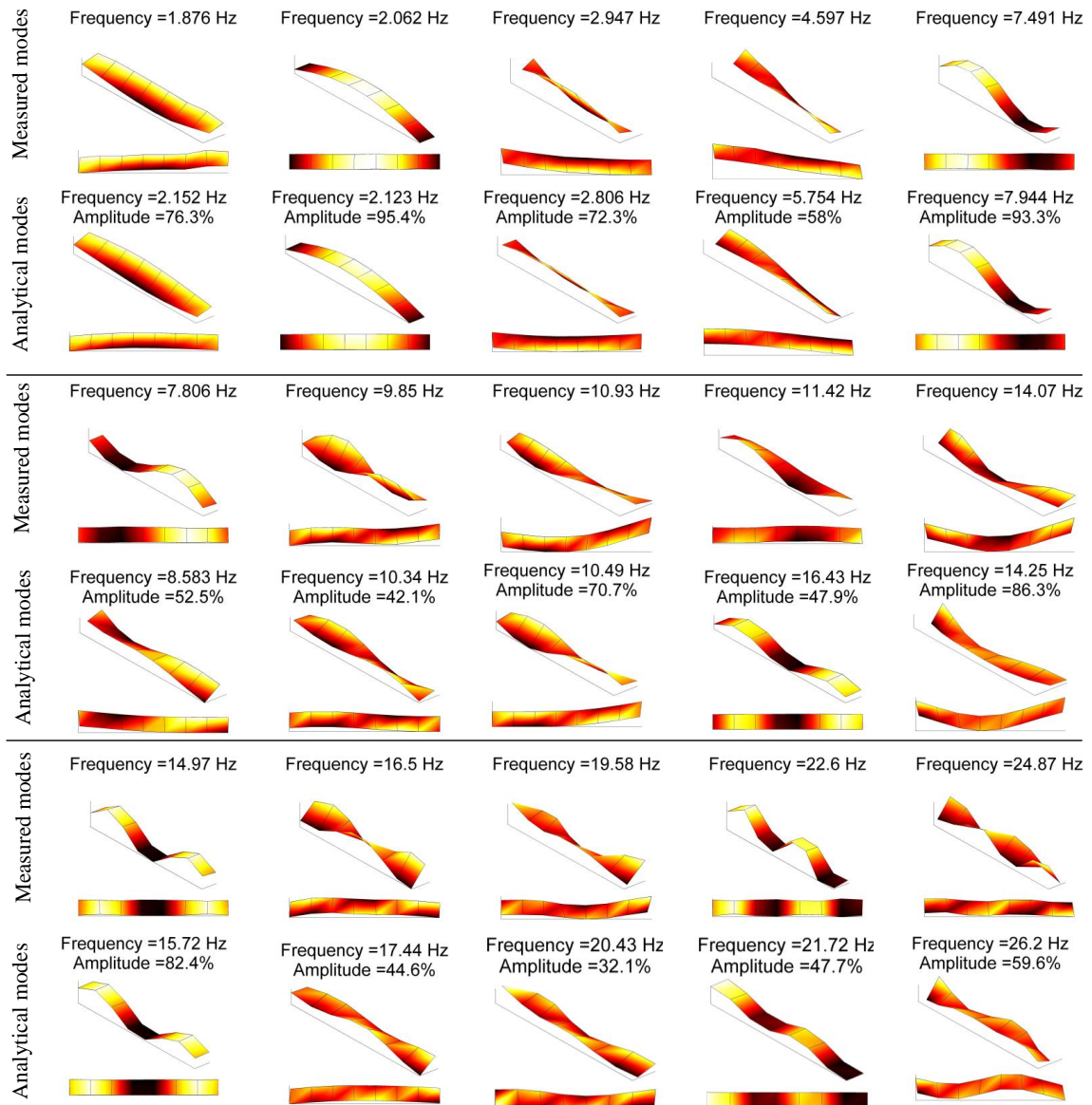


FIGURE 4.8: Comparison of modal parameters from the idealized finite element model to experimental estimates

## 4.2 Structural Identification for Model Calibration

### 4.2.1 Parameterization of the Model

Comparison of the modal parameters of the idealized finite element model to the experimental estimates within the prior section revealed generally good correlation.

However, there are several instances where the discrepancy between estimated and measured natural frequencies is very significant and, additionally, where mode shapes exhibit poor correlation to the measurement, as indicated by low MAC values. To minimize these differences and generate an analytical model that is dynamically more consistent with the experimental measurements, structural identification, or finite element model updating, was applied to the model using the experimental modal parameter estimates. This process will be described in this section and was completed through the use of a genetic algorithm to search for globally optimal values for uncertain parameters within the model.

While the genetic algorithm ultimately determined the parameter assignments that would produce modal parameter estimates closest to the experimental results, it was first necessary to determine the subset of uncertain parameters in the model to be updated. This is a critical step in the structural identification process since including too few parameters in the calibration would limit the improvement in the model calibration, while the genetic algorithm would have difficulty arriving at the globally optimal solution if too many parameters were included as the combinations of parameters in the search space would be too large. Furthermore, the chosen parameters needed to be significant enough to effectively change the modal parameters of the finite element model on which the model correlation is based. Lastly, it was further necessary that the selected parameters were linear properties of the finite element model. This last constraint allows for the ease of constructing parameter specific stiffness and mass matrices using superposition of linearly scaled matrix contributions rather than assembling the matrices from individual elements for each individual analysis.

The parameters were selected based off of differences observed between eigenanalysis of the idealized finite element model and the experimental modal parameter estimates. It was observed that the idealized model appeared stiffer than the response exhibited in the experimental estimates and it particularly exhibited less relative lateral motion than was observed in the experimental mode shapes. The selected parameters were therefore chosen for the reasons that they should theoretically affect the stiffness and bending properties of the model. As will be explained later, a quantitative basis of ranking potential uncertain parameters by evaluating the effects produced through the adjustment of individual parameters on the modal parameters of the model was used to ensure selection of the most significant set of uncertain parameters.

It was determined that parameters within the deck should be updated, as the deck is an integral component of the model and influences bending in both the vertical and lateral directions. The actual bending properties of the deck were not known, as neither the steel decking nor the reinforcement within the concrete slab was included in the as-built plans used when modeling the structure. Therefore, the uncertainty in these parameters was addressed through application of property modifiers applied to the major axis and minor axis flexural stiffness of the deck area elements.

Many of the link elements used throughout the model were also selected as uncertain parameters in the structural identification routine. With the exception of the link elements used to model composite action between the concrete deck slab and the diaphragms, the remaining link elements are associated with mechanisms that significantly affect the torsional properties of the span, the interaction between ad-

jacent spans, and the effect of boundary conditions on each span. Since both the natural frequencies and the mode shapes are sensitive to such properties and since the link elements in the idealized finite element model approximate the behavior with idealized conditions, the assigned stiffnesses of link elements was favored as potential uncertain parameters in the structural identification routine. The set of uncertain parameters selected included the stiffness of the link elements representing the pin and hanger assemblies, the link elements used to connect the columns to the diaphragms, and the link elements connecting the concrete deck slab to the girder web. However, the stiffness of each link element is specified for six degrees of freedom, represented by three local translational and three local rotational degrees of freedom. Updating each directional stiffness assignment for all link element sections would result in an impractically large set of unknowns. Therefore, only certain degrees of freedom were specified for each link element. In order to determine which of the degrees of freedom would yield the most significant benefit to the model correlation through updating, the sensitivity of the model to changes in the stiffness of each degree of freedom was examined for each link element. This was accomplished by changing each of the degrees of freedom individually and examining the effects on the modal characteristics of the idealized finite element model. This method of ranking the sensitivity of each parameter will be explained later in more detail, as a similar process was completed for each of the uncertain parameters. For the link element representing the pin and hanger assembly, the axial stiffness and the shear stiffness of the hanger in the direction parallel to the longitudinal direction of the concrete slab were selected as uncertain parameters. For the link element connecting the end diaphragms of

TABLE 7: Global coordinate degree of freedom assignments for the link elements used in model updating

Idealized finite element model joint assignments						
Idealized link element	$U_x$	$U_y$	$U_z$	$R_x$	$R_y$	$R_z$
Pin and hanger	Fixed	Fixed	Fixed	Free	Fixed	Free
Diaphragm to column	Fixed	Fixed	Fixed	Fixed	Free	Free
Bridge deck to girder	Fixed	Fixed	Fixed	Free	Free	Free
Field calibrated finite element model joint assignments						
Updated link element	$U_x$	$U_y$	$U_z$	$R_x$	$R_y$	$R_z$
Pin and hanger	Updated	Fixed	Updated	Free	Fixed	Free
Diaphragm to column	Fixed	Updated	Fixed	Updated	Free	Free
Bridge deck to girder	Fixed	Updated	Fixed	Free	Free	Free

each span to the supporting columns, the shear stiffness of the element in the lateral direction and the rotational stiffness about the axis longitudinal to the bridge deck were selected. These parameters significantly affect the relative lateral and torsional motion at the column supports. Since several experimental mode shape estimates exhibited relatively large lateral and torsional motion at the end of the instrumented span supported by a column, relative to the idealized finite element model, these parameters were deemed necessary for improved model correlation. Lastly, the axial stiffness of the link element connecting the bridge deck to the girder web was selected for updating. The degree of freedom assignments for each link element in global coordinates are summarized in Table 7, which presents the assignments used in the idealized model as well as those adopted in the field calibrated model.

As in static structural analysis, the dynamic properties of a finite element model are often highly sensitive to the boundary conditions in the model (Živanović et al., 2007). Consequently, the boundary conditions associated with the rocker bearings at the abutments were included in the structural identification routine. Within the idealized

finite element model, these boundary conditions had been specified as idealized pin supports. To model the rocker bearing with partial translational fixity in the direction of rocking, the restraint on this degree of freedom was removed for updating and was replaced by a linear elastic spring element. The stiffness assignment of this spring was included in the set of uncertain parameters. The final uncertain parameter selected for the structural identification routine was the mass of the highway sign attached to one of the I-girders, since this asymmetric added mass has the potential to significantly affect the symmetry of the mode shapes and was assigned by estimation in the idealized finite element model.

To limit the size of the search space over the uncertain parameters and limit the solution to reasonable parameter assignments, upper and lower bounds were established for each parameter. For the link element and boundary condition stiffness assignments, the desired bounds were associated with the full range between the fully fixed and friction free conditions. However, practical upper bounds were established for these parameters since at some point increased stiffness would no longer have any significant effect on the modal parameters of the model. This is similarly true for decreased stiffness assignments associated with the lower bounds. Therefore, optimal upper and lower bounds were determined by changing each parameter assignment individually and observing the changes in natural frequency estimates. The upper and lower bounds of these parameters were selected as the values at which a change in the parameter assignments no longer affected the first ten natural frequencies. For the total mass of the supported sign and the property modifiers associated with the bending stiffness of the deck, lower and upper bounds were established by engineering

TABLE 8: Sensitivity analysis of the uncertain parameter for the column link stiffness

Mode number	Lower bound result (Hz)	Upper bound result (Hz)	% difference
1	0.976	2.123	117.520
2	1.529	2.145	40.288
3	2.120	2.249	6.085
4	2.244	2.508	11.765
5	2.347	2.797	19.173
6	2.871	3.065	6.757
7	3.053	3.530	15.624
8	3.256	3.680	13.022
9	3.621	3.990	10.191
10	4.034	5.287	31.061
		Sensitivity	27.149

judgment.

To quantify the relative impact of each uncertain parameter on the dynamic properties of the model, a sensitivity analysis was performed over the bounds of the parameter assignments. For this sensitivity analysis, the first ten natural frequencies of the finite element model were calculated with each individual parameter assigned to its lower and then upper bound limit. The percentage difference between each natural frequency calculated when the parameter was set equal to the lower bound and to the upper bound was then calculated. A single index used to quantify the relative impact of each uncertain parameter on the dynamic properties of the model was then established using the average absolute percentage difference over the first ten natural frequencies. This calculation is illustrated in Table 8 for the parameter associated with the rotational stiffness of the link element connecting end diaphragms to the supporting columns. A summary of the final set of uncertain parameters included in the structural identification routine is presented in Table 9, which presents

TABLE 9: Summary of uncertain parameters included in the structural identification routine

Uncertain parameter	Idealized value	$\underline{\theta}$	$\bar{\theta}$	Sensitivity
Pin and hanger shear stiffness (kN/m)	Fixed	100	100000	70.8
Column link rotational stiffness (kN-m/Rad)	Fixed	1000	1000000	27.1
Pin and hanger axial stiffness (kN/m)	Fixed	1000	1000000	24.6
Column link shear stiffness (kN/m)	Fixed	1000	1000000	18.8
Deck and girder link shear stiffness (kN/m)	Fixed	1000	1000000	12.9
Rocker bearing spring stiffness (kN/m)	Free	1000	1000000	11.2
Mass of highway sign (kg)	250	0	500	3.5
Deck bending modifier M22	1	0.5	2.5	0.6
Deck bending modifier M11	1	0.5	2.5	0.4

the value associated with the idealized finite element model, the lower bound ( $\underline{\theta}$ ), the upper bound ( $\bar{\theta}$ ), and the sensitivity computed for each parameter. The parameters are arranged from most sensitive to least sensitive, according to the simple index associated with only the natural frequencies of the model.

#### 4.2.2 Global Optimization Using Genetic Algorithm

The genetic algorithm requires assembly and analysis of a large number of models with unique combinations of uncertain parameter assignments. The values populating these sets of uncertain parameter assignments were initially selected at random from within their respective upper and lower bounds. These sets could be referred to as the individuals of the genetic algorithm, which together form a population. To converge

on an optimal solution, the genetic algorithm requires the evaluation of a large number of populations, and for each individual within the population the genetic algorithm requires the estimation of natural frequencies and mode shapes of the specific model using the assembled mass and stiffness matrices. To efficiently allow for assembly of these models with any given set of parameter assignments, the individual models were assembled through superposition of linear mass and stiffness matrix contributions normalized to the uncertain parameters. This is demonstrated in Equations 10 and 11, which show changes in the stiffness and mass matrices incorporated into the initial, baseline matrices for each parameter.

$$K = K_{Baseline} + \Delta K_1\theta_1 + \Delta K_2\theta_2 + \Delta K_3\theta_3 + \dots\Delta K_N\theta_N \quad (10)$$

$$M = M_{Baseline} + \Delta M_1\theta_1 + \Delta M_2\theta_2 + \Delta M_3\theta_3 + \dots\Delta M_N\theta_N \quad (11)$$

$K_{Baseline}$  and  $M_{Baseline}$  are the stiffness and mass matrices of the model with lower bound parameter assignments and  $\Delta K_i$  and  $\Delta M_i$  are the normalized changes in the stiffness and mass matrices of the model associated with a unit change in parameter  $\theta_i$ . The decomposition and superposition of the stiffness and mass matrices allowed for the reconstruction of the matrices by any combination of linear parameters. Implementation of this technique required the initial assembly of the stiffness and mass matrices of the baseline idealized model and of the model featuring each individual uncertain parameter. The assembly of the matrices for each case of the finite element model was completed through the use of SAP2000 in conjunction with MATLAB through the open application programming interface. The script used to complete

this assembly is presented in Appendix A.

Following development of the baseline and parameter contribution matrices, the genetic algorithm was implemented within the MATLAB computing environment using the global optimization toolbox. Global optimization seeks to find the optimal combination of assignments for uncertain parameters in the model to achieve the best correlation with the experimental estimates according to a single objective function. Consequently, differences between each of the predicted natural frequencies and mode shapes and the experimental estimates had to be distilled into a single function suitable for minimization. In structural identification of civil infrastructure, this is typically done by a weighted sum of eigenvalue residuals and eigenvector residuals (Zárate and Caicedo, 2008). The objective function used for this analysis is

$$J(\theta) = \sum_{i=1}^{10} \alpha_i \left| \frac{f_i^a - f_i^e}{f_i^e} \right| + \beta_i (1 - MAC(\phi_i^e, \phi_i^a)) \quad (12)$$

where  $f_i^a$  and  $f_i^e$  are the undamped natural frequency estimates obtained from the finite element model and the experimental analysis, respectively, for mode  $i$  after mode pairing and  $MAC(\phi_i^e, \phi_i^a)$  is the modal assurance criterion value computed for this same pair of modes. Weighting factors,  $\alpha_i$  and  $\beta_i$ , are applied to express preference for minimizing the residuals associated with specific modes. In this study, the weighting factors were prescribed as

$$\alpha_i = \frac{1}{f_i^e}$$

$$\beta_i = \frac{1}{2f_i^e}$$

which weights the lower frequency modes with more significance than the higher

frequency modes and weights the eigenvalue residuals with twice the significance of the eigenvector residuals. The rationale behind weighting the lowest frequency modes with more significance is that these modes were within the bandwidth excited by pedestrian loading. A better correlation was desired for these lowest frequency modes to ensure the fidelity of subsequent time history analysis of pedestrian loadings performed with the field calibrated model. The greater weighting applied to the eigenvalue residuals expresses greater confidence in these experimental estimates than the corresponding eigenvectors (Živanović et al., 2007).

The first ten modal parameter estimates from the experimentally measured data were considered in the calculation of the objective value, which compared the set of experimentally measured modes to the ten most similar modal parameters from the finite element model. The number of experimental modal parameter estimates considered was limited to ten for the purpose of obtaining the optimal match for the lower frequency modes. Including additional modes in the objective function would have resulted in effectively weighting the lower frequency modes with less relative significance in the objective function and may have been detrimental to the quality of the correlation achieved for the lower frequency modes, which are of greater importance when examining pedestrian loading models.

A particular challenge in structural identification is the automated correct pairing of analytical modes with the corresponding experimental modes to compute the correlations in the objective function (Friswell and Mottershead, 1995). Often, the modal assurance criterion alone is used to pair modes. However, the discrepancy between the limited measurement of a single span and the finite element model of

the full structure required an additional strategy to encourage correct mode pairing. The previously discussed method of calculating the eigenvector amplitudes of the analytical modal estimates was again used to characterize the mode shape estimates of the field calibrated finite element model. Furthermore, an additional step to ensure that the correct modes were automatically paired during the optimization process leveraged natural frequency differences. For every analytical modal parameter estimate considered in the comparison, the percent difference between the experimental and analytical natural frequency was first considered. For cases where the percentage error in the undamped natural frequency was greater than 30 percent, the MAC value associated with the potential mode pairing was penalized by applying a scale factor of 0.1.

The objective values of the entire population are used to form consecutive populations, which, due to the nature of genetic algorithm, typically reflected improved objective values. For this research, the genetic algorithm was performed with a population size of 5,000 individuals and a stopping criteria of 25 populations. This resulted in a total of 125,000 analyses per optimization run. The number of elite individuals for each population was set to 25, and the remaining individuals in each population were produced using a 60 percent crossover rate and 40 percent mutation rate. These population settings consistently resulted in convergence of the solution prior to the completion of the 25th population.

In addition to the uncertain parameters subject to updating by genetic algorithm, there were two additional uncertain parameters in the model that were calibrated indirectly due to the nature of their effects on the model. These two parameters were

the thickness and unit weight of the concrete deck, which were unknown due to deck replacement. However, both of these parameters exhibit significant influence on the modal parameters of the finite element model. Including the thickness of the area elements used to model the deck as an uncertain parameter using the efficient approach implemented to reconstruct the mass and stiffness matrices by linear superposition is not possible since the stiffness of the area elements is not proportional to thickness. Although the mass of the deck could be treated as a linear parameter, requiring the genetic algorithm to optimize significant stiffness and mass parameters concurrently leads to uniqueness issues in the inverse eigenvalue problem (Kenigsbuch and Halevi, 1998). Consequently, the optimal combination of deck thickness and unit weight assignments was determined by applying the genetic algorithm to multiple models, with each model prescribed with a different combination of stationary deck thickness and unit weight assignments. The combination associated with the lowest objective value after application of the genetic algorithm was selected as the field calibrated model featuring the optimal combination of deck unit weight and thickness. The values of deck thickness and unit weight to be used in the models were determined based on common values for these properties and on observations made during field experimentation. Different unit weights were paired with deck thicknesses of either 10.16 cm, 12.70 cm, or 15.24 cm (4 in, 5 in, or 6 in). For each deck thickness, the unit weight was adaptively adjusted by  $24.5 \text{ kg/m}^3$  ( $10 \text{ lb/ft}^3$ ) intervals around  $196.01 \text{ kg/m}^3$  ( $120 \text{ lb/ft}^3$ ) until the minimum in the objective function was observed. Figure 4.9 presents the results obtained for all combinations analyzed, ordered by deck thickness. As can be seen in the results, the optimization is more sensitive to the unit

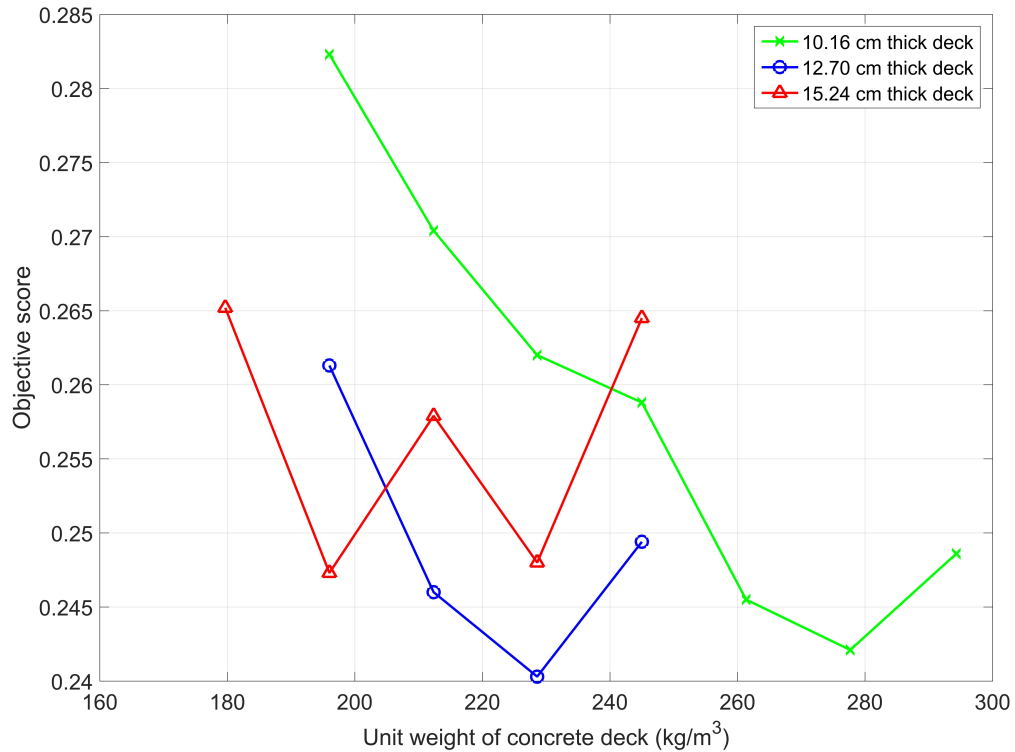


FIGURE 4.9: Minimum objective scores obtained when varying deck unit weight and thickness

weight assigned than the deck thickness prescribed. The minimum objective function obtained across the combinations was associated with a deck thickness of 12.70 cm (5 in) and unit weight of 228.68 kg/m<sup>3</sup> (150 lb/ft<sup>3</sup>). This combination of deck unit weight and thickness, with the associated uncertain parameter assignments identified for the combination by the genetic algorithm, were used for the final field calibrated model. Table 10 presents a comparison of the identified parameter assignments to the parameter assignments in the idealized model.

#### 4.2.3 Comparison of Field Calibrated Model to Experimental Data

Following identification of the set of parameter assignments yielding the lowest objective score, the finite element model was updated to reflect the optimized parameter

TABLE 10: Comparison of idealized and updated finite element model parameters

Uncertain parameter	Idealized value	$\underline{\theta}$	Updated value	$\bar{\theta}$
Pin and hanger shear stiffness (kN/m)	Fixed	100	27500	100000
Column link rotational stiffness (kN-m/Rad)	Fixed	1000	795000	1000000
Pin and hanger axial stiffness (kN/m)	Fixed	1000	228000	1000000
Column link shear stiffness (kN/m)	Fixed	1000	104000	1000000
Deck and girder link shear stiffness (kN/m)	Fixed	1000	22000	1000000
Rocker bearing spring stiffness (kN/m)	Free	1000	744000	1000000
Mass of highway sign (kg)	250	0	411	500
Deck bending modifier M22	1	0.5	2.26	2.5
Deck bending modifier M11	1	0.5	2.26	2.5

assignments. After updating the model, the modal parameters of the finite element model were compared to the modal parameter estimates obtained through experimental testing. A comparison of the natural frequencies and MAC values is presented in Table 11. It should be noted that, while the objective function minimized by the genetic algorithm included only the modal parameter estimates from the first ten modes, the table presents the correlation for all fifteen of the experimental modal parameter estimates. This extended comparison is provided to support the plausibility of the updated model. In general, a strong correlation between natural frequency estimates and generally good correlation in the mode shape estimates was achieved. It can be seen that, while differences still exist between the experimental and analytical data, the MAC values and percentage errors in estimated undamped natural

TABLE 11: Comparison of modal parameters obtained through experimentation and predicted by the field calibrated finite element model

Mode	$f_{exp}$ (Hz)	Field calibrated			Improvement	
		$f_{FEA}$ (Hz)	% Error	MAC	$\Delta\%$ Error	$\Delta$ MAC
1	1.876	1.994	6.272	0.978	-8.432	0.040
2	2.062	2.062	0	0.994	-2.953	0.006
3	2.947	2.906	-1.399	0.690	-3.407	0.079
4	4.597	5.198	13.073	0.877	-12.089	0.085
5	7.491	7.254	-3.160	0.977	-2.896	-0.019
6	7.806	7.724	-1.045	0.870	-8.918	0.678
7	9.850	9.450	-4.063	0.985	-0.868	0.437
8	10.933	9.308	-14.861	0.867	10.810	0.143
9	11.420	14.657	28.335	0.316	-15.566	0.003
10	14.070	14.478	2.890	0.895	1.618	0.061
11	14.971	14.916	-0.368	0.686	-4.618	-0.277
12	16.499	16.458	-0.247	0.676	-5.428	-0.024
13	19.577	19.040	-2.747	0.856	-1.603	0.143
14	22.597	22.691	0.416	0.551	-3.472	-0.184
15	24.872	25.208	1.352	0.690	-3.996	0.326
		Average	5.349	0.794	-4.120	0.167

frequencies are significantly improved over the idealized model. This is especially true for the lower frequency modes, which are of greater importance when modeling the response under pedestrian loading. The average improvement in percentage error of natural frequency over the 15 experimentally measured modes is 4.12%, and the average improvement in the MAC correlation is 0.167. Graphical representation of the mode shapes predicted by the field calibrated finite element model are presented in Figure 4.10. As in the previous comparison of the modal parameters from the idealized model, the experimental mode shape estimates are included for comparison, and the mode shapes from the finite element model are plotted only at the corresponding sensor locations to facilitate a direct comparison.

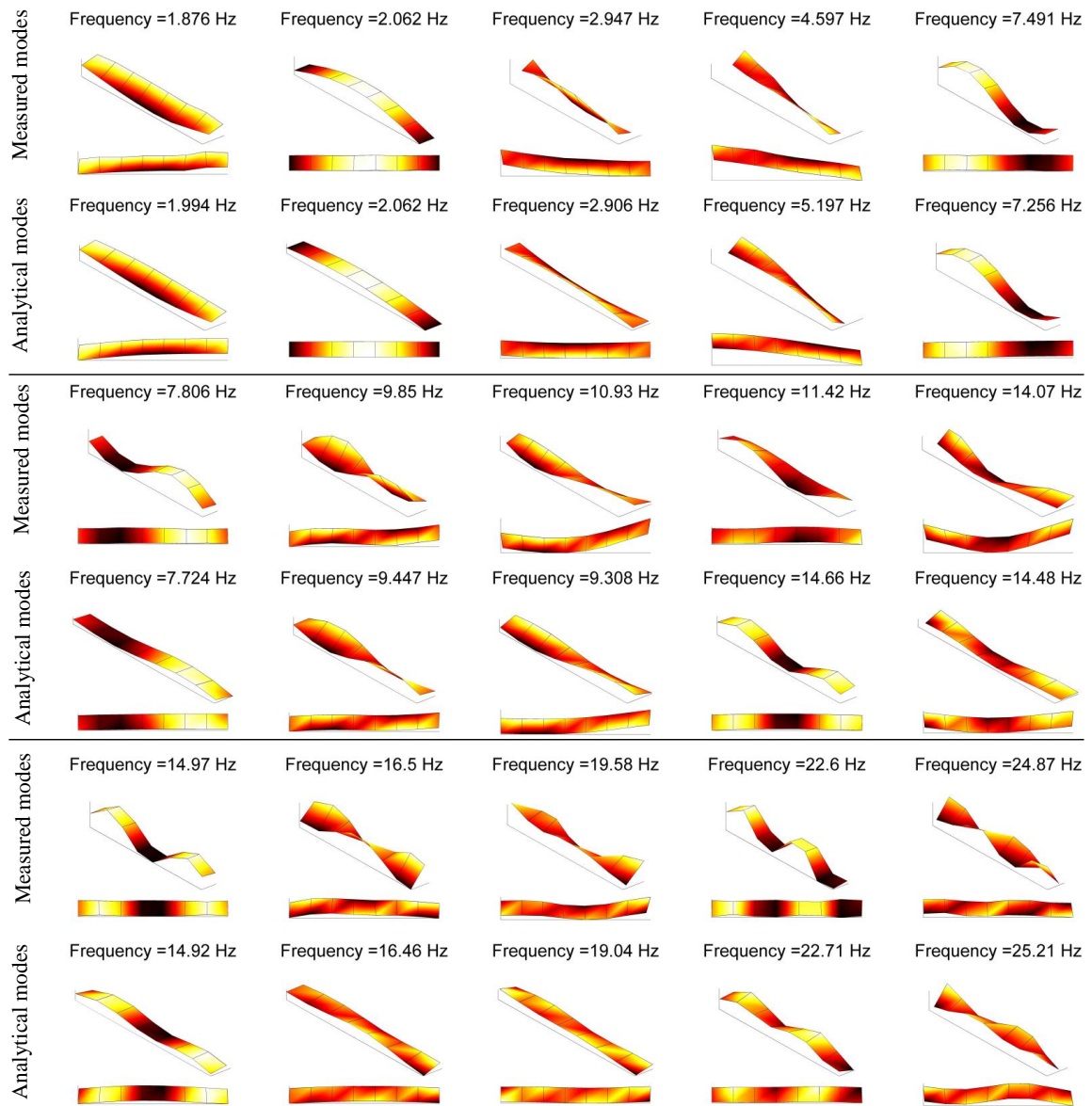


FIGURE 4.10: Comparison of modal parameters from field calibrated finite element model to experimental estimates

## CHAPTER 5: COMPARISON OF PEDESTRIAN FOOTFALL MODELS TO EXPERIMENTAL DATA

In this chapter, the analytical evaluation of various footfall loading models through finite element analysis is described with comparison to experimental measurements obtained from the case study structure. The pedestrian footfall models presented in three different standards are applied to the field calibrated finite element model of the pedestrian bridge to predict acceleration time histories at the instrumented locations of the span. The results obtained through application of each footfall model are compared to the experimental results to assess the relative predictive fidelity of each approach. Following the comparison of the results obtained using the code recommended standards, optimization techniques are employed to calibrate parameters in each model to improve the correlations to the experimentally measured response. Based on the results obtained through the recommended and optimized pedestrian footfall models, modifications to the evaluated loading models are suggested.

### 5.1 Modal Superposition Time History Simulation of Pedestrian Excitation

The finite element model used for all subsequent analysis is the parametrized model presented in Chapter 4 with the field calibrated parameter assignments summarized in Table 10. The modal parameters of this model were presented in Figure 4.10, and the model correlation with the modal parameter estimates obtained through operational modal analysis are summarized in Table 11. To prescribe damping to the finite

element model, the relative damping factors associated with all of the experimentally estimated modes were assigned using the pairs of natural frequency and damping ratios. By these assignments, the modal responses associated with the modes that featured an experimental comparison are prescribed the same relative damping as experimentally estimated for that mode. For the remaining modes, the relative damping is interpolated between the assigned pairs of natural frequencies and associated damping ratios. The three pedestrian footfall models selected for evaluation using the field calibrated finite element model were those recommended in AISC Design Guide 11 (Murray et al., 2003), ISO 10137 (ISO, 2007), and the BSI UK National Annex to Eurocode 1 (BSI, 2008).

To perform time history analysis, pedestrian footfall loading models needed to be applied as forces varying with both time and location to simulate the motion of a pedestrian across the bridge span. This required the preliminary step of establishing the forcing functions associated with each node in the model loaded during the pedestrian motion. Since the determination of these functions depended on several parameters, such as pacing frequency and both amplitude and phase coefficients in each footfall model, a MATLAB script was developed to construct forcing functions for each node and assign them to the field calibrated SAP2000 model using the open application programming interface (API). This script is provided in Appendix B.

The forcing functions for each model could be imported into SAP2000 as user specified time history functions. Imported forcing functions were matched to nodes generated in the model to correspond with footfall locations based on pacing frequency and stride length. Since the locations of these nodes that correspond to footfall

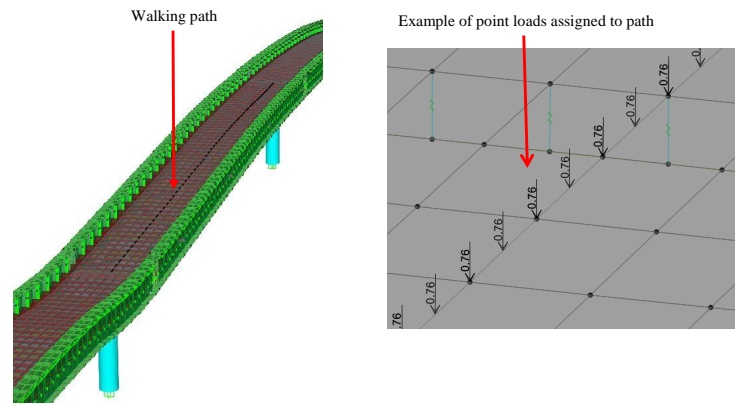


FIGURE 5.1: SAP2000 model displaying frame elements used to prescribe pedestrian loading

locations were not coincident with nodes of the area elements representing the deck surface, frame elements with insignificant stiffness were introduced to the model to efficiently distribute the loads from the footfall nodes to the area elements of the bridge deck. These frame elements were located at the center of the bridge deck relative to the twin I-girders and along the span of the deck to define the path along which the pedestrian footfall loads could be applied. This is demonstrated in Figure 5.1. It should be noted that due to the minimal cross-sectional dimensions of these members, the frame elements did not significantly affect the stiffness or mass of the model nor the modal parameters. Since the spacing of the nodes along the frame elements that would receive footfall load time histories could vary with each time history function, the assignment of these nodal locations and associated functions was completed through MATLAB. The locations of the nodes were determined based on the spacing of a stride length of 1 m (3.3 ft) at a specified pacing frequency.

For each model, time history analyses were conducted using modal superposition

to generate analytical predictions of the acceleration time histories at each of the instrumented locations to permit comparison with the experimentally measured responses. The pedestrian footfall models that were evaluated followed the functional forms presented in Chapter 2, with each forcing function featuring a unique set of variables associated with the functional form of the model. For each model, the variable assignments recommended by each respective standard were applied to generate the time histories of the footfall loading function. Comparison of the predicted responses for each model relative to the experimental measurement are presented in the following section. Subsequently, an optimization analysis is presented to determine calibrated variable assignments required to obtain optimal correlation with the field experiment.

## 5.2 Performance Evaluation of Standardized Pedestrian Excitation Models

The predictive fidelity of each standardized pedestrian footfall model was assessed using comparisons to experimental measurements of accelerations induced by controlled passage of a single pedestrian. For these comparisons, the experimental load cases examined in this chapter were limited to passage of a single pedestrian from the western end of the instrumented span to the eastern end.

In order to facilitate the comparison between experimental and analytical data, several steps were taken during preprocessing of the measured data. To permit direct comparison of the acceleration time histories produced by the finite element model to the experimental data, a strategy was developed to align the two sequences of data. Since the time at which the pedestrian load started in the experimental test

could not be precisely determined from the recorded data, this strategy accounts for time shifts in the experimental data relative to the predictions from the finite element model. Specifically, an algorithm was produced to determine the optimal time shift to apply to a time window of the experimental test data. First, to reduce the measurement time window to the duration of response with strong signal-to-noise ratio, only 14 seconds were used from each recorded time history. This time window included six seconds prior to the instant of peak recorded accelerations and eight seconds after this instant. Then, incremental time shifts were introduced to this windowed data and the mean squared error of the corresponding analytical data over the same time period was calculated. The optimal time shift was determined as the one that produced the lowest mean squared error. Time aligning of the data allowed for direct comparison of the experimental and analytical time histories overlaid on the same axis. In addition to visual comparison, the differences in the predicted and measured accelerations could also be numerically quantified. This quantification of the model correlation was later necessary to construct an objective function for optimizing parametric assignments associated with each pedestrian footfall model.

### 5.3 Evaluation of Single Pedestrian Loading Models Using Recommended Coefficients

Each loading model was initially evaluated using the parameter assignments recommended by each respective standard. The results obtained by modal superposition time history analysis incorporating the first 15 modes of the field calibrated finite element model are presented in this section, along with a comparison of these results to

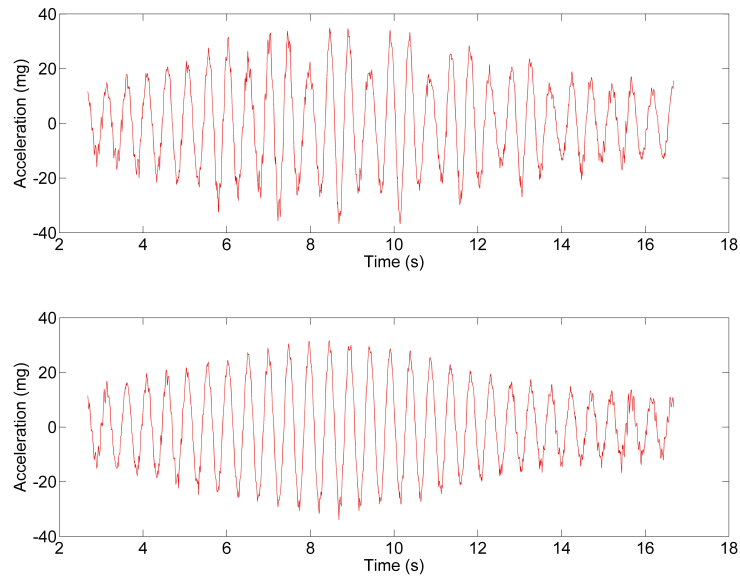


FIGURE 5.2: Peak amplitude acceleration time histories of the experimental load cases used for comparison to the predicted response

experimental data for each loading model. For each analysis, the modal superposition time history analysis was conducted with a time step of 0.008 seconds to coincide with the sampling rate used in the experimental test program.

Two sets of experimental acceleration time histories were used for comparison to the predicted response of the model. Both time histories are representative of the loading case of one pedestrian crossing the bridge and are generally consistent with one another. The peak accelerations were 34.858 mg and 31.687 mg, respectively, for each case, which results in an average peak acceleration of 33.272 mg. The peak accelerations were observed at the location of sensor 10, and representative time history plots of the accelerations observed at sensor 10 are presented in Figure 5.2.

### 5.3.1 American Institute of Steel Construction (AISC) Model

The loading model presented in AISC Design Guide 11 (Murray et al., 2003) was evaluated first. This pedestrian footfall model takes the form:

$$F_n(t) = P \left[ 1 + \sum_{n=1}^4 \alpha_n \cos(2\pi n f_s t + \psi_n) \right] \quad (13)$$

with the recommended amplitude coefficients presented in Table 12. The pacing frequency of the forcing function was taken to be 2.062 Hz in order to match the undamped natural frequency of the first vertical bending mode of the instrumented bridge span, as recommended by the standard. The weight of the pedestrian was set as 0.76 kN (170 lb) in order to correspond with the weight of the pedestrian providing the excitation during the experimental testing. A comparison of the acceleration response predicted by the finite element model to the experimental data is displayed in Figure 5.3. The response shown is associated with the accelerations in the gravitational direction for the location of sensor 10. The peak acceleration observed in the predicted results was 11.262 mg at the location of sensor 9. Consequently, the AISC pedestrian footfall model underestimates the peak acceleration by 66.2% when the recommended parameter assignments are used. It should be noted that sensor 9 is located at the same longitudinal location in the span as sensor 10, where the peak measured acceleration was recorded, but on the opposite side of the bridge deck.

### 5.3.2 International Standards Organization (ISO) Model

The pedestrian acceleration response analysis was repeated using the loading model presented in ISO 10137 (ISO, 2007). As indicated in Chapter 2, this forcing function

TABLE 12: AISC recommended dynamic coefficients for one pedestrian walking (Murray et al., 2003)

Harmonic	$\alpha$	$\psi$
1	0.5	0
2	0.2	$\pi/2$
3	0.1	$\pi/2$
4	0.05	$\pi/2$

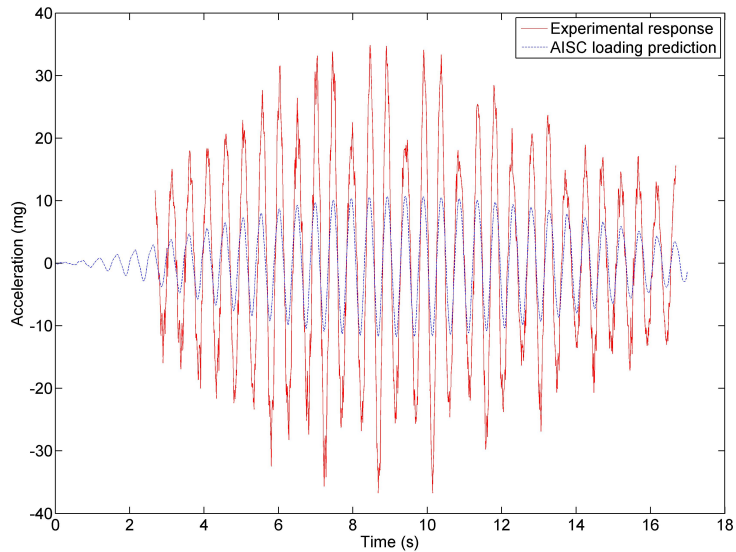


FIGURE 5.3: Experimental bridge deck response compared to AISC loading model predicted response

is nearly identical to the model presented in Murray et al (2003) and takes the form:

$$F_P(t) = G \left[ 1 + \sum_{i=1}^{i=5} \alpha \sin(2\pi i f t + \psi_i) \right] \quad (14)$$

However, the model varies in the recommended coefficient values and the number of harmonics considered. The dynamic coefficients recommended by ISO for the case of one person walking are shown in Table 13. A pacing frequency of 2.062 Hz and pedestrian weight of 0.76 kN were again used in the simulation for consistency. The predicted acceleration response is presented in Figure 5.4 with comparison to the

TABLE 13: ISO recommended coefficients for one pedestrian walking (ISO, 2007)

Harmonic	$\alpha$	$\psi$
1	0.393	0
2	0.1	0
3	0.06	0
4	0.06	0
5	0.06	0

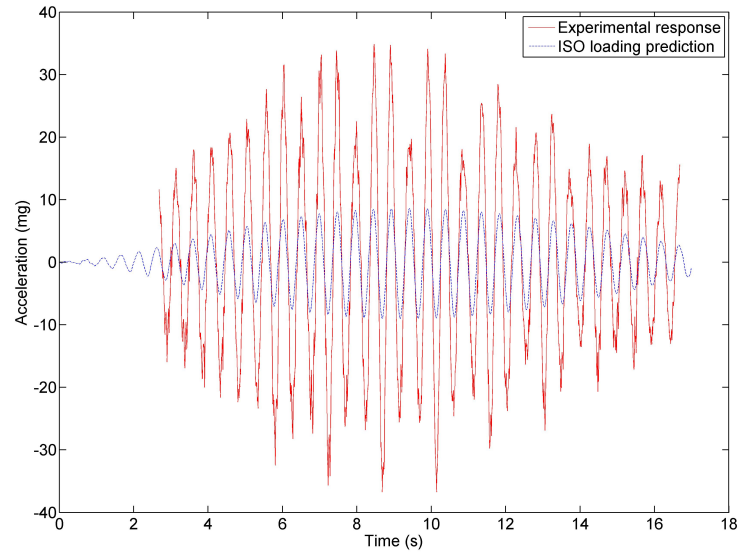


FIGURE 5.4: Experimental bridge deck response compared to ISO loading model predicted response

experimental response. As in the previous case, the response at the location of sensor 10 is presented. The predicted peak acceleration using this model was 9.116 mg, which occurred at the location of sensor 9 and represents an underestimation of 72.6% of the measured peak acceleration during passage of a single pedestrian.

TABLE 14: BSI recommended coefficients for one pedestrian walking (BSI, 2008)

Coefficient	Value
$k(f_v)$	1.0
$\lambda$	1.0

### 5.3.3 British Standards Institute (BSI) Model

Lastly, the response of the finite element model to the footfall model recommended by BSI (2008) was evaluated. This footfall model takes the form:

$$F = F_0 k(f_v) \sqrt{1 + \lambda(N - 1)} \sin(2\pi f_v t) \quad (15)$$

The coefficients recommended in the standard for this model are presented in Table 14. As in the previous analyses, the pacing frequency and pedestrian weight were taken to be 2.062 Hz and 0.76 kN, respectively. A comparison of the acceleration responses at sensor 10 obtained from the modal superposition time history analysis and the experimental measurement is presented in Figure 5.5. The peak acceleration predicted through the model was 23.391 mg, which occurred at sensor 9. While this footfall model compared significantly more favorably to the measured response, this estimate represents an underestimation by 29.7% of the measured peak acceleration during the passage of one pedestrian.

## 5.4 Evaluation of Calibrated Single Pedestrian Excitation Loading Models

### 5.4.1 Optimization of Single Pedestrian Excitation Models

The previous analysis reveals that the standardized pedestrian models with recommended parameter assignments produce predicted responses in the field calibrated finite element model that are significantly different than the experimentally measured

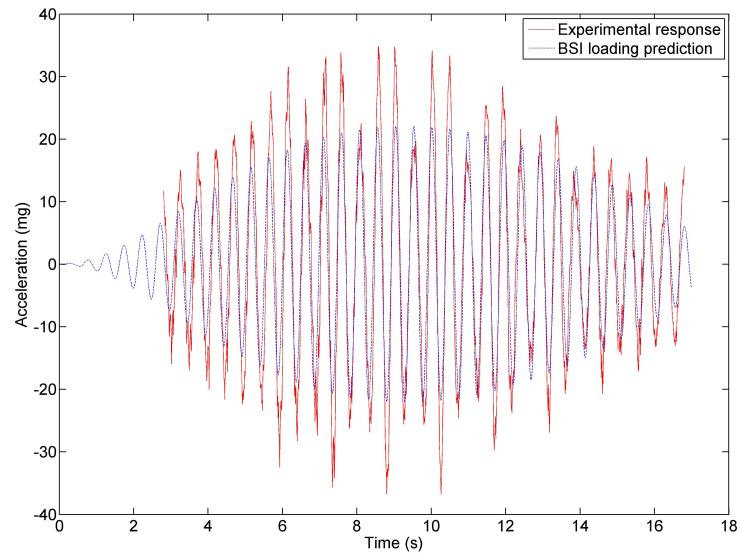


FIGURE 5.5: Experimental bridge deck response compared to BSI loading model predicted response

response of the case study structure. The loading models recommended in AISC Design Guide 11 (Murray et al., 2003) and ISO 10137 (ISO, 2007) significantly underestimated the peak acceleration of the instrumented span, while the loading model recommended by BSI (BSI, 2008) moderately underestimated the peak acceleration. To explore the sensitivity of each pedestrian footfall model to the corresponding set of parameter assignments, an optimization was performed to identify the parameter assignments associated with the greatest correlation between the analytical estimates and the experimental results.

Optimization was necessarily performed independently for each of the three loading models in order to determine the optimal parameter assignments for use within each model. In addition to the amplitude and phase parameters in each model, the forcing frequency used within each loading model was included as an uncertain parameter within the optimization process. This measure was taken to acknowledge that the pre-

dominant step frequency in the experimental test may not have corresponded exactly with the undamped natural frequency of the first vertical bending mode. Therefore, a different excitation frequency would be required to avoid biasing the optimization as a result of accumulated phase errors over the time history due to differences in the excitation frequency. Additionally, a random excitation was introduced to all nodes of the bridge deck in the model to simulate ambient excitations present during testing, such as wind and vehicular traffic beneath the bridge that provided additional, measurable accelerations during the testing. The amplitude of this broadband excitation was included as an uncertain parameter within the optimization scheme. Similar to the structural identification performed in the prior chapter, the calibration of uncertain parameters within each pedestrian footfall model was performed by genetic algorithm using the MATLAB global optimization toolbox.

To facilitate optimization of parameter assignments, an objective function was developed to compare the time windowed analytical predictions and experimental measurements. The objective function was developed simply as the sum of the squares of the prediction error after aligning and time windowing the analytical predictions. This objective function,  $J$ , takes the form:

$$J = \sum_{i=1}^{\#Pts} \sum_{j=6}^{12} (a_{j,i}^{exp} - a_{j,i}^{FEA})^2 \quad (16)$$

where  $i$  indicates the time step,  $j$  indicates the sensor number, and  $a$  is the acceleration. Since there were two sets of experimental acceleration time histories, the sum of the objective function computed over each data set was used to produce an aggregate objective score.

The comparison was completed using the acceleration data measured by sensors 6 through 12, because these sensors correspond to the nodes along the midspan of the bridge where the response amplitude, and consequently the signal-to-noise ratio of the measurement, was the highest. It was found that the sensors closer to the ends of the span were affected by ambient excitation and were therefore less suitable for comparison with the analytical results. Consequently, although an acceleration response was measured for each of the twelve sensors, only the sensors near the midspan were used for the comparison to finite element analysis results. Furthermore, as presented in Chapter 3, the experimentally measured accelerations were subject to coordinate transformations to reorient the measurement directions to the global coordinate frame of the finite element model to permit direct comparison.

The genetic algorithm updating routine applied to the loading models followed a similar method to that used in Chapter 4 to update the finite element model. As both procedures utilized genetic algorithm updating routines, the fundamental methods remained the same concerning the use of individuals forming successive populations through elite survival, crossover, and mutation until converging on a globally optimal solution. However, due to the nature of the dynamic time history analysis using pedestrian loading models, there were significant differences in the routine used to evaluate individuals within each population. As within the modal calibration, the optimization process was performed using a script developed in MATLAB to initialize the optimization problem over the SAP2000 open API interface (Appendix B). However, since the dynamic analysis did not involve changing the stiffness or mass matrices of the model, it was no longer necessary to extract the matrices from the finite element

model. It was, however, necessary to extract the acceleration time histories obtained following modal superposition time history analysis using the parameter assignments for each individual within the population. Therefore, a routine was developed within the API to open the finite element model in SAP2000, assign the prescribed load time histories, run the modal superposition time history analyses, and export the results to MATLAB for post processing. By using modal superposition rather than direct time history analysis, the evaluation of individuals within a population was expedited, as the finite element model needed only to be assembled and eigenanalysis performed only once per generation. All prescribed load cases were assigned to the software for the parameter combinations of each individual in the population prior to the analysis so that an entire population could be evaluated sequentially from the results of the single eigenanalysis. These results were returned to the MATLAB host application as a matrix of acceleration time histories for each individual from which the time shifting, windowing, and objective function calculations could be performed across the set of two experimentally measured time histories. For each optimization run, 25 generations consisting of 200 individuals per generation were used, resulting in a total of 5,000 analyses completed per optimization run to ensure convergence. The populations were developed using an elite count of 10, while the remaining individuals were produced using a 60 percent crossover rate and 40 percent mutation rate.

#### 5.4.2 Evaluation of Field Calibrated AISC Loading Model

The forcing function presented in AISC Design Guide 11 (Murray et al., 2003) contained a total of eight uncertain parameters in addition to the amplitude of random

TABLE 15: Optimization of AISC forcing function: lower bounds, upper bounds, and field calibrated parameters

Variable	Lower boundary	Field calibrated value	Upper bound
$f_s(Hz)$	1.85	2.076	2.3
$\alpha_1$	0.5	1.270	2.0
$\alpha_2$	0.005	0.127	0.2
$\alpha_3$	0.005	0.037	0.2
$\alpha_4$	0.001	0.015	0.1
$\psi_1$	-1.571	-1.533	1.571
$\psi_2$	-1.571	-1.567	1.571
$\psi_3$	-1.571	1.158	1.571
Noise amplitude (N)	0	5.709	100

noise excitation parameter included in the optimization. The uncertain parameters in the pedestrian footfall model included the harmonic amplitude coefficients, phase angles of each harmonic, and pacing frequency. The parameter set was subjected to the previously described genetic algorithm optimization routine to determine the optimal solution.

The identified parameter assignments for optimal model correlation through the developed objective function are presented in Table 15, along with the lower and upper bounds applied to each variable during the optimization. The comparison of acceleration responses at sensor 10 is presented in Figure 5.6, and the peak amplitude of the predicted response was found to be 28.187 mg at sensor 9. This represents an underestimation of 15.0% of the peak measured acceleration, which corresponds to an improvement of 51.2 in the percentage error when compared to the prediction using the recommended parameters. The most significant result of the calibration was the increase in the amplitude of the first harmonic coefficient, which resulted in a significant increase in the amplitude of acceleration in the predicted response.

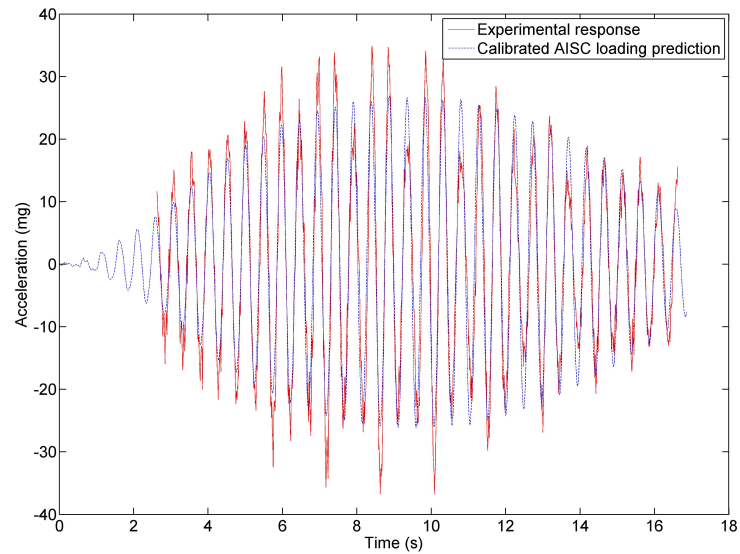


FIGURE 5.6: Experimental acceleration compared to field calibrated AISC loading model predicted acceleration

#### 5.4.3 Evaluation of Calibrated ISO Loading Model

The calibration of the ISO recommended pedestrian footfall model followed a nearly identical process to that followed for the case of the AISC loading model. The only significant difference was the additional harmonic term in the model, which introduced an additional uncertain parameter for both amplitude and phase. The field calibrated parameters identified through the genetic algorithm are displayed in Table 16 with the lower and upper bounds used in the optimization for each parameter. A comparison of the optimized response to the experimental response at the location of sensor 10 is presented in Figure 5.7. The peak acceleration was found to be 28.213 mg at sensor 9. This represents an underestimation of 15.2% of the peak measured acceleration, which corresponds to an improvement of 57.4 in the percentage error when compared to the prediction developed using the recommended parameters. As was the case when

TABLE 16: Optimization of ISO forcing function: lower bounds, upper bounds, and field calibrated parameters

Variable	Lower bound	Field calibrated value	Upper bound
$f_s(Hz)$	1.85	2.076	2.3
$\alpha_1$	0.5	1.264	2.0
$\alpha_2$	0.005	0.103	0.2
$\alpha_3$	0.005	0.0317	0.2
$\alpha_4$	0.005	0.0189	0.2
$\alpha_5$	0.001	0.0557	0.1
$\psi_1$	-1.157	-1.560	1.157
$\psi_2$	-1.157	-1.525	1.157
$\psi_3$	-1.157	0.883	1.157
$\psi_4$	-1.157	-1.4168	1.157
Noise amplitude (N)	0	12.800	0

using the parameters presented in (Murray et al., 2003), the most significant result of the calibration was the increase in the amplitude of the first harmonic coefficient. Furthermore, the field calibrated parameters agreed strongly with those yielded by field calibration of the AISC pedestrian footfall model. This is evidenced by the identical field calibrated pacing frequency and strong correlation between amplitude and phase assignments for the four harmonics present in both models. This similarity is expected due to the similarity of the two pedestrian footfall models.

#### 5.4.4 Evaluation of Field Calibrated BSI Loading Model

The calibration of the BSI pedestrian footfall model followed the same fundamental process of optimization by genetic algorithm that was followed for the previous two loading models. However, the functional form of this pedestrian footfall model differed significantly from the prior two models and resulted in only three uncertain parameters that could be optimized for the case of a single pedestrian loading. These were the pacing frequency, the combined factor  $k(f_v)$ , and the amplitude of the ran-

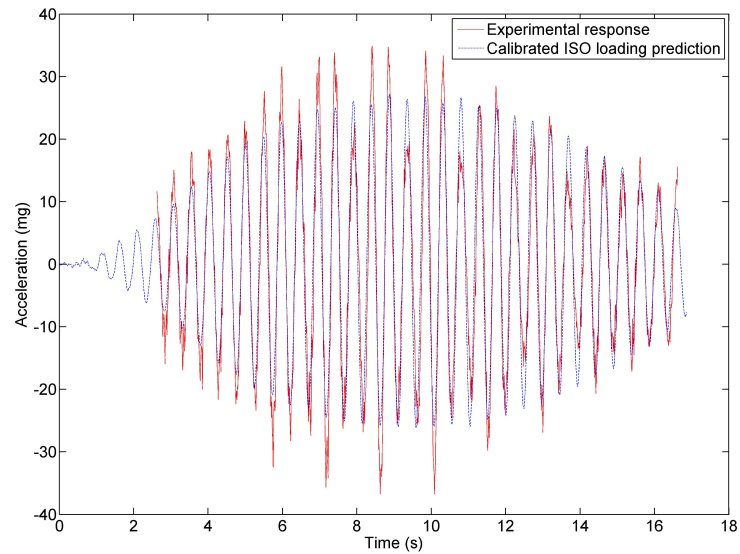


FIGURE 5.7: Experimental acceleration compared to field calibrated ISO loading model predicted acceleration

dom noise. The synchronization factor,  $\lambda$ , has no influence on the model when  $N$  is one, which is the case for the single pedestrian loading, so this parameter is not featured in the optimization.

The optimization resulted in the field calibrated parameter assignments presented in Table 17. The acceleration response produced from application of the field calibrated BSI model is presented in Figure 5.8 with comparison to experimentally measured data at the location of sensor 10. The peak acceleration predicted by the finite element analysis was found to be 28.049 mg, which occurred at sensor 9. This represents an underestimation of 15.7% of the peak measured acceleration, which corresponds to an improvement of 14.0 in the percentage error when compared to the prediction using the recommended parameters. As was the case with the previous two pedestrian footfall models, the pacing frequency parameter assignment again converged to 2.076 Hz.

TABLE 17: Optimization of BSI forcing function: lower bounds, upper bounds, and field calibrated parameters

Variable	Lower bound	Field calibrated value	Updated bound
$f_n(Hz)$	1.85	2.076	2.3
$k(f_v)$	0.8	1.285	1.5
Noise amplitude (N)	0	4.842	100

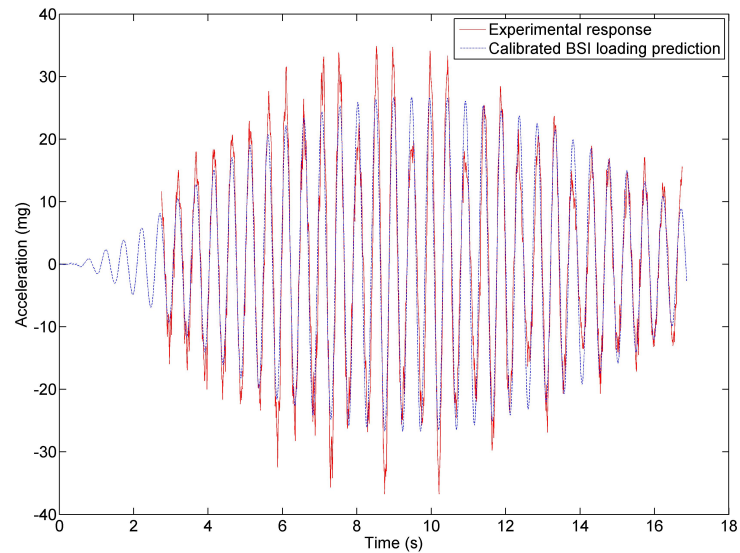


FIGURE 5.8: Experimental acceleration compared to field calibrated BSI loading model predicted acceleration

### 5.5 Summary of Comparisons Before and After Calibration

It can be seen from the evaluations of the finite element predictions that there was a significant discrepancy between the predicted accelerations determined using the standard recommended variables and using the parameter assignments determined through calibration of the AISC and ISO loading functions. Prior to calibration, the accelerations predicted using these loading models correlated poorly with the experimentally measured accelerations. In both cases, the analytical acceleration was significantly underestimated. The BSI model, however, returned a significantly more

accurate prediction of the bridge deck response.

The predictions produced following calibration show a significant improvement in the correlation with the experimental time histories. This is demonstrated in Table 18, which compares the peak responses within the experimental measurements and the analytical results calculated using both the recommended and field calibrated parameter values. However, due to the nature of the experimental response, it was impossible for any of the models to predict a response perfectly matching the data. This can be seen in Figures 5.6, 5.7, and 5.8. There is a noticeable decrease in the amplitude of the experimental response after the peak acceleration has been reached. This could not be duplicated through the finite element model with the given loading functions, which resulted in a more gradual increase and then decrease in acceleration amplitude. Therefore, the analytical response is initially under-predicted and then over-predicted in relation to the amplitude of the time history accelerations in order to obtain the best fit to the experimental data. Overall, the predicted responses of all three loading models returned similar time history responses and peak accelerations, with all three models showing significant improvement in correlation with the experimental response.

Several conclusions can be drawn from the results of the optimization runs. All three optimized models returned similar results, indicating that once the variables were updated, the predicted sinusoidal accelerations correlated almost equally well to the experimental response. Furthermore, optimization in every case indicated that optimal correlation was achieved using a forcing frequency of 2.072 Hz, despite the first vertical mode occurring at 2.062 Hz. This indicates that the pedestrian during

TABLE 18: Peak analytical accelerations before and after calibration compared to the experimentally measured peak acceleration

Load case	Average peak acceleration (mg)	% difference
Experimental	33.272	
Recommended footfall models		
AISC	11.262	-66.152
ISO	9.012	-72.914
BSI	23.391	-29.698
Field calibrated footfall models		
AISC	28.187	-15.283
ISO	28.213	-15.205
BSI	28.049	-15.698

experimental testing could have been walking at a frequency of 2.072 Hz, rather than at the estimated undamped natural frequency of the bridge.

The optimization results also indicate that the source of the initial underestimation seen in all three of the loading models can be attributed to the magnitude of the dynamic coefficient of the first harmonic. This was the most significant update to these forcing functions and resulted in significant increases in the amplitude of the predicted accelerations. This is most noticeable for the AISC and ISO loading functions and is therefore demonstrated in Figure 5.9. The predicted acceleration response shown was calculated using the AISC forcing function featuring all of the recommended variables with the exception of the first dynamic coefficient, which was set to equal the field calibrated value. The randomly generated noise was also omitted for this comparison. It can be seen that increasing the amplitude of the first harmonic alone results in improved correlation with the experimentally measured response that is similar to that achieved with inclusion of all additional harmonics. For the AISC and ISO loading functions, optimization produced minor changes in the higher order

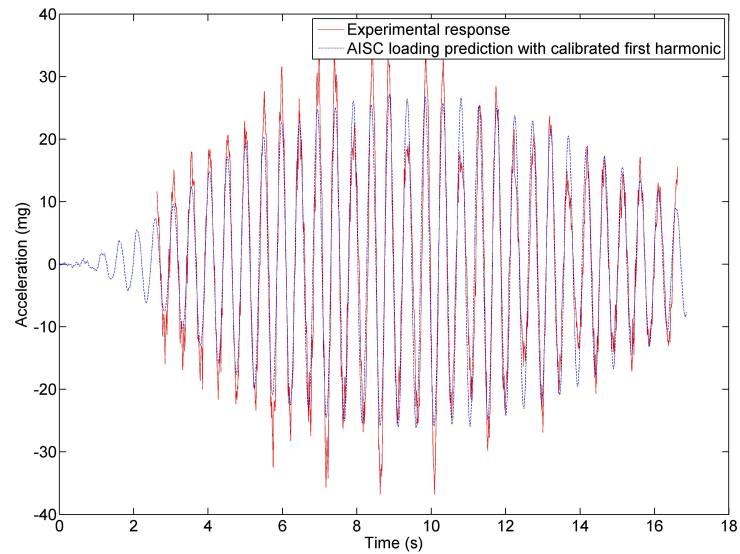


FIGURE 5.9: Experimental acceleration response compared to the AISC predicted response calculated using the AISC recommended forcing function in conjunction with the calibrated value for the first harmonic coefficient

harmonics, associated phase angle, and the amplitude of the random noise excitation. These parameter changes, however, produced less significant changes to the predicted response of the model.

In order to illustrate the similarities between the loading models after calibration, plots of the forcing functions before and after calibration were developed and are presented in Figure 5.10. Calibration in all three cases yielded similar forcing functions with nearly identical peak-to-peak force amplitudes. Furthermore, the insignificant contribution of the higher order harmonics to the calibrated forcing functions is readily apparent. In all cases, the first harmonic dominates the forcing function and suggests that a single harmonic periodic function can be used to predict the response of the structure to single pedestrian excitations for this case study.

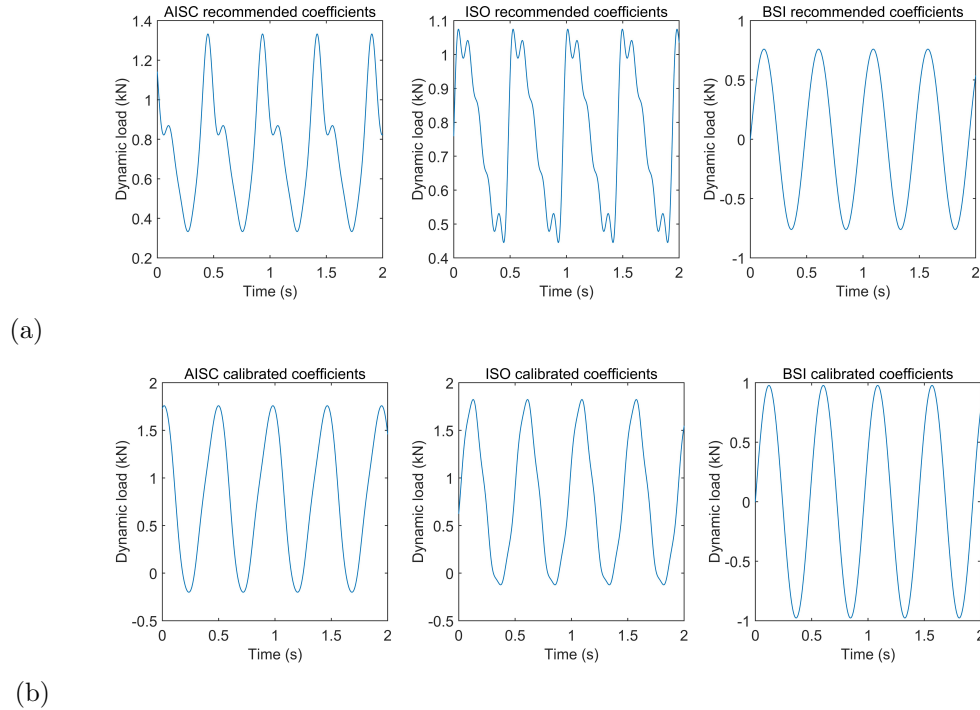


FIGURE 5.10: Single pedestrian footfall loading models using (a) recommended coefficients and (b) calibrated coefficients

## 5.6 Evaluation of Multiple Pedestrian Loading Models

For the previously examined loading models for single pedestrian loading, provisions exist to extend the model to multiple person footfall analysis. These methods introduce an amplification factor to the sinusoidal components of the forcing function in order to approximate both the increased weight of multiple pedestrians and the effect of synchronization of their loading. These methods result in higher amplitude forcing functions that take the same functional form as in the case of a single pedestrian. However, this disagrees with the experimentally measured accelerations induced by the multiple person loading cases in this study, which do not simply reflect increases in the amplitude of the acceleration time histories. This is demonstrated in Figure 5.11, which shows the experimentally measured acceleration time history

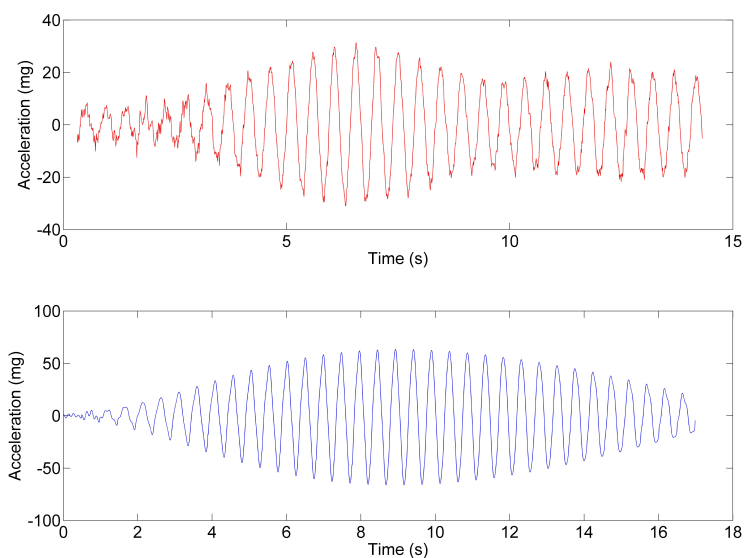


FIGURE 5.11: Experimentally measured response from two pedestrians (top) compared to the analytically predicted response for the same load case

and a typical acceleration time history produced using the ISO recommended forcing function for the loading case of two pedestrians. As can be seen, the envelope of the experimental acceleration time history does not correlate well with the envelope of the predicted acceleration time history. All three of the recommended loading functions predicted similar time history acceleration envelopes, none of which feature a response similar to that observed in the experimental response for the multiple person load case.

The discrepancies in the responses can likely be partially attributed to differences between the analytically pure forms of the pedestrian footfall models and the realities of actual pedestrian loadings, which are likely more stochastic. While measures were taken to ensure synchronization of the pedestrians as detailed in Chapter 3, it is likely that the multiple pedestrians did not maintain complete synchronization while walking the length of the bridge span, leading to one pedestrian matching the

natural frequency of the structure while the other did not. The interactions of the footfall loads could lead to unpredictable constructive and destructive interferences that are not explicitly considered in the analytical pedestrian footfall models. More importantly, this structure featured fairly closely spaced modes near the first vertical bending mode. The excitation of these modes could have produced the discrepancies with the analytical models that would not anticipate such modal interactions given the form of the multiple pedestrian footfall models.

Due to the difference between the experimental and analytical results, it was not feasible to complete an analysis comparing the responses and optimization parameters within each model. While increasing the number of pedestrians within the analytical analysis would result in fairly predictable increases in acceleration amplitude, the experimental responses did not behave in an accordingly predictable manner. Consequently, a thorough comparison of the multiple person experimental results to recommended and then calibrated loading models was not performed and is deferred as an area of recommended future research.

## CHAPTER 6: CONCLUSIONS

### 6.1 Summary of Research and Key Findings

The primary focus of this thesis is the evaluation of common footfall loading models to a case study structure and the development of a methodology for calibrating parameters in these excitation models to achieve improved correlation with the experimental measurements. However, the research presented is relevant to and offers contributions to the areas of operational modal analysis of civil structures and structural identification, or finite element model updating. Vibration testing and operational modal analysis were performed on a case study pedestrian bridge to estimate the modal parameters of the structure and characterize the structural response under prescribed pedestrian loading. A finite element model of the pedestrian bridge was developed and the dynamic properties of the model were calibrated to the experimentally obtained estimates using optimization by genetic algorithm.

The field calibrated finite element model was then used to predict the response of the bridge to single pedestrian walking loads using pedestrian footfall models recommended within several design guides and standards. The three pedestrian loading models evaluated were those presented in AISC Design Guide 11 (Murray et al., 2003), ISO 10137 (2007), and the BSI (2008). In each case, recommended coefficients for single pedestrian excitation during walking were used to develop the footfall func-

tions applied to the finite element model. Overall, the model recommended by the BSI provided the strongest correlation with the experimental measurements when the recommended parameter assignments were used. This footfall model produced a predicted response that modestly underestimated the accelerations across the bridge deck, while the loading models recommended by AISC and ISO were found to significantly underestimate the response.

The research also produced a method for calibrating coefficients within each analytical footfall function by optimizing the correlation with the measured acceleration. Following this calibration of the footfall functions, all three models produced similar results and correlated better with the experimentally measured response. Analysis of the parameters identified through the optimization indicated that the fidelity of the AISC and ISO models could be greatly improved by simply increasing the force amplitude of the first harmonic of the footfall functions. Furthermore, a comparison of the calibrated footfall models revealed strong consistency between the characteristics of the identified excitation in each case and suggested that a single harmonic periodic function with larger amplitude excitation than expected by any of the standardized models could be used to predict the actual experimentally measured response.

However, it is important to emphasize the challenges associated with controlled experimental testing on full scale structures, and it should be acknowledged that controlled application of footfall loads in the absence of additional ambient excitations is difficult to achieve. Consequently, the conclusions developed related to the performance of the various footfall models could have been affected by these external effects. Due to the unpredictability of human-structure interaction and possible am-

bient interference that could have occurred during experimentation of the case study structure, the analytical responses observed in this case study can only indicate which loading model proved most accurate when applied to this specific structure. These results do not yet provide sufficient evidence to forecast the performance of these models when applied to other structural models. Consequently, the conclusions developed should be limited to this particular case study unless supported by additional experimentation on a number of other structures.

## 6.2 Recommendations for Future Work

Through the course of this research, several challenges were encountered. It is recommended that these areas of research be addressed in future work.

- Accurately modeling connections and component interactions with the bridge, specifically the interface at the concrete slab cast around the transverse stiffeners on the girder, proved challenging and created difficulties when calibrating the finite element model. Simplified methods for modeling such connections in a way conducive to model updating should be investigated further in future research.
- The dynamic response of the structure predicted using the AISC and ISO loading models varied significantly from the experimentally measured response. Likewise, parameter identification of the excitation forces suggested that a single harmonic periodic function was sufficient for accurately modeling the excitation rather than the use of four or five harmonics, as suggested by these models. It is recommended that additional field experimentation be performed on full scale structures and that the methodology developed be applied to extend the anal-

ysis from this limited case study.

- It is suspected that the differences between the analytical predictions and measured responses are largely due to the loading models being developed using forcing data acquired from footfalls applied to hard, stable surfaces. This does not explicitly account for the interaction between the pedestrian and the vibrating structure. Therefore, future research into the effects of human-structure interaction and means to incorporate the impact within simplified models suitable for design is recommended.
- One of the original goals of this research was to extend the analysis of the pedestrian loading models to cases of multiple pedestrians. However, due to significant discrepancies between the experimentally measured acceleration time histories and those predicted by amplified footfall models, this analysis could not be completed, either directly using recommended coefficients or through optimization. Therefore, techniques for the analysis of simplified pedestrian footfall models extended to multiple pedestrian loading should be investigated in future research.

## REFERENCES

- AASHTO (2009). Lrfd guide specifications for the design of pedestrian bridges. Standard, American Association of State Highway Transportation Officials.
- Allemang, R. J. (2003). The modal assurance criterion—twenty years of use and abuse. *Sound and vibration*, 37(8):14–23.
- Bachmann, H. and Ammann, W. (1987). *Vibrations in Structures: Induced by Man and Machines*. International Association for Bridge and Structural Engineering, Zurich, Switzerland.
- Brandt, A. (2011). *Noise and vibration analysis: signal analysis and experimental procedures*. John Wiley & Sons.
- BSI, B. S. I. (2008). Uk national annex to eurocode 1. actions on structures. traffic loads on bridges. Design guide, British Standards Institution (BSI).
- Çatbaş, F. N., Kijewski-Correa, T., and Aktan, A. E. (2013). Structural identification of constructed systems. *Reston (VI): American Society of Civil Engineers*.
- Dallard, P., Fitzpatrick, T., Flint, A., Low, A., Smith, R., Willford, M., and Roche, M. (2001). London millennium bridge: Pedestrian-induced lateral vibration. *Journal of Bridge Engineering*, 6(6):412–417.
- Eurocode (2001). En 1990:2002+a1:2005(e) eurocode-basis of structural design. Standard, European Committee for Standardization.
- Ewins, D. J. (1984). *Modal Testing: Theory and Practice*. Research Studies Press, LTD., Taunton, Somerset, England.
- Friswell, M. and Mottershead, J. E. (1995). *Finite element model updating in structural dynamics*, volume 38. Springer Science & Business Media.
- Friswell, M., Penny, J., and Garvey, S. (1998). A combined genetic and eigensensitivity algorithm for the location of damage in structures. *Computers & Structures*, 69(5):547–556.
- Fujino, Y., Pacheco, B., Nakamura, S., and Warnitchai, P. (1993). Synchronization of human walking observed during lateral vibration of a congested pedestrian bridge. *Earthquake Engineering and Structural Dynamics*, 22(2):741–758.
- Goldberg, E. (1989). *Genetic Algorithms in Search, Optimization, and Machine Learning*. Addison-Wesley Publishing Company, Inc, Boston, USA.
- ISO (1989). Evaluation of human exposure to whole-body continuous vibration. Standard ISO 2631-2, International Organization for Standardization.

- ISO (2007). Bases for design of structures serviceability of buildings and walkways against vibrations. Standard ISO 10137, International Organization for Standardization.
- Kenigsbuch, R. and Halevi, Y. (1998). Model updating in structural dynamics: a generalised reference basis approach. *Mechanical Systems and Signal Processing*, 12(1):75–90.
- Kernicky, T. P., Whelan, M. J., Weggel, D. C., and Rice, C. D. (2015). Structural identification and damage characterization of a masonry infill wall in a full-scale building subjected to internal blast load. *Journal of Structural Engineering*, 141(1):D4014013.
- Levin, R. and Lieven, N. (1998). Dynamic finite element model updating using simulated annealing and genetic algorithms. *Mechanical Systems and Signal Processing*, 12(1):91–120.
- Matsumoto, Y., Nishioka, T., Shiojiri, H., and Matsuzaki, K. (1978). *Dynamic Design of Footbridges*. IABSE Foundation, Zurich, Switzerland.
- Mottershead, J. E., Link, M., and Friswell, M. I. (2011). The sensitivity method in finite element model updating: a tutorial. *Mechanical Systems and Signal Processing*, 25(7):2275–2296.
- Murray, T., Allen, D., and Ungar, E. (2003). Design guide 11: Floor vibrations due to human activity. Design guide, American Institute of Steel Construction (AISC).
- Nguyen, K., Freytag, B., Ralbovsky, M., and Rio, O. (2015). Assessment of serviceability limit state of vibrations in the uhpfr-c-wild bridge through an updated fem using vehicle-bridge interaction. *Computers & Structures*, 156:29–41.
- Pan, T. (1992). Vibration of pedestrian overpass. *Journal of Constructed Facilities*, 6(1):34–45.
- Peeters, B. and Roeck, G. D. (2001). One-year monitoring of the z24-bridge: environmental effects versus damage events. *Earthquake Engineering and Structural Dynamics*, 30(2):149–171.
- Ricciardelli, F. and Pizzimenti, A. D. (2007). Lateral walking-induced forces on footbridges. *Journal of Bridge Engineering*, 12(6):677–688.
- Roberts, T. (2005). Lateral pedestrian excitation of footbridges. *Journal of Bridge Engineering*, 10(1):107–112.
- Tedesco, J. W., McDougal, W. G., and Ross, C. A. (1999). *Structural Dynamics: Theory and Applications*. Addison Wesley Longman, Boston, MA.
- Van den Branden, B., Peeters, B., and De Roeck, G. (1999). Introduction to macecv2. 0: Modal analysis on civil engineering constructions. *Department of Civil Engineering. Katholieke Universiteit, Leuven, Belgium*.

- Van Overschee, P. and De Moor, B. (1996). *Subspace Identification for Linear Systems: Theory - Implementation - Applications*. Kluwer Academic Publishers, Dordrecht, Netherlands.
- Weaver, W. and Johnston, P. R. (1987). *Structural Dynamics by Finite Elements*. Springer Science & Business Media, New York, NY.
- Whelan, M. and Janoyan, K. (2009). Design of a robust, high-rate wireless sensor network for static and dynamic structural monitoring. *Journal of Intelligent Material Systems and Structures*, 20(5):849–863.
- Žárate, B. A. and Caicedo, J. M. (2008). Finite element model updating: Multiple alternatives. *Engineering Structures*, 30(12):3724–3730.
- Zivanovic, S., Pavic, A., and E.T., I. (2010). Modeling spatially unrestricted pedestrian traffic on footbridges. *Journal of Structural Engineering*, 136(10):1296–1308.
- Živanović, S., Pavic, A., and Reynolds, P. (2006). Modal testing and fe model tuning of a lively footbridge structure. *Engineering Structures*, 28(6):857–868.
- Živanović, S., Pavic, A., and Reynolds, P. (2007). Finite element modelling and updating of a lively footbridge: The complete process. *Journal of Sound and Vibration*, 301(1):126–145.

## APPENDIX A: SAP2000 MATRIX EXTRACTION CODE

```

1 % SAP2000 Matrix Extraction Code
2 % This code is used to define the stiffness and mass matrices
3 % (K and M) and changes in the matrices (delK and delM) resulting
4 % from parameter assignment modification. This script is applied
5 % to the idealized SAP2000 model prior to genetic algorithm
6 % updating.
7
8 % Define the lower and upper parameter bounds
9 clear all
10 % Define lower bounds
11 lb=[0.5;
12 0.5;
13 1;
14 1;
15 1;
16 1;
17 10;
18 1;
19 0];
20 % Define upper bounds
21 ub=[1.5;
22 1.5;
23 1000;
24 1000;
25 1000;
26 1000;
27 1000;
28 1000;
29 500];
30 % Define scale factor applied to lower and upper bounds
31 sc=[1;
32 1;
33 1000;
34 100;
35 1000;
36 1000;
37 1000;
38 1000;
39 1];
40 % Establish updating parameter assignments
41 Pop(1, :)=lb;
42 for k=1:numel(lb)
43 Pop(k+1, :)=Pop(1, :);
44 Pop(k+1, k)=ub(k);
45 end
46 for k=1:numel(lb)
47 Pop(:, k)=Pop(:, k)*sc(k);
48 end
49
50 %Establish Model

```

```

51 root=strcat(cd, '\');
52 % Establish Global Optimization Problem
53 for k=1:length(lb)+1
54 % Initialize SAP2000 model
55 clear SapObject SapModel
56 feature('COM_SafeArraySingleDim',1);
57 feature('COM_PassSafeArrayByRef',1);
58 SapObject = actxserver('sap2000v15.SapObject');
59 SapObject.ApplicationStart(6, 'True');
60 SapModel = SapObject.SapModel;
61 ret = SapModel.InitializeNewModel(6) %#ok<*NASGU>
62 ret = SapObject.SapModel.File.OpenFile(strcat(root, ...
63 '/FEModel/SAPModel.sdb'))
64 fprintf('Set Model Units to kN, m, C\n')
65 ret=SapObject.SapModel.SetPresentUnits(6)
66 fprintf('Delete Results\n')
67 ret=SapObject.SapModel.Analyze.DeleteResults('MODAL',1)
68 fprintf('Unlock Model\n')
69 ret=SapObject.SapModel.SetModelIsLocked(false)
70 fprintf('Set Model Units to kN, m, C\n')
71 ret=SapObject.SapModel.SetPresentUnits(6)
72 fprintf('Set Gravity Load\n')
73 ret = SapObject.SapModel.AreaObj.SetLoadGravity('ALL', ...
74 'DEAD',0,0,1,true, 'GLOBAL',1)
75
76 % Apply parameter changes to the SAP2000 model
77
78 % Set the Bending property modifiers of the deck slab area elements
79 fprintf('Set Bending Modifiers of Deck')
80 ret = SapObject.SapModel.AreaObj.SetModifiers('DeckAll', [...
81 1,1,1,Pop(k,1),Pop(k,2),1,1,1,1,1]',1)
82
83 % Set the link element properties
84 % Properties of the pin and hanger link element
85 fprintf('Set Span Link Properties')
86 ret = SapObject.SapModel.PropLink.SetLinear('SPANLINK', [true, ...
87 true,true,false,true,false]', ...
88 [false,false,true,false,true,false]', [Pop(k,3),Pop(k,4), ...
89 0,0,0,0]', [0,0,0,0,0,0]',0,0)
90 % Properties of the column-to-diaphragm connection link element
91 fprintf('Set Column Link Properties')
92 ret = SapObject.SapModel.PropLink.SetLinear('COLUMNLINK', [...
93 true,true,true,true,false,false]', ...
94 [true,true,false,false,false,false]', [0,0,Pop(k,5), ...
95 Pop(k,6),0,0]', [0,0,0,0,0,0]',0,0)
96 % Properties of the girder web-to-deck slab link element
97 fprintf('Set Web Deck Link Properties')
98 ret = SapObject.SapModel.PropLink.SetLinear('WebDeckLink', [...
99 true,true,true,false,false,false]', ...
100 [false,true,true,false,false,false]', [Pop(k,7),0,0,0,0,0]', ...
101 [0,0,0,0,0,0]',0,0)
102
103 % Set the properties of the boundary condition spring element
104 fprintf('Set BC Springs')

```

```

105 ret=SapObject.SapModel.PointObj.SetSpring('BCSpring',[...
106 Pop(k,8),0,0,0,0,0]',1,true,true)
107
108 % *****
109 %           RUN THE INITIAL MODEL ANALYSIS
110 % *****
111 ret = SapObject.SapModel.File.Save(strcat(root,'/FEModel/MK',...
112 num2str(k-1),'.sdb')); % Need to Save Model Before Analysis
113 ret = SapObject.SapModel.Analyze.SetRunCaseFlag('Linear',0);
114 ret = SapObject.SapModel.Analyze.SetRunCaseFlag('MODAL',1);
115 ret = SapObject.SapModel.Analyze.RunAnalysis();
116 ret = SapObject.SapModel.Results.Setup.SetCaseSelectedForOutput(...
117 'MODAL',1); % Set case and combo output selections
118 ret = SapObject.SapModel.Results.Setup.SetCaseSelectedForOutput(...
119 'Linear',0);
120 SapObject.ApplicationExit(true);
121
122 % *****
123 %   EXTRACT EQUATION NUMBERS AND DEVELOP MAPPING OF MATRICES
124 % *****
125 %Import Stiffness Matrix file
126 TK=importdata(strcat(root,'/FEModel/MK',num2str(k-1),'.TXK'));
127 TK=TK.data;
128 %Import Mass Matrix file
129 TM=importdata(strcat(root,'/FEModel/MK',num2str(k-1),'.TXM'));
130 TM=TM.data;
131 %Determine full matrix size
132 n=max(TK(:,1));
133 %Populate other half of symmetric matrix
134 TK=[TK(:,1);TK(:,2)],[TK(:,2);TK(:,1)],[TK(:,3);TK(:,3)]];
135 %Remove duplicate reference to diagonal entries
136 TK=unique(TK,'rows');
137 K{k}=sparse(TK(:,1),TK(:,2),TK(:,3),n,n);
138 clear TK;
139 TM=[TM(:,1);TM(:,2)],[TM(:,2);TM(:,1)],[TM(:,3);TM(:,3)]];
140 TM=unique(TM,'rows');
141 M{k}=sparse(TM(:,1),TM(:,2),TM(:,3),n,n);
142 clear TM n;
143 end
144 for k=2:numel(lb)+1
145 delK{k-1}=K{k}-K{1};
146 delM{k-1}=M{k}-M{1};
147 end
148 K=K{1};
149 M=M{1};
150 fid=fopen(strcat(root,'/FEModel/MK0.TXC'));
151 fgetl(fid);
152 flag=0;
153 k=1;
154 while(flag==0)
155 A=fgetl(fid);
156 if (A==-1)
157 flag=1;
158 else

```

```

159 CONS(k, :)= [str2num(A(1:12)), str2num(A(13:26)), ...
160 str2num(A(27:52))];
161 k=k+1;
162 end
163 end
164 fclose(fid);
165
166 % *****
167 %   EXTRACT EQUATION NUMBERS AND DEVELOP MAPPING OF MATRICES
168 % *****
169 fid=fopen(strcat(root, '\FEModel\MK0.TXE'));
170 fgetl(fid);
171 flag=0;
172 kj=1;
173 while(flag==0)
174 A=fgetl(fid);
175 B=fgetl(fid);
176 if (B==-1)
177 flag=1;
178 else
179 if isempty(strfind(A(1:10), 'NULL'))
180 if isempty(strfind(A(1:10), 'CElement'))
181 Eqtemp(kj, :)= [str2num(A(1:10)), str2num(A(11:24)), ...
182 str2num(A(25:38)), str2num(A(39:52)), ...
183 str2num(A(53:66)), str2num(A(67:80)), str2num(B(1:14))];
184 kj=kj+1;
185 end
186 end
187 end
188 end
189 fclose(fid);
190 clearvars -except K M delM delK Eqtemp CONS
191
192 % Establish highway sign parameter lower and upper bounds
193 % (This is added separately because it directly affects the
194 % mass matrix)
195 masslb=[0];
196 massub=[1103.26];
197 % Define the location of the sign mass
198 SignJoints=[141;407;1830];
199 [ILC, LOCB]=ismember(SignJoints, Eqtemp(:, 1));
200 SignIndices=reshape(Eqtemp(LOCB, 2:4), length(LOCB)*3, 1);
201 I=find(SignIndices<1);
202 SignIndices(I)=[];
203 % Apply the sign mass to the mass matrix
204 delM{9}=sparse(SignIndices, SignIndices, massub(1)/32.2/1000, ...
205 size(M, 1), size(M, 2));
206 delK{9}=sparse(1, 1, 0, size(M, 1), size(M, 2));
207
208 % Clear workspace of unnecessary data and save remaining workspace
209 clearvars -except K M delM delK Eqtemp CONS
210 save MK.Brooklyn.mat

```

## APPENDIX B: SCRIPTS USED TO OPTIMIZE COEFFICIENTS IN PEDESTRIAN FOOTFALL MODELS

```

1 % Footfall model updating script
2 % This code is used to initialize and run the genetic algorithm in
3 % MATLAB to calibrate the pedestrian footfall loading models.
4 % Define parameter lower bounds
5 lb=[0.5,...
6 0.005,...
7 0.005,...
8 0.005,...
9 0.001,...
10 -pi/2,...
11 -pi/2,...
12 -pi/2,...
13 -pi/2,...
14 0,...
15 1.85];
16
17 % Define parameter upper bounds
18 ub=[2.0,...
19 0.2,...
20 0.2,...
21 0.2,...
22 0.1,...
23 pi/2,...
24 pi/2,...
25 pi/2,...
26 pi/2,...
27 100,...
28 2.3];
29
30 % Set genetic algorithm options
31 options=gaoptimset(@ga);
32 options=gaoptimset('OutputFcns',...
33 @SaveFunctionMATLAB_RunSAP_ReturnAccelerations);
34 options.PlotFcns={};
35 options.PopulationSize=[200];
36 options.TolFun=0;
37 options.TolCon=0;
38 options.EliteCount=10;
39 options.Generations=25;
40 options.CrossoverFraction=0.6;
41 options.CrossoverFcn=@crossoverheuristic;
42 options.PopInitRange=[lb;ub];
43 options.UseParallel='never';
44 options.Vectorized='on';
45 format shortg
46 ['Starting the Genetic Algorithm']
47 nparams=11;
48 [x,fval,exitflag,output,population,scores]=...
49 ga(@MATLAB_RunSAP_ReturnAccelerations,nparams,[],[],[],[],...
50 lb(1:nparams),ub(1:nparams),[],[],options)

```

```

1 % MATLAB to SAP2000 Interface for Pedestrian Traffic
2 % This code is used to establish the SAP2000 model for application
3 % of pedestrian load cases, apply the pedestrian loading model to
4 % the finite element model, and extract the acceleration response
5 % of specified nodes.
6 function Objective = MATLAB_RunSAP_ReturnAccelerations(params)
7 params
8 % Preliminary step - Opening field calibrated SAP2000 model
9 root=cd; % Opening SAP2000
10 feature('COM_SafeArraySingleDim',1);
11 feature('COM_PassSafeArrayByRef',1);
12 SapObject = actxserver('sap2000v15.SapObject');
13 SapObject.ApplicationStart(1,'True');
14 SapModel = SapObject.SapModel;
15 ret = SapModel.InitializeNewModel; % Opening SAP2000
16 ret = SapObject.SapModel.File.OpenFile(...
17 strcat(root, '\FieldCalibratedSAPModel.sdb'));
18
19 % Step 1 - Determining Frame/Points where step load is to be
20 % applied
21 ret = SapObject.SapModel.FrameObj.SetSelected('PATH',true,1);
22 numberframe=double(0);
23 framenames=cellstr('');
24 [ret,numberframe,framenames]=...
25 SapObject.SapModel.FrameObj.GetNameList(numberframe,...
26 framenames);
27 framesel=logical(zeros(numberframe,1));
28 for k=1:numberframe
29 [ret,framesel(k)]=...
30 SapObject.SapModel.FrameObj.GetSelected(framenames{k},...
31 framesel(k));
32 end
33 I=find(framesel==1);
34 framenames=framenames(I);
35 numberframe=length(I);
36 point1='';
37 point2='';
38 x=0; y=0; z=0;
39 for k=1:numberframe
40 [ret,point1,point2]=...
41 SapObject.SapModel.FrameObj.GetPoints(framenames{k},...
42 point1,point2);
43 Pt1{k}=point1;
44 Pt2{k}=point2;
45 [ret,x,y,z]=SapObject.SapModel.PointObj.GetCoordCartesian(...
46 Pt1{k},x,y,z);
47 Pt1x(k)=x; Pt1y(k)=y; Pt1z(k)=z;
48 [ret,x,y,z]=SapObject.SapModel.PointObj.GetCoordCartesian(...
49 Pt2{k},x,y,z);
50 Pt2x(k)=x; Pt2y(k)=y; Pt2z(k)=z;
51 end
52 [Pt1x,order]=sort(Pt1x);
53 Pt1y=Pt1y(order);
54 Pt1z=Pt1z(order);

```

```

55 Pt2x=Pt2x(order);
56 Pt2y=Pt2y(order);
57 Pt2z=Pt2z(order);
58 framenames=framenames(order);
59 for k=1:numberframe
60 framelength(k)=...
61 sqrt((Pt2x(k)-Pt1x(k))^2+(Pt2y(k)-Pt1y(k))^2+...
62 (Pt2z(k)-Pt1z(k))^2);
63 end
64 framedist=cumsum(framelength);
65
66 % STEP 2 - Applying footstep loads to the model
67 d=3.3; % Distance between footsteps (in m or ft);
68 weight=0.7; % Weight of pedestrian (in kN or k);
69 nsteps=floor(framedist(end)/d);
70 for k=1:nsteps
71 temp=find(k*d<framedist);
72 I=temp(1);
73 if I==1
74 reldist=k*d;
75 else
76 reldist=k*d-framedist(I-1);
77 end
78 ret=SapObject.SapModel.LoadPatterns.Add(strcat('nstep',...
79 num2str(k)),8,0,true);
80
81 ret=SapObject.SapModel.FrameObj.SetLoadPoint(framenames{I},...
82 strcat('nstep',num2str(k)),...
83 1,10,reldist,weight,'Global',false,true,0)
84 end
85
86 % STEP 2 for random noise - apply randomly generated loads to the
87 % model deck
88 ret=SapObject.SapModel.LoadPatterns.Add('rng',8,0,true)
89 ret=SapObject.SapModel.PointObj.SetLoadForce('DeckNodes','rng',...
90 [0.001,0.001,-0.001,0,0,0],true,'GLOBAL',1)
91
92 % STEP 3 - Load in the walking and random noise forcing functions
93 % Pedestrian loading forcing function (the ISO function is shown)
94 for kGen=1:length(params)
95 G=1;
96 alpha=[params(kGen,1);params(kGen,2);params(kGen,3);...
97 params(kGen,4);params(kGen,5)];
98 fs=params(kGen,11);
99 speed=fs*d;
100 phi=[params(kGen,6),params(kGen,7),params(kGen,8),params(kGen,9)];
101 i=[1;2;3;4];
102 t = linspace(0,1/fs,1000);
103 for al=1:1
104 Fp(:,al)=G*(1+alpha(1,al)*cos(2*pi*i(1)*fs*t)+...
105 alpha(2,al)*cos(2*pi*i(2)*fs*t+phi(1))+...
106 alpha(3,al)*cos(2*pi*i(3)*fs*t+phi(2))+...
107 alpha(4,al)*cos(2*pi*i(4)*fs*t+phi(3)));
108 end

```

```

109 t(end+1)=t(end)+(t(end)-t(end-1));
110 ft=Fp(:,hk);
111 ft(end+1)=0;
112 ret=SapObject.SapModel.Func.FuncTH.SetUser(['Walking',...
113 num2str(kGen)],length(t),t',ft);
114
115 % Random noise forcing function
116 rng(1);
117 RRForce=(rand(size(ft))-0.5)*params(kGen,10)/100;
118 t2 = linspace(0,(1/fs)*nsteps,1000);
119 ret=SapObject.SapModel.Func.FuncTH.SetUser(['RandomNoise',...
120 num2str(kGen)],length(t2),t2',RRForce);
121
122 % STEP 4 - Setup linear modal time history load case
123 DampFreq=[1.876,2.062,2.947,4.597,7.491,7.806,9.85,...
124 10.93,11.42,14.07,14.97,16.5,19.58,22.6,24.87];
125 RelDamp=[0.0439,0.00881,0.00793,0.0959,0.012,0.0219,...
126 0.012,0.0236,0.0688,0.0426,0.0111,0.0245,0.0767,0.0173,...
127 0.00256];
128 timestep=1/125;
129 duration=nsteps*d/speed;
130 ntimesteps=duration/timestep;
131 ret=SapObject.SapModel.LoadCases.ModHistLinear.SetCase(...
132 ['ModalTime',num2str(kGen)]);
133 ret=...
134 SapObject.SapModel.LoadCases.ModHistLinear.SetDampInterpolated(...
135 ['ModalTime',num2str(kGen)],6,15,DampFreq',RelDamp');
136 ret=SapObject.SapModel.LoadCases.ModHistLinear.SetTimeStep([...
137 'ModalTime',num2str(kGen)],ntimesteps,timestep);
138 for k=1:nsteps
139 loadtype{k,1}='Load';
140 loadname{k,1}=strcat('nstep',num2str(k));
141 func{k,1}=['Walking',num2str(kGen)];
142 sf(k)=1;
143 tf(k)=1;
144 at(k)=(k-1)*d/speed;
145 CSys{k,1}='Global';
146 Ang(k)=0;
147 end
148 ret=SapObject.SapModel.LoadCases.ModHistLinear.SetLoads([...
149 'ModalTime',num2str(kGen)],...
150 nsteps+1,[loadtype;'Load'],[loadname;'rng'],[func;[...
151 'RandomNoise',num2str(kGen)]],[sf';1],[tf';1],[at';0],...
152 [CSys;'GLOBAL'],[Ang';0])
153 end
154
155 % STEP 5 - Run analysis
156 ret=SapObject.SapModel.File.Save(strcat(root,'\MATLABBRIDGERUN',...
157 num2str(hk+20)));
158 ret = SapObject.SapModel.Analyze.SetRunCaseFlag('DEAD',0);
159 ret = SapObject.SapModel.Analyze.SetRunCaseFlag('MODAL',0);
160 ret = SapObject.SapModel.Analyze.SetRunCaseFlag('DEAD2',0);
161 ret = SapObject.SapModel.Analyze.SetRunCaseFlag('rng',0);
162 ret = SapObject.SapModel.LoadCases.ModalEigen.SetNumberModes(...

```

```

163 'MODAL',20,20);
164 ret = SapObject.SapModel.Analyze.RunAnalysis();
165
166 % Step 6 - Extract results
167 for kGen=1:length(params)
168 ret = SapObject.SapModel.Analyze.SetRunCaseFlag([...
169 'ModalTime',num2str(kGen)],1);
170 ret = SapObject.SapModel.Results.Setup.SetCaseSelectedForOutput(...
171 ['ModalTime',num2str(kGen)],1);
172 ret = SapObject.SapModel.Results.Setup.SetCaseSelectedForOutput(...
173 'DEAD',0);
174
175 SapObject.SapModel.Results.Setup.SetOptionDirectHist(2);
176 SapObject.SapModel.Results.Setup.SetOptionModalHist(2);
177 SapResult= zeros(7,1,'double');
178 NumberResults = 0;
179 Obj = cellstr(' ');
180 Elm = cellstr(' ');
181 ACase = cellstr(' ');
182 StepType = cellstr(' ');
183 StepNum = zeros(1,1,'double');
184 U1 = zeros(1,1,'double');
185 U2 = zeros(1,1,'double');
186 U3 = zeros(1,1,'double');
187 R1 = zeros(1,1,'double');
188 R2 = zeros(1,1,'double');
189 R3 = zeros(1,1,'double');
190 GroupElm = 2;
191 ret = ...
192 SapModel.Results.Setup.DeselectAllCasesAndCombosForOutput;
193 ret = SapModel.Results.Setup.SetCaseSelectedForOutput([...
194 'ModalTime',num2str(kGen)]);
195 [ret, NumberResults, Obj, Elm, ACase,...
196 StepType,StepNum, U1, U2, U3,...
197 R1, R2, R3]=...
198 SapModel.Results.JointAcc('SENSORS', ...
199 GroupElm, NumberResults, Obj, Elm,...
200 ACase,StepType, StepNum, U1, U2, U3,...
201 R1, R2, R3);
202 nl=length(U1)/16;
203 for cm=1:16 %Establishing predicted accelerations
204 SU1(cm,:)=U1(1+(nl*(cm-1)):(nl*cm));
205 SU2(cm,:)=U2(1+(nl*(cm-1)):(nl*cm));
206 SU3(cm,:)=U3(1+(nl*(cm-1)):(nl*cm));
207 end
208 Objective(kGen,:)=Correlation(SU3)
209 clear SU1 SU2 SU3; %Results must be cleared for the next
210 % generation
211 end
212 ret=SapObject.ApplicationExit(true);
213 end

```

```

1 % Pedestrian footfall correlation code
2 % This code is used to compute the objective score calculated for an
3 % analytical acceleration time history compared to an experimental
4 % acceleration time history
5 function Objective = Correlation(SU3) % The correlation of the
6 % vertical acceleration
7 % Match the first dataset
8 load('SinglePersonCase1'); % Experimental acceleration file 1
9 mlen=length(CAccel(:,1));
10 SU3g=SU3/32.2*1000; % Converting accelerations to mg
11 for j=1:(length(SU3(1,:))-mlen)
12 for k=6:12
13 % Calculation of the objective score for one load case
14 Error(k)=sum((CAccel(:,32+k)-SU3g(k,j:j+mlen-1)).^2);
15 end
16 CError(j)=sum(Error(k));
17 end
18 [M,I]=min(CError);
19 EXPFFT1=mean(abs(fft(CAccel(:,33:48))),2);
20
21 % Match the second dataset
22 load('SinglePersonCase2') % Experimental acceleration file 2
23 mlen=length(CAccel(:,1));
24 SU3g=SU3/32.2*1000;
25 for j=1:(length(SU3(1,:))-mlen)
26 for k=6:12
27 % Calculation of the objective score for one load case
28 Error(k)=sum((CAccel(:,32+k)-SU3g(k,j:j+mlen-1)).^2);
29 end
30 CError(j)=sum(Error(k));
31 end
32 [M2,I2]=min(CError);
33 Objective=M+M2; % Summation of the objectives
34
35 % Plotting the comparison between experimental and analytical
36 % acceleration time histories
37 for csensor = 6:12
38 figure
39 set(gca,'FontSize',18)
40 stime=1/125:1/125:length(SU3g)/125;
41 mtime=1/125:1/125:mlen/125;
42 plot(stime(I)+mtime,CAccel(:,csensor+32),'r')
43 hold on
44 plot(stime,SU3g(csensor,:), '--');
45 legend('Experimental response','SAP2000 predicted response')
46 xlabel('Time (s)')
47 ylabel('Acceleration (mg)')
48 end
49 end

```